# $H_6^+$ ions in solid hydrogen

**SHIMIZU Yuta**

# $H_6^+$ ions in solid hydrogen

**SHIMIZU Yuta**

*Department of Applied Chemistry*

*Graduate School of Engineering*

*Nagoya University*

*Nagoya 464-8603, Japan*

*2011*

# Contents

# 1 Introduction

## 1.1 Chemistry of hydrogen molecules and ions in gaseous phase

"Hydrogens" are in the most abundant atoms and molecules in the universe.[1] Organisms are mainly composed of water, organic molecules as proteins, lipids, DNA and so on, so that most of them include hydrogen atoms in these molecules. Protons play the most important roles for living organisms, for example, DNA molecules can make double helix structure due to hydrogen bonds between two bases in each strand, ATP synthesis can be proceed by a proton gradient in the membrane of mitochondria. Hydrogen molecules are also used for the synthesis of ammonia or hydrogenation of unsaturated hydrocarbons in industrial use. Recently hydrogen molecules in fuel cells are in attention of environmental protection. Tremendous amounts of protons have been ejected from sun as a result of huge energy production by nuclear fusion of hydrogen atoms, so that these proton beams travel in space and reach to the atmosphere to produce 2$^{nd}$ cosmic ray falling to the surface or inside of the earth. Hydrogen atoms, molecules, protons are, therefore, very deeply related to our life.

Because hydrogen atoms and molecules are fundamental and the simplest chemicals, both experimental and theoretical approaches have been made for developing the theory of quantum mechanics including molecular orbital. Especially hydrogen molecular ion as an $H_2^+$ is known as the most fundamental molecular ion for the study of molecular orbital approximation by linear combination of atomic orbital.

Although an $H_2^+$ is the most famous molecular ion and simply thought to be observed by ionizing radiation to hydrogen molecules, it is impossible to detect it in condensed phase as described below.

The protonated hydrogen molecule, $H_3^+$ is the most abundant molecular ion in the universe and play a pivotal role in interstellar chemistry.[1-5] As the simplest of all polyatomic molecules, $H_3^+$ is fascinating to both physicists and chemists, but lately research in astronomy has been an important driver of both laboratory work and theory. $H_3^+$ was discovered in 1911 by J. J. Thomson.[6] First observed as an "evanescent" trace product of a discharge in $H_2$, its abundance was soon found to exceed that of both $H^+$ and $H_2^+$ in most hydrogen plasmas, demonstrating both its ease of formation and stability. It was realized that $H_3^+$ was being formed by the efficient reaction,

$$H_2^+ + H_2 \rightarrow H_3^+ + H. \qquad (1.1)$$

$H_3^+$ is highly reactive, happily dominating a proton to almost every atom and molecule it encounters. In astrophysical environments, the principal seed is cosmic rays, which, as they traverse interstellar clouds, leave trails of $H_2^+$ ions in their wakes, which are rapidly converted to $H_3^+$ by the aforementioned reaction (1.1).

Although the presence of $H_3^+$ in dense clouds, which are characterized by very low temperature (~10 K) and high densities ($10^4 - 10^8$ $cm^{-3}$), could be inferred, direct detection of $H_3^+$ proved to be elusive. The only method of observing the molecule in space is via the $\nu_2$ vibration-rotation band whose fundamental occurs near a wavelength of 4 μm. This spectrum was observed in the laboratory in 1980.[7] It took 16 additional years before $H_3^+$ was detected in interstellar space.[4]

Over the last three decades, millimeter and submillimeter spectroscopy revealed that dense clouds contain a large variety of molecules.[3, 8] In such clouds, $H_3^+$ ion is

thought to be a cornerstone of ion-molecule gas-phase chemistry.[3] $H_3^+$ ion will transfer its proton to other species such as O and CO to make $OH^+$ and $HCO^+$, respectively. It can also charge transfer with trace metal atoms such as iron.[3]

Recently, it is becoming increasingly clear that chemical reactions on cosmic dust in dense clouds play an important role rather than in gas-phase ion-molecule reactions.[9] In 2010, Kaneda *et al*. obtain clear evidence that the polycyclic aromatic hydrocarbons emission comes predominantly from the cosmic dust lane of the galaxy.[10] They also detect molecular hydrogen line emissions from the dust lane.[10]

Unfortunately, direct observations of the solid-phase chemistry of dense clouds are difficult to come by. In the absence of direct evidence, we have to resort to laboratory studies. A wealth of data has been gathered on gas-phase ion molecule reactions, but investigations on solid-phase reactions remain scare, although there have been experimental studies of molecular hydrogen formation on the surface of cosmic dust analogs[11].

Based on the gas phase studies, it was expected that the $H_3^+$ ions should also be produced in irradiated solid hydrogens. Souers *et al*.[12-16] in 1980's carried out infrared absorption (IR) study of solid hydrogens containing radioactive species of tritium. Brooks *et al*.[17-19] extended their studies using high-energy proton beams as a radiation source. Since 1990's, Oka *et al*.[20-23] have reinvestigated these studies using a technique of high-resolution IR spectroscopy in γ-ray irradiated solid parahydrogen ($p\text{-}H_2$) matrices. In all studies charge-induced IR lines of hydrogen molecules neighboring on ionic species were observed, showing that hydrogen ions were produced; however, no one observed any IR lines of the ions themselves.

## 1.2 Matrix isolations in solid hydrogen

### 1.2.1 Properties of solid parahydrogen

Solid p-$H_2$ has a various quantum effects features because of small mass and intermolecular interactions. Because of the small mass and the weak interactions, the rotational angular moment $J$ of each hydrogen molecule is still a good quantum number in solid as was discovered by McLenann and McLeod.[24] The largest of the orientation-dependent interactions is the electric quadrupole-quadrupole (EQQ) interaction, which is on the order of magnitude of ~4 K. Because the EQQ interaction is much smaller than the rotational constant of $H_2$ (B = 85.2 K), the rotational states of $H_2$ are almost undistorted by neighbors.[25]

The Pauli exclusion principle requires that the rotational states having even quantum numbers couple with the $I = 0$ nuclear spin states where $I$ is the total nuclear spin number, while those having odd quantum numbers couple with $I = 1$ nuclear spin state, exclusively as shown in Table 1.1.[25] The former is called parahydrogen (p-$H_2$), and the latter orthohydrogen (o-$H_2$). At very low temperatures, p-$H_2$ occupies only the $J = 0$ rotational state, while o-$H_2$ occupies the $J = 1$ state. Relaxation from the $J = 1$ to the $J = 0$ rotational state is extremely slow even in solid hydrogen, so that p-$H_2$ and o-$H_2$ can be treated as almost different molecules in the solid.[25]

Since the $J = 0$ rotational wavefunction has a spherical shape, p-$H_2$ molecules at liquid helium (LHe) temperatures have no permanent electric moments of any order.[25] Thus, the p-$H_2$ crystal provides a homogeneous environment for a solute embedded in it. On the other hand, o-$H_2$ molecules occupying the $J = 1$ rotational quantum number have a small permanent electric quadrupole moment.[25] The quadrupole moment of the o-$H_2$

Table 1.1. Allowed combinations of $I$ and $J$ for $H_2$ and $D_2$.

| molecule | $I$ | $J$ | Designation |
|---|---|---|---|
| $H_2$ ($I_N$ = 1/2) | 0 | Even | para |
| | 1 | Odd | ortho |
| $D_2$ ($I_N$ = 1) | 1 | Odd | ortho |
| | 0, 2 | Even | para |

in $J$ = 1 state provides slightly stronger interaction with its surroundings than the p-$H_2$ in $J$ = 0 state. The concentration of o-$H_2$ in p-$H_2$ matrices, therefore, needs to be as low as possible in order that solute molecules in solid p-$H_2$ may have least electric and magnetic perturbation. Since the o-$H_2$ in $J$ = 1 state has 170.5 K higher energy than the p-$H_2$ in $J$ = 0 state as shown in Figure 1.1, the concentration of o-$H_2$ can be reduced to less than 0.05% by immersing FeO(OH) into liquid normal $H_2$ at just above the melting point of 13.8 K. The concentrations of o-$H_2$ in samples described in this thesis are always less than 0.2%.

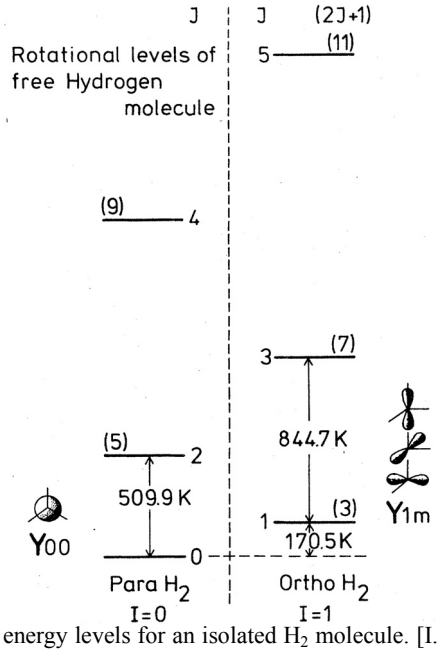


Figure 1.1. The molecular rotational energy levels for an isolated $H_2$ molecule. [I. F. Silvera, Rev. Mod. Phys. **52** 393 (1980)] The same diagram applies to $D_2$ but scaled down by about a factor of 2 due to the larger moment of inertia. The angular distribution of the two lowest rotational states are also indicated ($Y_{10}$ and $Y_{11} \pm Y_{1-1}$ are actually shown). $I$ is the total nuclear spin composed of two nuclear spins of proton $I_N$ = 1/2 aligned in antiparallel ($I$ = 0) or in parallel ($I$ = 1). Numbers in parenthesis are the $m$ degeneracies, where $m$ is the $z$-component of therotational quantum number.

Table 1.2. Physical properties of molecular crystals [I. F. Silvera, Rev. Mod. Phys. **52**, 393 (1980), T. Momose, H. Hoshina, M. Fushitani, and H. Katsuki, Vibrational Spectroscopy **34**, 95 (2004).]

| Properties | | p-$H_2$ | Ne | Ar |
|---|---|---|---|---|
| Triple point (K) | | 13.80 | 24.56 | 83.81 |
| Boiling point[a] (K) | | 20.28 | 27.07 | 87.29 |
| Lattice constant (Å) | | 3.793 | 3.16 | 3.76 |
| Crystal structure | | *hcp* | *fcc*/*hcp* | *fcc*/*hcp* |
| Lennard-Jonse parameter | $\varepsilon^b$ (K) | 37 | 35.6 | 119.3 |
| | $\sigma^b$ (Å) | 2.92 | 2.74 | 3.45 |

[a] At a pressure of 0.1 MPa.
[b] The Lennard-Jonse potential is defined as $V(r) = 4\varepsilon[(\sigma/R)^{12} - (\sigma/R)^6]$.

Another important feature is large amplitude of zero-point vibration. The root-mean-square width of the single particle distribution function is about 18% of the nearest neighbor distance (3.793 Å[25]) (*cf*. Table 1.2). This large zero-point motion is a result of the weak isotropic intermolecular potential and the light mass. As a result, the intermolecular distance in solid p-$H_2$ is considerably larger than the interatomic distance in solid Ne, although the Lennard-Jones type of pair potentials between $H_2$ molecules is similar to the potential between Ne atoms as shown in Figure 1.2.[25, 26]

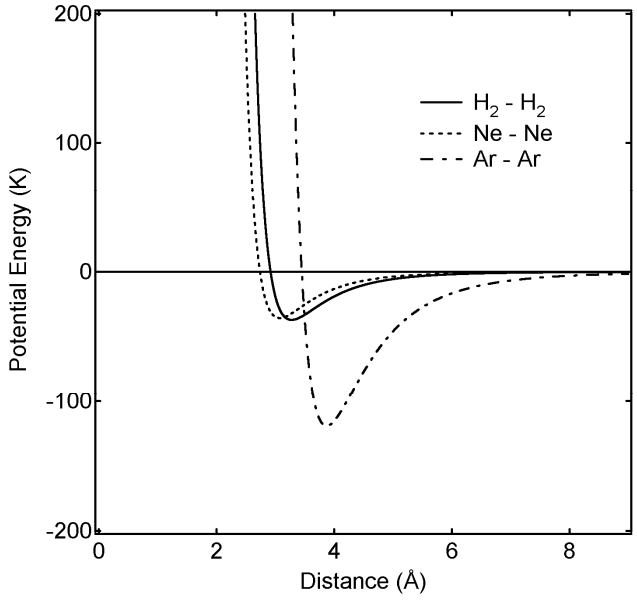


Figure 1.2. Lennard-Jones pair potential of $H_2$-$H_2$, Ne-Ne, and Ar-Ar using Lennard-Jones parameter listed in Table 1.2.

The crystal structure of solid p-$H_2$ was firstly determined by Keesom *et al* in 1930.[25, 27] Their seven X-ray reflections could be fit to the hexagonal closest packed (*hcp*) lattice. It is known that the crystal structures of Ne and Ar matrices consist both of hexagonal-close-packed (*hcp*) and face-centered-cubic (*fcc*) structures as listed in Table 1.2.[25, 26] The mixtures of different crystal structures in Ne and Ar matrices cause additional complexity and broadening in their optical spectra that makes the spectral analysis impossible in some cases. On the other hand, the crystal structure of solid p-$H_2$ is a pure *hcp*, which has provided highly resolved spectra of IR, ESR, and other spectroscopy.[26, 28-53]

### 1.2.2 Spectroscopy using solid parahydrogen

Solid hydrogen is one of the most feasible and ideal media for the study of matrix isolation spectroscopy. Thanks to the quantum nature, solid p-$H_2$ has a self-annealing character, in which defects and imperfections of the solid p-$H_2$ crystal produced during both the crystal growth and the harsh irradiation are eliminated.[20, 41, 42, 54, 55] Unlike in other molecular crystals, spectroscopic data measured in solid parahydrogen are highly reproducible and independent on scheme of sample preparation. Secondly, spectral linewidth of ESR lines of solute molecules becomes highly resolved because p-$H_2$ molecules having a spherical shape of the $J = 0$ rotational wavefunction do not have permanent electric and magnetic moments.[41, 42, 45, 54] Third, solute molecules are in almost free from the cage effect because of the softness of p-$H_2$ as a quantum crystal. A variety of chemical reactions can be taken place in solid p-$H_2$ at liquid helium

temperature by light or ionizing radiation.[50, 53, 56-61] Availing these unique properties, solid p-$H_2$ matrix has been applied to the spectroscopic studies for physical and chemical processes of solute molecules by several groups.[26, 28-53]

Miyazaki *et al*.[45] has pointed out that solid p-$H_2$ is useful for high-resolution ESR spectroscopy, because p-$H_2$ has no nuclear magnetic moment therefore yielding no superhyperfine interaction with guest radicals which broaden ESR linewidth. We have reported highly resolved ESR lines of H,[41] $CH_3$,[45] $C_2H_5$,[42] $O_2$,[44] $e^-$,[43, 46] and $H_6^+$[46-52] in solid p-$H_2$. Solid p-$H_2$ matrix can provide large benefit on the measurement of FT-IR spectroscopy too. Oka and Momose have been studied on reaction intermediates in γ-ray irradiated solid p-$H_2$ by FT-IR spectroscopy.[53, 56-61] They have observed sharp infrared spectral lines in ionized para-$H_2$ crystals.[23] They assigned the lines to the $Q_1(0)$ ($v = 1 \leftarrow 0, J = 0 \leftarrow 0$) transition of $H_2$ near $H_3^+$ and $H^-$, which becomes optically active due to Stark shift from Coulomb field of the ions.[22, 23] However, any signal of ion itself could not be detected.

## 1.3 $H_6^+$ ions and its isotopomers in solid parahydrogen

### 1.3.1 "Six" is the magic number for even-membered $H_n^+$

$H_6^+$ ion was firstly observed in $H_2$ gas phase with electron beam using mass spectroscopy by Kirchner and Bowers.[62] Although odd-membered hydrogen ions are mainly observed from hydrogen gas irradiated by elecrtron beam, yield of $H_6^+$ ions was the largest by far among even-membered hydrogen ions ($H_6^+ >> H_8^+ > H_{10}^+ > H_4^+$). Fiegele *et al*.[63] have reproduced the results by using deuterium ions. Although mass and

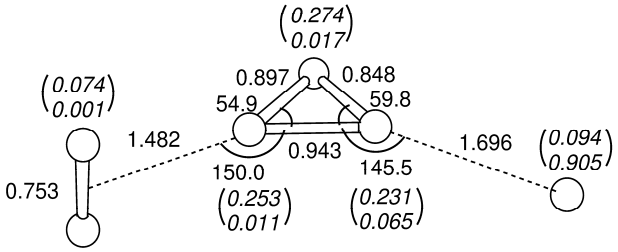


**(a) $H_3^+$-core $H_6^+$ ($C_s$)**

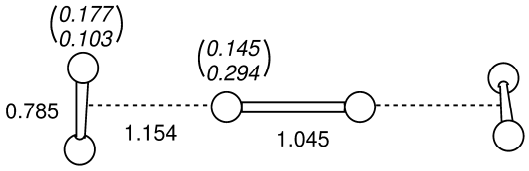


**(b) $H_2^+$-core $H_6^+$ ($D_{2d}$)**

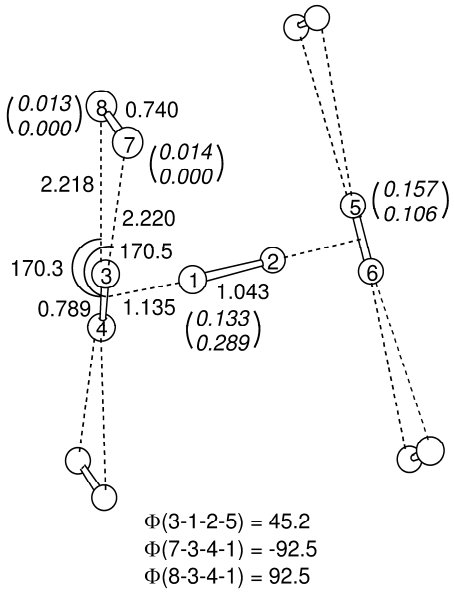


**(c) $H_2^+$-core $H_{14}^+$ ($D_2$)**

Figure 1.3. Optimized geometries of (a) $H_3^+$-core $H_6^+$, (b) $H_2^+$-core $H_6^+$, and (c) $H_2^+$-core $H_{14}^+$ at MP2/cc-pVTZ level reported by Kurosaki and Takayanagi in 1998 [Y. Kurosaki and T. Takayanagi, J. Chem. Phys. **109**, 4327 (1998)]. Bond lengths in Å and angles in degrees. In parentheses are shown atomic net charge and spin density in the upper and lower lines, respectively.

charge of $H_6^+$ were clear from the mass spectroscopy, it was impossible to get chemical structural information. Kirchner and Bowers expected that a $H_6^+$ was a cluster composed of $H_3^+$, H, and $H_2$ because $H_3^+$ occupies largest majority in the products of cation. In the same year, Montgomery and Michels proposed that $H_6^+$ has two isomers, a

$H_3^+$-core type with $C_s$ symmetry and a $H_2^+$-core type with $D_{2d}$ symmetry (*cf*. Figure 1.3), and that the $H_2^+$-core isomer is about 0.1 eV lower in energy than the $H_3^+$.[64] This prediction is surprising because it has been widely accepted that all $H_n^+$ cluster geometries are composed of a $H_3^+$-core and surrounding $H_2$ molecules weakly bound to it. In 1998, Kurosaki and Takayanagi did an extensive treatment of the $H_2^+$-core $H_6^+$ ion.[65, 66] They found a reaction path connecting the two $H_6^+$ isomers. They also pointed out that "six" is the magic number for even-membered $H_n^+$. Their calculations predict that the central $H_6^+$ is almost unperturbed in all even-membered $H_n^+$ ($n \geq 6$), and outer $H_2$'s are very weakly bound to its corners. As shown in Figure 1.3(c), structure of central $H_6^+$ in $H_{14}^+$ is found to be almost the same as that in Figure 1.3(b), and charge and spin densities on outer four $H_2$'s are negligible. The total binding energy of four $H_2$'s to $H_6^+$ in $H_{14}^+$ is only 0.05 eV, which is negligible compared to the exothermic $H_2^+ + 2H_2 \rightarrow H_6^+$ reaction of 2.12 eV. It means that, when $H_6^+$ is generated in solid $H_2$, the positive charge remains localized on unperturbed $H_6^+$.

Although theoretical approach on $H_2^+$-core $H_6^+$ ions has been accumulated for over a decade from 1987, no experimental results, which support chemical structure of $H_2^+$-core $H_6^+$ ions, has been appeared until we have published ESR spectroscopic results on $H_{6-n}D_n^+$ ions in γ-ray irradiated solid p-$H_2$-$D_2$ or HD mixtures.[48]

### 1.3.2 Strange doublet ESR lines in γ-ray irradiated solid p-$H_2$

Independent of the mass spectroscopy works, Miyazaki *et al*.[45, 67, 68] in the middle of 1990's developed a technique of high-resolution ESR spectroscopy using

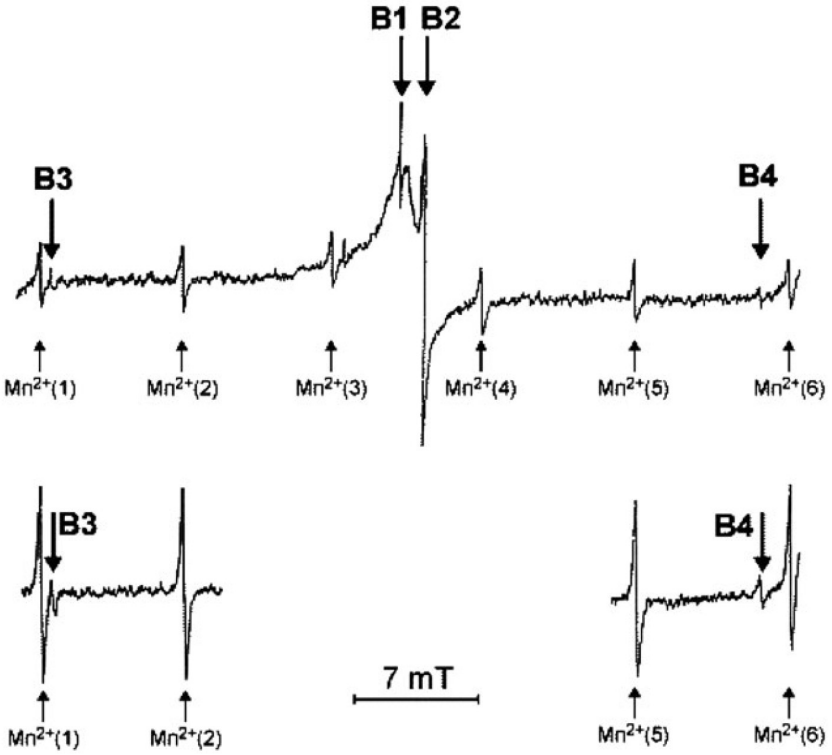


Figure 1.4. ESR spectra at 4.2 K in g-irradiated solid p-$H_2$ reported by Kumada *et al*. [T. Kumada, H. Inagaki, T. Nagasawa, Y. Aratono, and T. Miyazaki, Chem. Phys. Lett. **251**, 219 (1996)]

solid p-$H_2$ matrices. In 1995, Miyazaki *et al*.[67] found a very narrow isotropic doublet lines in the ESR spectrum in γ-ray irradiated solid p-$H_2$ at 4.2 K with a separation of 1.24 mT and a mid-point *g*-value of 2.007. They designated the two signals temporally as radical pairs comprising trapped electron and $H_2^+$ ion. However, Symons pointed out that these novel lines might be due to a second order splitting of the nuclear spin moment and its *z*-component [$I$, $I_z$] = [1, 0] and [0, 0] features.[69] The two ionic hydrogen species, $H_2^+$ and $H_2^-$, were considered as possibilities. Symons suggested that the species was $H_2^-$ ion. He assigned a real *g*-value of 2.0033 to the spectrum, and the $^1$H-hyperfine splitting, estimated from the 1.24 mT, was 20.3 mT for two equivalent protons, so that the two outer lines due to [$I$, $I_z$] = [1, 1] and [1,] features could be predicted.[69]

In 1996, Kumada *et al*.[68] found two broadened lines at ±20.3 mT from the line at $g$ = 2.0033 as Symons had predicted, and four lines due to [$I$, $I_z$] = [1, 0], [0, 0], [1, 1], and [1, −1] features were denoted as B1 to B4, as shown in Figure 1.4.[68] Since [$I$, $I_z$] = [1, 1], [1, −1] species of a $H_2^+$ ion, which was found in the gas phase, showed 28.7 mT in $^1$H-hyperfine splitting,[70] the observed spectrum showed $^1$H-hyperfine splitting of 20.3 mT, which was 30% smaller than that of 28.7 mT in $H_2^+$ ion. This 30% reduction of $^1$H-hyperfine splitting of $H_2^+$ ion in solid phase is very difficult to explain. In addition, $H_2^+$ ion have never been observed in solid hydrogen because of reaction (1.1).[20, 21]

When Miyazaki *et al*. measured the ESR spectrum of doublet lines (B1 and B2), they did not use any microwave frequency counters. Only the third and fourth lines of $Mn^{2+}$ in MgO were used as the $g$-value standard in the conventional method, which is a less reliable way of measurement for obtaining a precise g-value. Kumagai *et al*.[52] succeeded in observing much highly resolved lines in highly purified solid p-$H_2$ and determined the ESR parameters, $A$ =20.441 mT and $g$ = 2.002 120 ± 0.000 012, which consistently account for all of position and lineshape of the quartet lines. The $g$-value was smaller than that of free electron as 2.002319.

During the course of refining experimental ESR parameters of the species, Suter *et al*.[71] pointed out that $H_6^+$ ions, having $H_2^+$-core type $H_6^+$ with $D_{2d}$ symmetry as Montgomery and Michels predicted, may show isotropic hyperfine coupling constant of 572 MHz (= 20.4 mT) on their DFT calculation. The value of calculated isotropic hyperfine coupling constant was very close to that experimentally obtained. Tachikawa calculated $g$-value of $H_2^+$-core $H_6^+$ ions by B3LYP/6-311G++(3df, 3pd) level as 2.00228 which is smaller than that of free electron, and it was also consistent with experimental one qualitatively.[52]

Although the experimental *g*-value and isotropic hyperfine coupling constants are consistent with those of $H_2^+$-core $H_6^+$ theoretically calculated, these experimental values were still not enough to confirm whether the species are $H_2^+$-core $H_6^+$ or $H_2^-$. According to the theoretical calclation of Suter *et al*, side-on $H_2$ of $H_2^+$-core $H_6^+$ should have isotropic hyperfine coupling constant of ≈ 9 mT but corresponding lines have not been observed in the ESR spectrum. Kumada *et al*. pointed out that the splitting could "disappear" if side-on $H_2$s on $H_6^+$ are allowed to rotate freely along the main axis due to $J = 0$ at 4.2 K combined with $I = 0$. The free rotation of side on $H_2$ may be allowed theoretically but was difficult to confirm whether the side-on $H_2$ exist or not from experimental result.

### 1.3.3 Experimental assignment of $H_6^+$ and its isotopomers in γ-ray irradiated solid p-$H_2$ ESR spectroscopy

In order to confirm the assignment, we have performed to put small portion of $D_2$ or HD in solid p-$H_2$ to generate isotopomers of $H_6^+$.[48] Table 1.1 shows the allowed combinations of *I* and *J* for $H_2$ and $D_2$ molecules. $D_2$ has $I = 2$ and 0 at $J = 0$ although $H_2$ has only $I = 0$ at $J = 0$. The splitting of five ESR lines due to hyperfine coupling constant of side-on $D_2$ in $I = 2$ at $J = 0$ should be observed if $H_2^+$-core $H_4D_2^+$ are produced.

In the course of my doctoral study, we have succeeded in observing sharp ESR lines assigned to $H_5D^+$, $H_4D_2^+$, and $H_2D_4^+$ in γ-ray irradiated solid p-$H_2$ containing ortho-$D_2$ (o-$D_2$) and HD only at 1 mol%. The experimental ESR parameters almost

satisfy the theoretical values of $H_{6-n}D_n^+$. This is the first direct observation and confirmation of hydrogen ions in solid hydrogen.. In addition the experimental results revealed that distribution of unpaired electron is depend on protons or deuterons, which is not expected by theoretical calculation under Born-Oppenheimer approximation. In Chapter 2, the ESR study on $H_6^+$ and its isotopomers will be discussed on the assignment scheme and spectroscopic properties.

### 1.3.4 Rotational motions of $H_6^+$ and its isotopic analogues

There is a long history on the studies of rotational and librational motions of molecules trapped in cryocrystals.[20, 44, 54, 55, 72-83] Theses studies were mainly carried out using infrared absorption spectroscopy (IR); however, electron spin resonance (ESR) spectroscopy is also applicable for the rotational and librational motions.[55, 79-82] Advantage of ESR over IR is that ESR measures pure rotational and librational motions, whereas IR excites ro-vibrational transitions.

When rotation of radicals in cryocrystals is hindered or stopped, ESR lines are broadened via anisotropic *g*-values and hyperfine interactions. On the contrary, when radicals rotate freely, such a broadening disappears due to motional narrowing.[81, 82] Kumada[44] found by analysis of ESR lines of $O_2$ in isotopic solid hydrogens that the libration amplitude does not decrease but increases with an increase in pressure. This result indicates that cage distortion rather than size of cage is important factor which determine the librational motion.[83] In order to study the rotational and librational motions by ESR spectroscopy, highly resolved lines are essential. Solid para-$H_2$ (p-$H_2$)

is the ideal matrix for high-resolution ESR spectroscopy[41-43, 45-51, 55] as mentioned in Chapter 1.2.

$H_6^+$ is the radical ion, whose spectroscopic data were firstly reported by our group by using highly resoluted ESR spectroscopy with p-$H_2$ matrices.[46-48, 51] The validity of assignment of $H_6^+$ and its isotopomers were precisely confirmed in Chapter 2. Isotropic hyperfine-coupling constants (HFCCs) $A^{iso}$ experimentally determined show excellent agreement with those calculated, indicating that the calculation properly optimizes the geometry of $H_6^+$.

Anisotropic HFCCs, $A^{ani}$, however, differ greatly from the theoretical ones.[49, 52] Recently, we carried out ESR measurements on $H_6^+$ and $H_4D_2^+$, both at 4.2 and 1.7 K, to conclude that the difference should be due to large precessional motion. In Chapter 3, we present the ESR results and discuss possible precession modes in solid p-$H_2$.

### 1.3.5 Electrons and $H_6^+$ ion trapping by isotopic molecules in solid parahydrogen

When gaseous $H_2$ molecules are subjected to ionizing radiation,[12, 84] the ionization of $H_2$ molecules initially produce $H_2^+$ as:

$$H_2 \xrightarrow{\gamma\text{-ray}} e^- + H_2^+ . \qquad (4.1)$$

The $H_2^+$ ions disappear immediately by reacting with neighboring $H_2$ molecules to form $H_3^+$ as:

$$H_2^+ + H_2 \rightarrow H_3^+ + H . \qquad (4.2)$$

The $H_3^+$ ions recombine with electrons to produce H atom radicals under irradiation:

$$H_3^+ + e^- \rightarrow H_3^* \rightarrow 3H \text{ or } H_2 + H . \quad (4.3)$$

H atom radicals are also generated by dissociation of $H_2$ in an excited state:

$$H_2 \xrightarrow{\gamma\text{-ray}} H_2^* \rightarrow 2H . \quad (4.4)$$

Not only these ions and H atom radicals but also $H_6^+$ ions are expected to be produced in irradiated solid hydrogen. Although electrons produced in irradiated gaseous $H_2$ they recombine with the cations immediately, very small portions of $e^-$ can be trapped in the solid phase to form $e_t^-$.

Electrons trapped in solids at cryogenic temperature have been extensively studied since four decades in the field of radiation chemistry for aqueous matrices,[85-90] alcohols,[91-100] hydrocarbons,[95, 101-104] and hetero compounds.[93, 96-98, 105-111] Although most electrons produced by the radiolysis of solid matter recombine with the parent cations, some of them are trapped in local potential minima like defects, cracks, and distortions to form trapped electrons ($e_t^-$)[84, 112, 113]. Yields of $e_t^-$ in solids usually depend on solid crystallinity and polarity. Electrons in glassy solids can be stabilized as $e_t^-$ by local rearrangement of surrounding molecules to produce larger free volumes for reducing kinetic energy.[112-115] Polar molecules in solids assist in reducing the potential energy of electron by charge polarization[92]. On the other hand, no electron can be trapped in irradiated molecular crystals, except in irradiated single crystals of $D_2O$, [116] trehalose[117], and crystals of diols.[91] Large crystallization energy hinders the local rearrangements of molecules in crystals.[84]

Ten years ago, the yields of $e_t^-$ produced by radiolysis of solid p-$H_2$ were found to significantly increase with increasing $D_2$ or HD concentrations, whereas no $e_t^-$ could be detected in their absence by ESR spectroscopy.[118] Recently, we succeeded in detecting $e_t^-$ in pure p-$H_2$ and found that the isotope effect on $e_t^-$ yields was 10−24-fold

with increasing $D_2$ and HD concentrations (~1−8 mol%) in solid p-$H_2$. This experimental result addresses the following outstanding issues. First, the isotope effect on $e_t^-$ yields is observed for small concentrations of isotopic hydrogen molecules in irradiated solid p-$H_2$. Isotope effects on $e_t^-$ yields in condensed matter have been studied by several researchers.[116, 119, 120] Wang and Willard have reported that $e_t^-$ yields produced in fully deuterated saturated hydrocarbons like 3-methylpentane-$d_{14}$, methylcyclohexane-$d_{14}$, and 3-methylheptane-$d_{18}$ glasses irradiated using γ-rays at 77 K were around 1.5 times larger than in protiated hydrocarbons.[119] Regarding liquid phases, the survival probability of $e_t^-$ in liquid $D_2O$ has been reported to be about 1.1 times higher than in liquid $H_2O$.[120, 121] Hase and Kawabata have detected $e_t^-$ in irradiated crystalline $D_2O$ at 4 K using electron spin resonance and photo absorption spectroscopy, in particular, when $H_2O$ contents in $D_2O$ were below 3% in volume.[116] Because isotope effects on $e_t^-$ yields in fully deuterated irradiated solvents were below twofold increases in these reports, except for crystalline $D_2O$, 10−24-fold increases obtained by increasing $D_2$ and HD concentrations (~1−8 mol%) in solid p-$H_2$ were astonishingly large. In addition, significant amounts of $e_t^-$ have been yielded in irradiated solid hydrogens that are not in amorphous but crystalline phase. The detection of $e_t^-$ in solid p-$H_2$ crystals containing small amounts of isotopic hydrogen molecules is unusual. Solid hydrogen crystals must be perfect for the following reasons. Hydrogen molecules in solid hydrogen have large zero-point motions, which repair cracks, distortions, and imperfections maintaining high homogeneity of solid without annealing.[20, 54, 122-124] These occur because molecular hydrogen is light and undergoes small intermolecular interactions. In particular, p-$H_2$ molecules exclusively have a $J = 0$ rotational quantum state with no electric quadrupole moment. Therefore, solid p-$H_2$ is free from

inhomogeneous electric quadrupole−quadrupole interactions between neighboring p-$H_2$ molecules. Neither an $H_2$ nor a $D_2$ has dipole moment and an HD has a negligible dipole moment.[125-127] The present model of electron trapping cannot account for this isotope effect as the trapping depends on inhomogeneity and polarity in solids.[84, 112-114, 125-127]

Similar to the $e_t^-$ yields, the total yields of $H_6^+$ and its isotopomes $H_{6-n}D_n^+$ ($4 \geq n \geq 1$) increased with increasing ortho-$D_2$ (o-$D_2$) or HD concentrations. However, these increases have only been investigated by qualitative analysis. In Chapter 4, we performed a quantitative decay analysis for the concentrations of $H_6^+$ and $H_{6-n}D_n^+$ ($4 \geq n \geq 1$) in irradiated solid p-$H_2$ at 4.2 K and performed a kinetic analysis for isotope condensation reactions between $H_6^+$ and hydrogen isotopic molecules. In other words, $H_6^+$ were trapped by o-$D_2$ and/or HD molecules in solid p-$H_2$. Therefore, isotopic hydrogen molecules in solid p-$H_2$ play an important role in trapping $H_6^+$ and electrons. In Chapter 4 isotope effects on the yields and decays of $e_t^-$ and $H_6^+$ in solid p-$H_2$, p-$H_2$−o-$D_2$, and p-$H_2$−HD will be reported with discussion of the trapping mechanisms. We propose new trapping mechanisms of electron and cation by hydrogen isotopic molecules, which have not been accurately considered in the history of radiation chemistry.

# References


[1] T. R. Geballe and T. Oka, Science **312**, 1610 (2006).

[2] B. J. McCall, T. R. Geballe, K. H. Hinkle, and T. Oka, Science **279**, 1910 (1998).

[3] A. G. G. M. Tielens, *The physics and chemistry of the interstellar medium* (Cambridge University Press, Cambridge, 2005).

[4] T. R. Geballe and T. Oka, Nature **384**, 334 (1996).

[5] E. Herbst and Klempere.W, Astrophys. J. **185**, 505 (1973).

[6] J. J. Thomson, Philosophical Magazine **21**, 225 (1911).

[7] T. Oka, Phys. Rev. Lett. **45**, 531 (1980).

[8] T. Miyazaki, *Atom Tunneling Phenomena in Physics, Chemistry and Biology* (Springer, Berlin, 2004).

[9] T. J. Millar and D. A. Williams, *Dust and chemistry in astronomy* (Institute of Physics Pub., Bristol, 1993).

[10] H. Kaneda, T. Onaka, I. Sakon, T. Kitayama, Y. Okada, T. Suzuki, D. Ishihara, and M. Yamagishi, Astrophys. J. Lett. **716**, L161 (2010).

[11] V. Pirronello, C. Liu, L. Y. Shen, and G. Vidali, Astrophys. J. **475**, L69 (1997).

[12] P. C. Souers, *Hydrogen Properties for Fusion Energy* (University of California Press, Berkeley, 1986).

[13] P. C. Souers, D. Fearon, R. Garza, E. M. Kelly, P. E. Roberts, R. H. Sanborn, R. T. Tsugawa, J. L. Hunt, and J. D. Poll, J. Chem. Phys. **70**, 1581 (1979).

[14] P. C. Souers, E. M. Fearon, P. E. Roberts, R. T. Tsugawa, J. D. Poll, and J. L. Hunt, Phys. Lett. A **77**, 277 (1980).

[15] P. C. Souers, E. M. Fearon, R. L. Stark, and R. T. Tsugawa, Can. J. Phys. **59**, 1408 (1981).

[16] J. D. Poll, J. L. Hunt, P. C. Souers, E. M. Fearon, R. T. Tsugawa, J. H. Richardson, and G. H. Smith, Phys. Rev. A **28**, 3147 (1983).

[17] R. L. Brooks, S. K. Bose, J. L. Hunt, J. R. Macdonald, J. D. Poll, and J. C. Waddington, Phys. Rev. B **32**, 2478 (1985).

[18] R. L. Brooks, J. L. Hunt, J. R. Macdonald, J. D. Poll, and J. C. Waddington, Can. J. Phys. **63**, 937 (1985).

[19] J. J. Miller, R. L. Brooks, J. L. Hunt, and J. D. Poll, Can. J. Phys. **66**, 1025 (1988).

[20] T. Oka, Ann. Rev. Phys. Chem. **44**, 299 (1993).

[21] M. C. Chan, M. Okumura, and T. Oka, J. Phys. Chem. A **104**, 3775 (2000).

[22] T. Momose, C. M. Lindsay, Y. Zhang, and T. Oka, Phys. Rev. Lett. **86**, 4795 (2001).

[23] T. Momose, Y. Zhang, and T. Oka, Physica B **284**, 387 (2000).

[24] J. H. M. J.C. McLennan, Nature **123**, 160 (1929).

[25] I. F. Silvera, Rev. Mod. Phys. **52**, 393 (1980).

[26] T. Momose, H. Hoshina, M. Fushitani, and H. Katsuki, Vibrational Spectroscopy **34**, 95 (2004).

[27] W. H. Keeson, J. de Smedt, and H.H.Mooy, Commun. Kamerlingh Onnes Lab., Univ. Leiden **19,** 2090 (1930).

[28] T. Momose and T. Shida, Bull. Chem. Soc. Jpn. **71**, 1 (1998).

[29] M. E. Fajardo and S. Tam, J. Chem. Phys. **108**, 4237 (1998).

[30] S. Tam and M. E. Fajardo, Rev. Sci. Instrum. **70**, 1926 (1999).

[31] N. Sogoshi, Y. Kato, T. Wakabayashi, T. Momose, S. Tam, M. E. DeRose, and M. E. Fajardo, J. Phys. Chem. A **104**, 3733 (2000).

[32] M. E. Fajardo and S. Tam, J. Chem. Phys. **115**, 6807 (2001).

[33] S. Tam and M. E. Fajardo, Appl. Spectrosc. **55**, 1634 (2001).

[34] D. T. Anderson, R. J. Hinde, S. Tam, and M. E. Fajardo, J. Chem. Phys. **116**, 594 (2002).

[35] R. J. Hinde, D. T. Anderson, S. Tam, and M. E. Fajardo, Chem. Phys. Lett. **356**, 355 (2002).

[36] K. Yoshioka and D. T. Anderson, J. Chem. Phys. **119**, 4731 (2003).

[37] X. F. Wang, L. Andrews, S. Tam, M. E. DeRose, and M. E. Fajardo, J. Am. Chem. Soc. **125**, 9218 (2003).

[38] M. E. Fajardo, S. Tam, and M. E. DeRose, J. Mol. Struct. **695**, 111 (2004).

[39] Y. J. Wu, X. M. Yang, and Y. P. Lee, J. Chem. Phys. **120**, 1168 (2004).

[40] H. Hoshina, Y. Kato, Y. Morisawa, T. Wakabayashi, and T. Momose, Chem. Phys. **300**, 69 (2004).

[41] T. Kumada, M. Sakakibara, T. Nagasaka, H. Fukuta, J. Kumagai, and T. Miyazaki, J. Chem. Phys. **116**, 1109 (2002).

[42] T. Kumada, J. Kumagai, and T. Miyazaki, J. Chem. Phys. **114**, 10024 (2001).

[43] T. Kumada, S. Mori, J. Kumagai, Y. Aratono, and T. Miyazaki, J. Phys. Chem. A **103**, 8966 (1999).

[44] T. Kumada, J. Chem. Phys. **117**, 10133 (2002).

[45] T. Miyazaki, K. Yamamoto, and J. Arai, Chem. Phys. Lett. **219**, 405 (1994).

[46] T. Kumada, Y. Shimizu, T. Ushida, and J. Kumagai, Rad. Phys. Chem. **77**, 1318 (2008).

[47] T. Kumada, H. Tachikawa, and T. Takayanagi, Phys. Chem. Chem. Phys. **7**, 776 (2005).
[48] J. Kumagai, H. Inagaki, S. Kariya, T. Ushida, Y. Shimizu, and T. Kumada, J. Chem. Phys. **127** (2007).
[49] Y. Shimizu, T. Kumada, and J. Kumagai, J. Magn. Reson. **194**, 76 (2008).
[50] Y. Shimizu, M. Inagaki, T. Kumada, and J. Kumagai, J. Chem. Phys. **132** (2010).
[51] T. Kumada, T. Takayanagi, and J. Kumagai, J. Mol. Struct. **786**, 130 (2006).
[52] J. Kumagai, M. Hanabusa, H. Inagaki, and S. Kariya, Phys. Chem. Chem. Phys. **6**, 4363 (2004).
[53] T. Momose, M. Fushitani, and H. Hoshina, Int. Rev. Phys. Chem. **24**, 533 (2005).
[54] S. Tam, M. E. Fajardo, H. Katsuki, H. Hoshina, T. Wakabayashi, and T. Momose, J. Chem. Phys. **111**, 4191 (1999).
[55] T. Kumada, N. Kitagawa, T. Noda, J. Kumagai, Y. Aratono, and T. Miyazaki, Chem. Phys. Lett. **288**, 755 (1998).
[56] M. Fushitani, N. Sogoshi, T. Wakabayashi, T. Momose, and T. Shida, J. Chem. Phys. **109**, 6346 (1998).
[57] T. Momose, H. Hoshina, N. Sogoshi, H. Katsuki, T. Wakabayashi, and T. Shida, J. Chem. Phys. **108**, 7334 (1998).
[58] N. Sogoshi, T. Wakabayashi, T. Momose, and T. Shida, J. Phys. Chem. A **105**, 3077 (2001).
[59] M. Fushitani and T. Momose, Low Temp. Phys. **29**, 740 (2003).
[60] H. Hoshina, M. Fushitani, T. Momose, and T. Shida, J. Chem. Phys. **120**, 3706 (2004).
[61] S. Tam, M. Macler, and M. E. Fajardo, J. Chem. Phys. **106**, 8955 (1997).
[62] N. J. Kirchner and M. T. Bowers, J. Chem. Phys. **86**, 1301 (1987).
[63] T. Fiegele, G. Hanel, O. Echt, A. Stamatovic, P. Scheier, and T. D. Mark, J. Phys. B-Atomic Molecular and Optical Physics **37**, 4167 (2004).
[64] J. A. Montgomery and H. H. Michels, J. Chem. Phys. **87**, 771 (1987).
[65] Y. Kurosaki and T. Takayanagi, Chem. Phys. Lett. **293**, 59 (1998).
[66] Y. Kurosaki and T. Takayanagi, J. Chem. Phys. **109**, 4327 (1998).
[67] T. Miyazaki, K. Yamamoto, and Y. Aratono, Chem. Phys. Lett. **232**, 229 (1995).
[68] T. Kumada, H. Inagaki, T. Nagasawa, Y. Aratono, and T. Miyazaki, Chem. Phys. Lett. **251**, 219 (1996).
[69] M. C. R. Symons, Chem. Phys. Lett. **247**, 607 (1995).
[70] A. Carrington, I. R. McNab, and C. A. Montgomerie, J. Phys. B-Atomic Molecular and Optical Physics **22**, 3551 (1989).
[71] H. U. Suter, B. Engels, and S. Lunell, in *Advances in Quantum Chemistry, Vol 40: New Perspectives in Quantum Systems in Chemistry and Physics, Pt 2* (Academic Press Inc, San Diego, 2001), Vol. 40, p. 133.
[72] V. A. Apkarian and N. Schwentner, Chem. Rev. **99**, 1481 (1999).
[73] V. E. Bondybey, A. M. Smith, and J. Agreiter, Chem. Rev. **96**, 2113 (1996).
[74] G. Schallmoser, A. Thoma, B. E. Wurfel, and V. E. Bondybey, Chem. Phys. Lett. **219**, 101 (1994).
[75] W. H. Flygare, J. Chem. Phys. **39**, 2263 (1963).
[76] B. E. Wurfel, N. Caspary, J. Agreiter, A. Thoma, A. M. Smith, and V. E. Bondybey, J. Chim. Phys. **92**, 351 (1995).
[77] Friedman.H and S. Kimel, J. Chem. Phys. **43**, 3925 (1965).
[78] H. Hoshina, T. Wakabayashi, T. Momose, and T. Shida, J. Chem. Phys. **110**, 5728 (1999).
[79] T. Yamada, K. Komaguchi, M. Shiotani, N. P. Benetis, and A. R. Sornes, J. Phys. Chem. A **103**, 4823 (1999).
[80] K. Komaguchi, T. Kumada, T. Takayanagi, Y. Aratono, M. Shiotani, and T. Miyazaki, Chem. Phys. Lett. **300**, 257 (1999).
[81] C. P. P. Jr., *Electron Spin Resonance* (Dover, Mineola, 1983).
[82] A.Abragam, (Oxford University Press, Oxford, 1961).
[83] Z. Li and V. A. Apkarian, J. Chem. Phys. **107**, 1544 (1997).
[84] Y. Tabata, Y. Ito, and S. Tagawa, *CRC handbook of radiation chemistry* (CRC Press, Boca Raton, 1991).
[85] B. G. Ershov and A. K. Pikaev, Adv. Chem. Series, 1 (1968).
[86] B. G. Ershov, Khodzhae.Of, and A. K. Pikaev, Doklady Akademii Nauk Sssr **179**, 911 (1968).
[87] J. Zimbrick and L. Kevan, J. Chem. Phys. **47**, 2364 (1967).
[88] B. G. Ershov and A. K. Pikaev, Russ. J. Phys. Chem. **41**, 1394 (1967).
[89] L. Kevan, J. Am. Chem. Soc. **87**, 1481 (1965).
[90] M. J. Blandamer, M. C. R. Symons, and L. Shields, J. Chem. Soc., 4352 (1964).
[91] M. Ogasawara, M. Lindgren, A. Lund, and G. Nilsson, Chem. Phys. Lett. **117**, 254 (1985).
[92] T. Sasaki, Kawatsur.K, and S. Ohno, Chem. Lett., 91 (1972).
[93] L. Kevan and D. H. Chen, J. Chem. Phys. **49**, 1970 (1968).
[94] Habersbe.A, Collect. Czechoslovak Chem. Commun. **33**, 1925 (1968).
[95] A. Ekstrom and J. E. Willard, J. Phys. Chem. **72**, 4599 (1968).
[96] C. Chachaty, J. Chimi. Phys. **64**, 614 (1967).
[97] L. Shields, J. Phys. Chem. **69**, 3186 (1965).
[98] Blandame.Mj, L. Shields, and M. C. R. Symons, J. Chem. Soc., 1127 (1965).

[99] C. Chachaty and E. Hayon, J. Chimi. Phys. **61**, 1115 (1964).
[100] C. Chachaty, Comptes Rendus Hebdomadaires Des Seances De L Academie Des Sciences **259**, 2219 (1964).
[101] J. Lin, K. Tsuji, and F. Williams, J. Am. Chem. Soc. **90**, 2766 (1968).
[102] K. Tsuji, H. Yoshida, and K. Hayashi, J. Chem. Phys. **46**, 810 (1967).
[103] K. Tsuji and F. Williams, J. Am. Chem. Soc. **89**, 1526 (1967).
[104] D. R. Smith, F. Okenka, and J. J. Pieroni, Can. J. Chem. **45**, 833 (1967).
[105] A. D. Grishina, A. V. Vannikov, and N. M. Alpatova, Radiat. Phys. Chem. **11**, 289 (1978).
[106] H. Yoshida, D. Feng, and L. Kevan, J. Chem. Phys. **58**, 4924 (1973).
[107] H. Yoshida, M. Ogasawara, T. Warashina, and T. Higashimura, J. Chem. Phys. **56**, 4238 (1972).
[108] H. Yoshida, L. Kevan, and D. F. Feng, J. Am. Chem. Soc. **94**, 8922 (1972).
[109] S. Noda, K. Fueki, and Z. Kuri, Chem. Phys. Lett. **8**, 407 (1971).
[110] K. Tsuji and F. Williams, J. Phys. Chem. **73**, 4017 (1969).
[111] Cronenwe.W and M. C. R. Symons, J. Chem. Soc., 2991 (1968).
[112] A. Lund and M. Shiotani, *Radical Ionic Systems* (Kluwer Academic Publishers, Boston, 1991).
[113] L. Kevan, J. Phys. Chem. **84**, 1232 (1980).
[114] L. Kevan, J. Phys. Chem. **82**, 1144 (1978).
[115] D. C. Walker, J. Phys. Chem. **84**, 1140 (1980).
[116] H. Hase and K. Kawabata, J. Chem. Phys. **65**, 64 (1976).
[117] P. O. Samskog, L. D. Kispert, and A. Lund, J. Chem. Phys. **78**, 5790 (1983).
[118] T. Kumada, S. Mori, J. Kumagai, Y. Aratono, and T. Miyazaki, J. Phys. Chem. A **103**, 8966 (1999).
[119] H. Y. Wang and J. E. Willard, J. Chem. Phys. **69**, 2964 (1978).
[120] Y. Gauduel, S. Pommeret, A. Migus, and A. Antonetti, J. Phys. Chem. **95**, 533 (1991).
[121] R. A. Crowell and D. M. Bartels, J. Phys. Chem. **100**, 17713 (1996).
[122] T. Kumada, M. Sakakibara, T. Nagasaka, H. Fukuta, J. Kumagai, and T. Miyazaki, J. Chem. Phys. **116**, 1109 (2002).
[123] T. Kumada, J. Kumagai, and T. Miyazaki, J. Chem. Phys. **114**, 10024 (2001).
[124] T. Kumada, N. Kitagawa, T. Noda, J. Kumagai, Y. Aratono, and T. Miyazaki, Chem. Phys. Lett. **288**, 755 (1998).
[125] S. M. Blinder, J. Chem. Phys. **35**, 974 (1961).
[126] S. M. Blinder, J. Chem. Phys. **32**, 582 (1960).
[127] S. M. Blinder, J. Chem. Phys. **32**, 105 (1960).

# 2 Electron spin resonance study on $H_6^+$, $H_5D^+$, $H_4D_2^+$, and $H_2D_4^+$ in solid parahydrogen

We carried out electron spin resonance (ESR) study on hydrogen ions produced by radiolysis of solid parahydrogen. In addition to quartet ESR lines proposed to be $H_2^+$-core $H_6^+$ ($D_{2d}$) ions in solid parahydrogen, we newly observed totally more than 50 resolved lines in γ-ray irradiated solid parahydrogen – orthodeuterium and parahydrogen – deuterium hydride mixtures. We assigned these lines to be isotopomers of $H_2^+$-core $H_6^+$ ions such as $H_5D^+$, $H_4D_2^+$, and $H_2D_4^+$ throughout the comparison of their ESR parameters with theoretical results. These results provide a conclusive evidence that $H_2^+$-core $H_6^+$ ions are generated in irradiated solid hydrogen. Analysis of ESR spectrum and *ab initio* calculations predicts $D_{2d}$ symmetry of the $H_6^+$ ions, whereas a lowering symmetry ($D_{2d} \rightarrow C_{2v}$) induced by asymmetric nuclear wave function is observed in $H_5D^+$ and $H_4D_2^+$.

## 2.1 Introduction

Ionized solid hydrogen has attracted attention as mentioned in Chapter 1.[1-8] Several absorption features induced by the ionization were reported by FT-IR spectroscopy although any signal of ion itself could not be detected.[12, 13] In 1995, Miyazaki *et al.*[15] found a very narrow isotropic doublet in the ESR spectrum in γ-ray irradiated solid p-$H_2$ at 4.2 K, which was soon found to be components of quartet ESR lines with *g*-value of 2.0033, hyperfine coupling constant (HFCC) of 20.3 mT. These four ESR lines due to [$I$, $I_z$] = [1, 0], [0, 0], [1, 1], and [1, −1] features were denoted as B1 to B4, as shown in Figure 1.4.[17] Although the two ionic hydrogen species, $H_2^+$ and $H_2^-$, were considered as possibilities, the quartet lines were initially attributed to $H_2^-$ because of follows. Since [$I$, $I_z$] = [1, 1], [1, −1] species of a $H_2^+$ ion, which was found in the gas phase, showed 28.7 mT in $^1$H-hyperfine splitting,[18] the observed spectrum showed $^1$H-hyperfine splitting of 20.3 mT, which was 30% smaller than that of 28.7 mT in $H_2^+$ ion. This 30% reduction of $^1$H-hyperfine splitting of $H_2^+$ ion in solid phase is very difficult to explain. In addition, $H_2^+$ ion have never been observed in solid hydrogen because of reaction (1.1).[19, 20]

When Miyazaki *et al*. measured the ESR spectrum of doublet lines (B1 and B2), they did not use any microwave frequency counters. Only the third and fourth lines of $Mn^{2+}$ in MgO were used as the *g*-value standard in the conventional method, which is a less reliable way of measurement for obtaining a precise g-value. Kumagai *et al.*[9] succeeded in observing much highly resolved lines in highly purified solid p-$H_2$ and determined the ESR parameters, $A$ =20.441 mT and g = 2.002 120 ± 0.000 012, which consistently account for all of position and lineshape of the quartet lines. The g-value

was smaller than that of free electron as 2.002319.

During the course of refining experimental ESR parameters of the species, Suter *et al*.[14] pointed out that $H_6^+$ ions, having $H_2^+$-core type with $D_{2d}$ symmetry as Montgomery and Michels predicted, may show isotropic hyperfine coupling constant of 572 MHz (= 20.4 mT) on their DFT calculation. The value of isotropic hyperfine coupling constant was very close to that experimentally obtained. Tachikawa calculated *g*-value of $H_2^+$-core $H_6^+$ ions by B3LYP/6-311G++(3df, 3pd) level as 2.00228, which is smaller than that of free electron and was also consistent with experimental one qualitatively.[9]

Although the experimental *g*-value and isotropic hyperfine coupling constants are consistent with those of $H_2^+$-core $H_6^+$ theoretically calculated, these experimental values are not enough to confirm whether the species are $H_2^+$-core $H_6^+$ or $H_2^-$. According to the theoretical calclation of Suter et al, side-on $H_2$ of $H_2^+$-core $H_6^+$ shoul have isotropic hyperfine coupling constant of ≈ 9 mT but corresponding lines have not been observed in the ESR spectrum. Kumada *et al*. pointed out that the splitting could "disappear" if side-on $H_2$s on $H_6^+$ are allowed to rotate freely along the main axis due to $J = 0$ at 4.2 K combined with $I = 0$. The free rotation of side on $H_2$ may be allowed theoretically but was difficult to confirm whether the side-on $H_2$ exist or not from experimental result.

In order to confirm the assignment, we have performed to put small portion of $D_2$ or HD in solid p-$H_2$ to generate isotopomers of $H_6^+$.[21] The splitting of five ESR lines due to hyperfine coupling constant of side-on $D_2$ in $I = 2$ at $J = 0$ state should be observed if $H_2^+$-core $H_4D_2^+$ are produced.

In the course of my doctoral study, we have succeeded in observing sharp ESR

lines assigned to $H_5D^+$, $H_4D_2^+$, and $H_2D_4^+$ in γ-ray irradiated solid p-$H_2$ containing ortho-$D_2$ (o-$D_2$) and HD only at 1 mol%. The experimental ESR parameters almost satisfy the theoretical values of $H_{6-n}D_n^+$. The direct detections and assignment of hydrogen ions in irradiated solid hydrogen is a first time in the decades of history of radiation chemistry in solid hydrogen. In addition the experimental results revealed that distribution of unpaired electron is depend on protons or deuterons, which is not expected by theoretical calculation under Born-Oppenheimer approximation. In this Chapter, the ESR study on $H_6^+$ and its isotopomers will be discussed on the assignment scheme and spectroscopic properties.

## 2.2 Experiment

Parahydrogen (p-$H_2$) molecules were obtained and purified by immersing iron hydroxide FeO(OH) into liquid normal $H_2$ ( > 99.99999%; Taiyo Nippon Sanso Co.) for 10 h at 14 K in a cryocooler (Daikin UV204SCL). Orthodeuterium (o-$D_2$) molecules were obtained from normal $D_2$ (n-$D_2$) (99.999 %; 99.96 atom % D; Isotec Inc.) in a similar manner at 18 K. All hydrogen gases, p-$H_2$, o-$D_2$, and HD (99.6 %; 96 atom % D; Isotec Inc.) were purified through seven condensation/vaporization cycles at condensation and vaporization temperatures of 10 and 25 K, respectively. The gases were recovered at 25 K. Five p-$H_2$ samples, namely, p-$H_2$, p-$H_2$–o-$D_2$ (1 and 8 mol%), and p-$H_2$–HD (1 and 8 mol%) were prepared using different isotopic hydrogen molecule contents. All samples contained 0.1 mol% of He gas (99.9999%; Taiyo Nippon Sanso Co.) for thermal contact. The samples were sealed in quartz cells and immersed in a

quartz Dewar filled with liquid He to prepare the solids. Solid samples were irradiated with γ-rays for *ca.* 1 h to the total dose of 2.88 kGy at the $^{60}$Co γ-ray irradiation facility (Nagoya University). The irradiated samples were placed in an *X*-band ESR spectrometer (JEOL JES-RE1X) to measure the time course of ESR lines at 4.2 K. Microwave frequency and magnetic field of the spectrometer were monitored using a microwave frequency counter (Hewlett-Packard, 53150A) and an NMR field meter (Echo Electronics Co. Ltd., EFM-2000AX), respectively. Microwave powers of 1.0 mW and 0.1–1 nW were used to measure the $H_6^+$ and $e_t^-$ lines, respectively.

## 2.3 Results

Figure 2.1(a) shows the ESR spectrum of γ-ray irradiated solid p-$H_2$ at g ≈ 2. Intense doublet lines at the magnetic fields $H_0$ = 304 and 355 mT belong to Hydrogen atom radicals. The lines at 332 mT marked by " * " is due to radicals produced in the irradiated quartz sample cells and Dewar. The singlet line at 327 mT named A line results form a forbidden transition of H atom radicals. The line named B1 – B4 are the quartet lines produced to be $H_2^+$-core $H_6^+$. Yield of the ion of B1 – B4 series of lines is ~ $10^{-4}$ ppm, which is $10^4$ times smaller than that of Hydrogen atom radicals. Figure 2.1(c) is the spectrum obtained by subtracting (b) from (a), such that only B1 – B4 are present in the difference spectrum. All ESR spectra from solid p-$H_2$-o-$D_2$ and p-$H_2$-HD mixtures shown in this chapter are the difference spectra after subtraction of background.

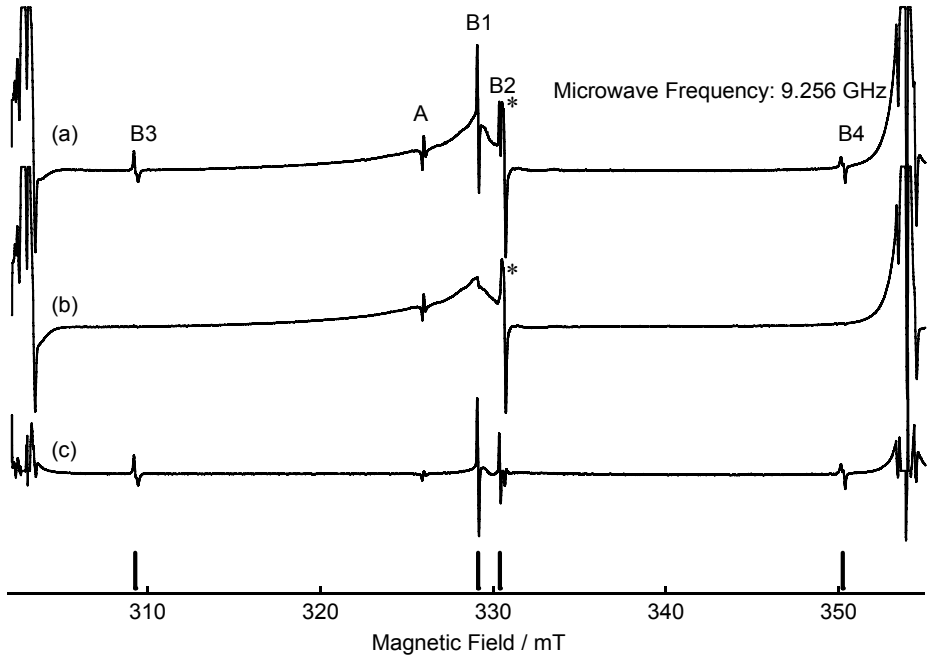


Figure 2.1. (a) ESR spectra of γ-ray irradiated solid p-$H_2$ measured at 4.2 K. (b) Same as (a) but 5 min illumination of the sample with an infrared lamp. (c) Difference spectrum generated by subtracting (b) from (a). Stic diagram shows line positions obtained by Eq. 2.7 with g = 2.0020, $I_{12}$ = 1 and 0, and $A_{ctr}$ = 20.44 mT. Note that B1 – B4 lines in spectrum are broadened due to over modulation and that intensity of B2 is saturated due to the high microwave power. The singlet line marked as A results from a forbidden transition of H atom radicals.

B1-B4 series of lines are composed of sharp doublet lines, B1 and B2, separated by 1.25 mT near g ≈ 2.002, and broad B3 and B4 lines with uniaxial asymmetry whose resonance magnetic fields are lower and higher than the center of B1 and B2 by 20.4 mT, respectively. Kumagai *et al.*[9] determined precisely the ESR parameters of B1-B4 lines, g = 2.00212, nuclear spin quantum numbers $I$ = 0 and 1, and hyperfine coupling constant A = 20.441 mT. B1, B3, and B4 are the lines corresponding to the total nuclear magnetic spin $I$ = 1 with projections $I_z$ = 0, 1, and -1, respectively, and B2 corresponds to $I = I_z = 0$. The splitting between B1 and B2 is due to the second-order hyperfine term $A^2 / H_0$.[22] As shown in a stick diagram in Figure 2.1, resonance magnetic fields of B1-B4 lines coincide with those determined by these ESR parameters. Microwave power-saturation behavior among $I$ = 1 species B1, B3, and B4 were the same, whereas

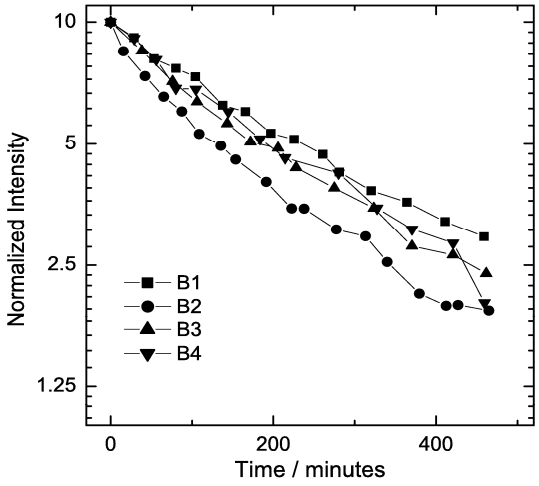


Figure 2.2. Tim-course of intensity of B1-B4 lines in γ-ray irradiated solid p-$H_2$ at 4.2 K. Intensities at t = 0 are normalized to 10.

$I = 0$ species B2 saturates with smaller microwave power probably due to the absence of relaxation path via hyperfine interaction. Although B3 and B4 lines are much broader and then look waker than B1 and B2, integrated intensities among B1-B4 lines are the same within experimental accuracy.[11] As shown in Figure 2.2, all B1-B4 lines decay in a similar manner. These results indicate that the quartet lines are a set of lines assigned to one chemical species.

Figure 2.3 shows an ESR spectrum of irradiated solid p-$H_2$-o-$D_2$ (1 mol%). Except for B1-B4 lines, three series of lines named C1-C16 were observed at around 310 mT (C1-C5), 330 mT (C6-C12), and 350 mT (C13-C16). At lower magnetic field, the quintet lines C1-C5 equally separated by 1.44 mT from the center, which is very close to position of B3 line, have ratio in intensity of roughly 1:1:2:1:1. At higher magnetic field, only four equally separated by 1.44 mT lines C13-C16 are detected. Since the ratio in intensity is 1:1:2:1 and C15 is very close toB4, C13-C16 are ecpected to be parts of quintet lines. The fifth line could not be measured due to overlapping with an intense line of hydrogen atom radicals. Figure 2.4(a) shows the enlarged portion of

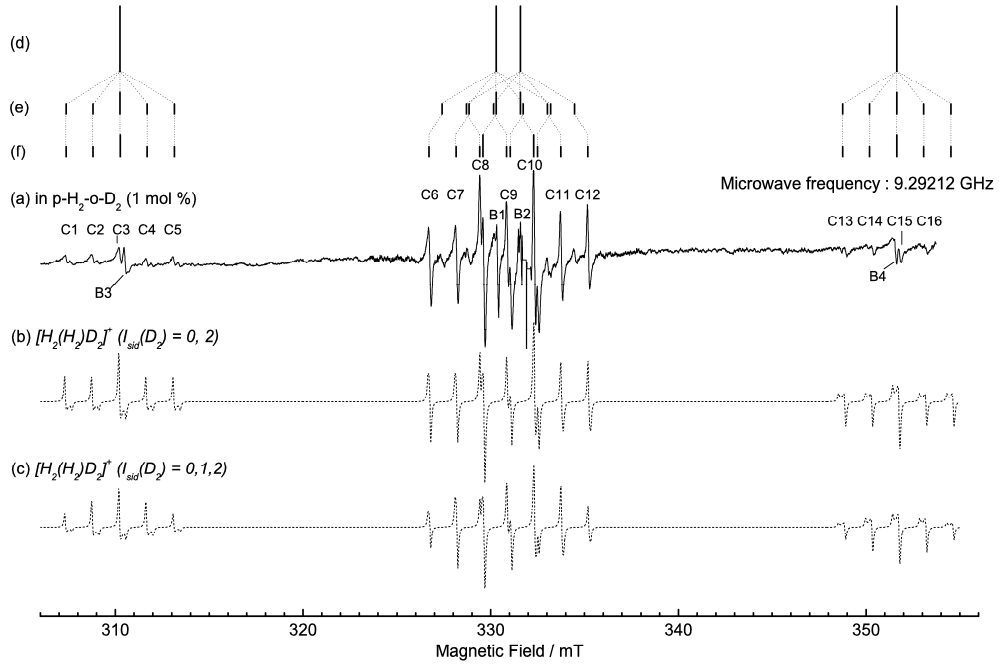


Figure 2.3. (a) An ESR spectrum of γ-ray irradiated solid p-$H_2$-o-$D_2$ (1 mol%) at 4.2 K. (b) A simulated spectrum of $H_2^+$-core $H_4D_2^+$with

the same spectrum at around 330 mT. Each of the C8, C9, and C10 lines appear as a doublet and more intense than C6, C7, C11, and C12, suggesting that each of C8–C10 is composed of two superimposed lines. Although it is less clear due to the overlap in C8–C10, an asymmetry of ESR line shape is observed in C6, C7, C10, and C11: the lower (upper) peak is higher than the upper (lower) one in C6 and C7 (C10 and C11) by ~50%. Since the sign of asymmetry has bilateral symmetry against the field of g=2.0020 ($H_0 \approx 332$ mT), it should be due to the asymmetry in hyperfine coupling constants. Figure 2.5 compares the decay behaviors of B1, B2, and C6–C12 lines in solid p-$H_2$–$D_2$ (1 mol%), whereas B3, B4, C1–C5, and C13–C16 are too weak to measure the decay. C6–C12 lines decay in a similar manner but slower than B1 and B2 lines. This result indicates that the C lines are the set of lines assigned to one chemical species other than that of B lines.

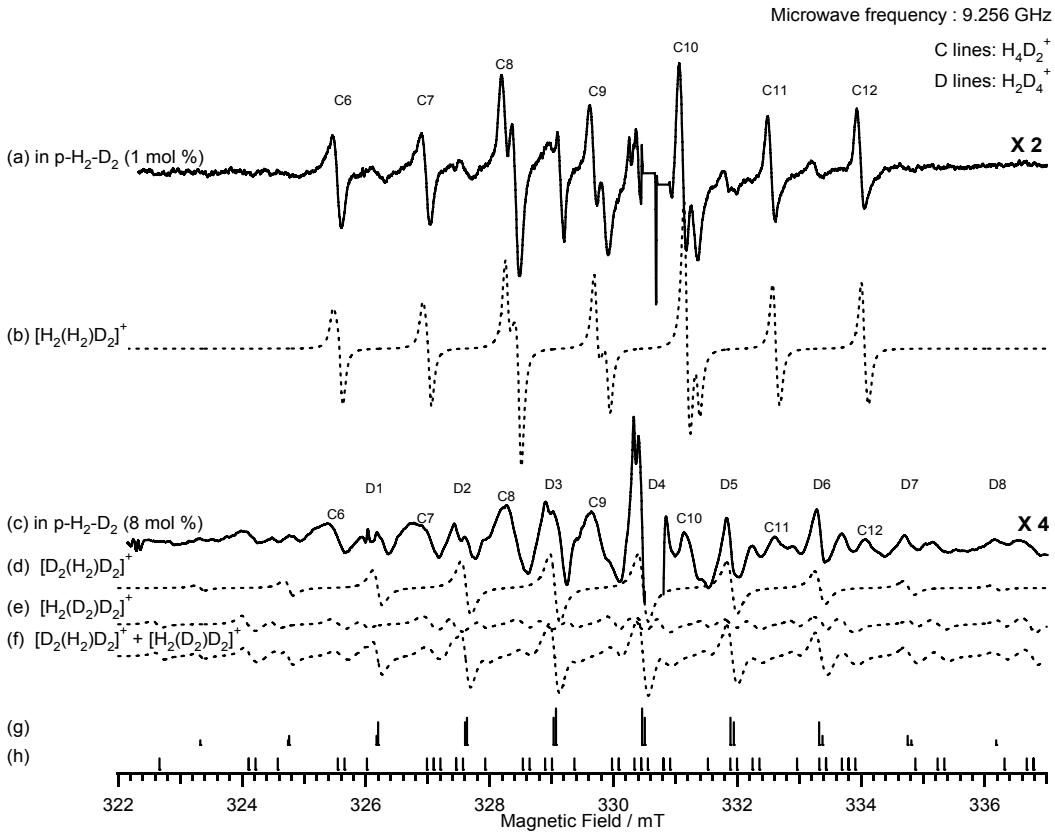


Figure 2.4. (a) An ESR spectrum of γ-ray irradiated solid p-$H_2$–o-$D_2$ (1 mol%) at 4.2 K. (b) A simulated spectrum of $H_2^+$-core $H_4D_2^+$ with $\Delta H_{FWHM}$ = 0.12 mT. (c) An ESR spectrum of irradiated p-$H_2$–o-$H_2$ (8 mol%) at 4.2 K. (d) A simulated spectrum of $H_2^+$-core $H_2D_4^+$ for $[I_{ctr}(H_2), I_{ctrz}(H_2)]$ =[1,0] and [0, 0] with $\Delta H_{FWHM}$ = 0.24 mT. Microwave frequency in (c) is normalized to 9.256 000 GHz. Stick diagram shows line positions of $H_2^+$-core $H_2D_4^+$ for $[I_{ctr}(H_2), I_{ctrz}(H_2)]$ =[1,0] and [0, 0].

Figures 2.4(a) and 2.4(c) show ESR spectra in irradiated solid p-$H_2$–o-$D_2$ (1 and 8 mol%) mixtures. A set of lines that becomes pronounced in Figure 2.4(c) is marked as D1–D8. Although some of them such as D1, D2, D5, and D6 are also observed in (a), the ratio in intensity of D to C lines in (c) is much higher than that in (a). No line is detected below 324 and above 340 mT in solid p-$H_2$–o-$D_2$ (8 mol%) except for very small C lines and intense hydrogen atom lines (not shown). Figure 2.6 compares the decay of C and D lines in solid p-$H_2$–$D_2$ (8 mol%). D lines decay slower than C. These results indicate that C and D series of lines belong to two distinct species.

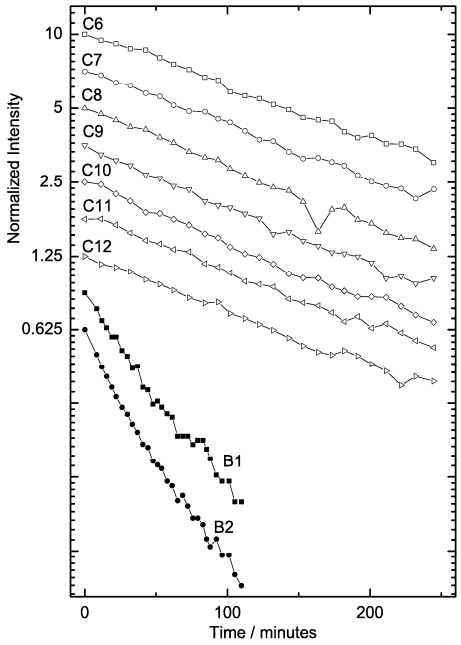


Figure 2.5. Time course of intensity of B and C lines in γ-ray irradiated solid p-$H_2$–o-$D_2$ (1 mol %) at 4.2 K. Intensities of all lines are normalized at $t$ = 0. The vertical scale is the same for all signals but offset to facilitate comparison of the decay.

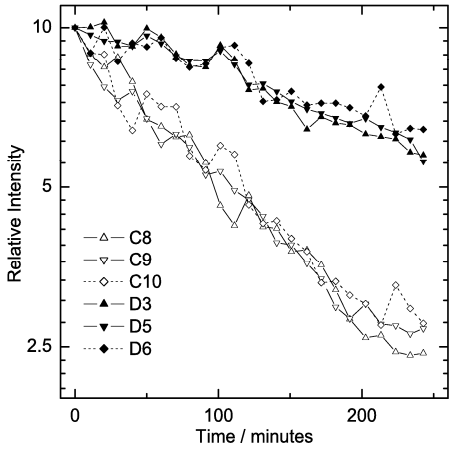


Figure 2.6. Time-course of intensity of C and D lines in γ-ray irradiated solid p-$H_2$–o-$D_2$ (8 mol%) at 4.2 K. Intensities of all lines at $t$=0 are normalized to 10.

Figure 2.7 shows an ESR spectrum of irradiated solid p-$H_2$–HD (1 mol%). Except for B lines, about 30 sharp lines named E and F were observed, whereas C and D lines were negligible. Figures 2.8(a) and 9(c) compare spectra in irradiated solid p-$H_2$–HD (1 and 8 mol%). The ratio in intensity of F to E lines in p-$H_2$–HD (8 mol %)

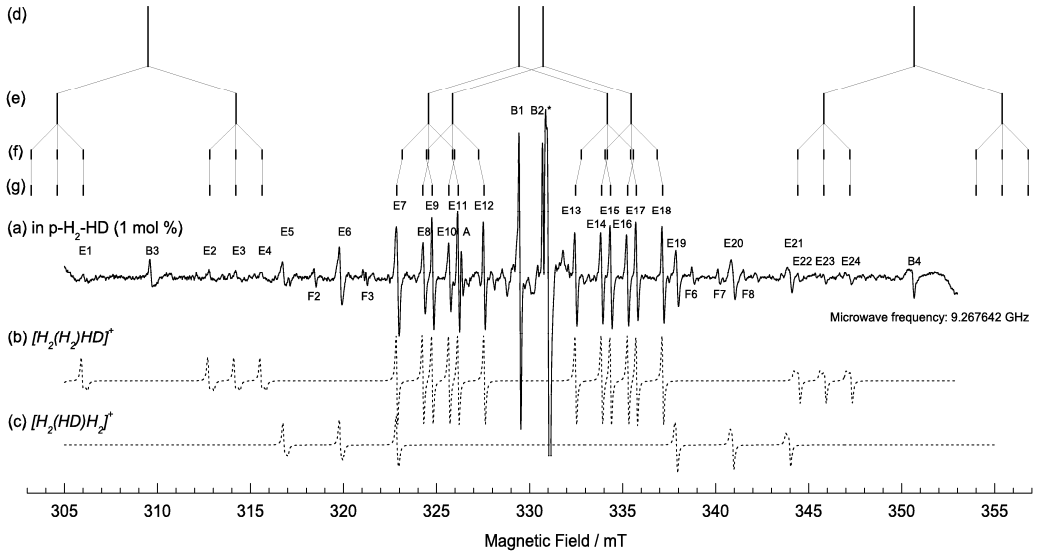


Figure 2.7. (a) An ESR spectrum of γ-ray irradiated solid p-$H_2$–HD (1 mol%) at 4.2 K. (b) and (c) Spectra of $H_2^+$-core $H_5D^+$ and $HD^+$-core $H_5D^+$ simulated with $\Delta H_{FWHM} = 0.15$ mT. Stick diagram shows line positions of $H_2^+$-core $H_5D^+$. The spectrum below 305 mT and above 354 mT could not be measured because of the overlapping of very intense signal of hydrogen atom radicals.

is larger than that in p-$H_2$–HD (1 mol %), suggesting that F lines should be assigned to the species which contains larger number of HD than those for E. Figure 2.9 shows the decay behavior of B and E lines in solid p-$H_2$–HD (1 mol%). All of E lines decay in a similar manner but slower than B lines, indicating that E lines should be assigned to one chemical species with a chemical composition different from that of B. F lines were so small that their decay cannot be measured.

Except for A–F lines, ESR signals of electron bubbles were observed at $g$=2.0023 in irradiated solid p-$H_2$–$D_2$ and p-$H_2$–HD mixtures.[23] The electron bubbles and/or H− ions produced by electron attachment to isolated hydrogen atom radicals, $H + e^- \rightarrow H^-$, should be the dominant negative ionic product in irradiated solid p-$H_2$. Study of electron bubbles is needed to understand the formation and decay dynamics of $H_6^+$ ions in irradiated solid p-$H_2$ and its mixtures. However, it is difficult to measure B–F lines and a signal of bubbles simultaneously, because the ESR parameters to measure

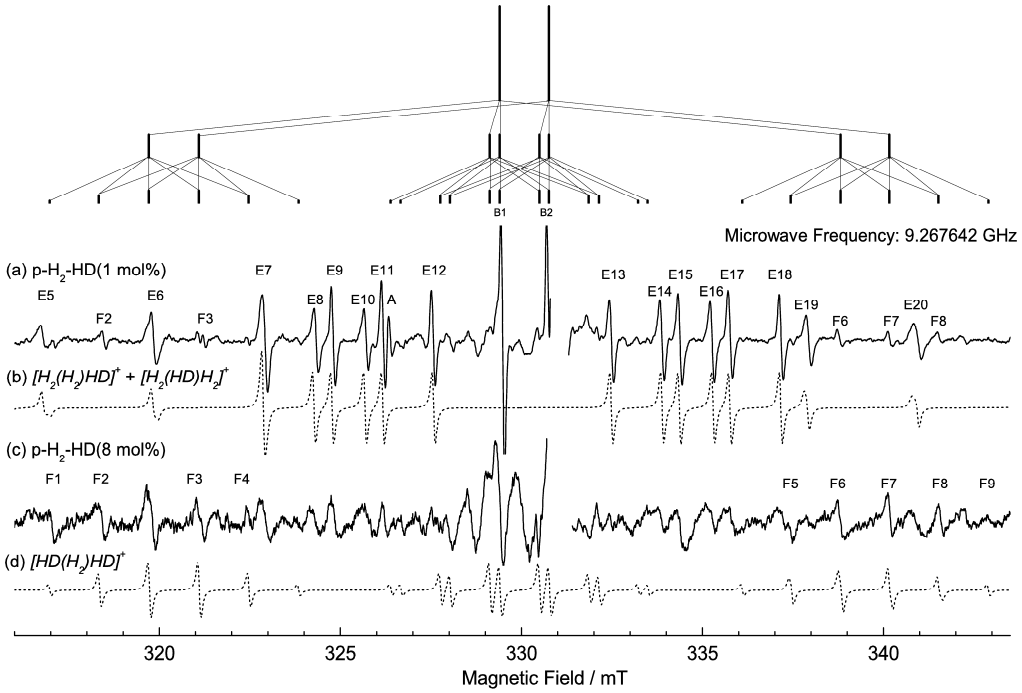


Figure 2.8. (a) An ESR spectrum of γ-ray irradiated solid p-H2–o-HD (1 mol%) at 4.2 K. (b) A simulated spectrum of $H_2^+$-core $H_5D^+$ and $HD^+$-core $H_5D^+$ with $\Delta H_{FWHM}$ = 0.15 mT. (c) An ESR spectrum of irradiated p-H2–o-H2 (8 mol%) at 4.2 K. (d) A simulated spectrum of $H_2^+$-core $H_4D^+$ (HD-sub.) for [$I_{ctr}(H_2)$ , $I_{ctrz}(H_2)$] =[1,0] and [0, 0] and [0, 0] and $\Delta H_{FWHM}$ = 0.15 mT. Microwave frequency in (c) is normalized to 9.267642 GHz. Stick diagram shows line positions of $H_2^+$-core $H_4D^+$ (HD-sub.) for [$I_{ctr}(H_2)$ , $I_{ctrz}(H_2)$]=[1, 0] and [0, 0].

electron bubbles are different from those for B–F lines. In this chapter, we mainly focus on the spectroscopic analysis of B–F lines.

## 2.4 Assignment

### 2.4.1 B lines to $H_6^+$

In this section, the ESR spectra of $H_6^+$ and its isotopomers will be simulated and compared with the experimental results. We shall follow the assignment scheme of B lines to $H_6^+$ radical validated in Ref. 11, and then apply the scheme to C–F lines and

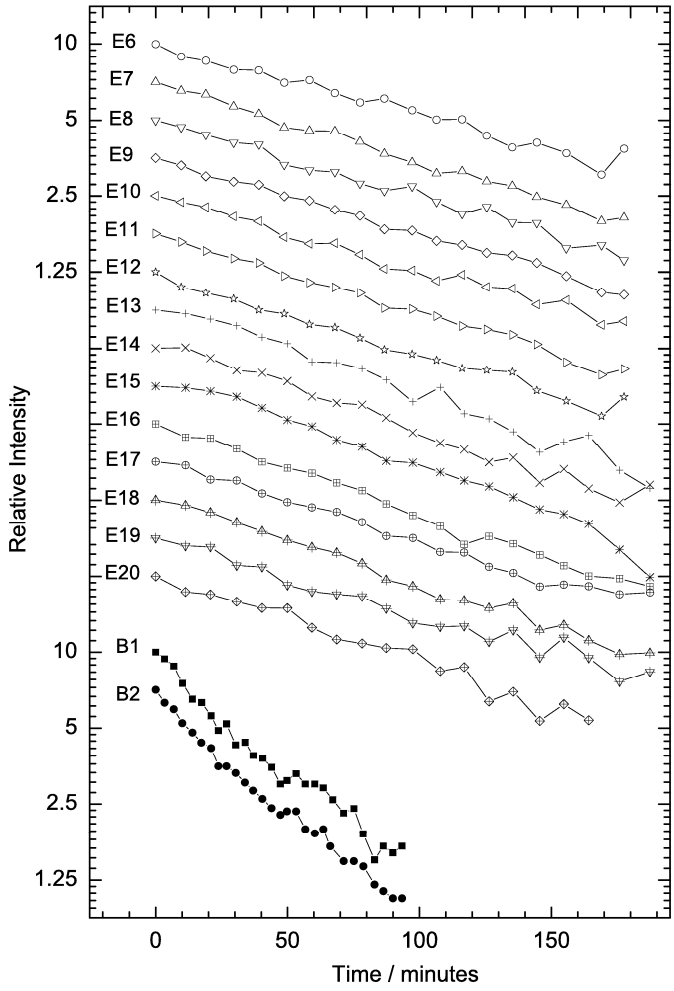


Figure 2.9. Time course of intensity of B and E lines in γ-ray irradiated solid p-$H_2$–HD (1 mol%) at 4.2 K. Intensities of all lines are normalized at $t = 0$. The vertical scale is the same for all signals but offset to facilitate comparison of the decay.

isotope substituents of $H_6^+$. Hereafter, isotopomers of $H_6^+$ are rewritten such as $[H_2(HD)H_2]^+$, where HD in the parentheses is the $HD^+$ core, and $H_2$'s in both ends correspond to side-on $H_2$'s.

Figure 2.10 shows energy levels for $H_6^+$. Spin Hamiltonian is given by

$$\mathrm{H} = g\mu_B S H_0 + \sum_i (-g_{ni}\mu_N I_i H_0 + g\mu_B A_i I_i S)\,, \qquad (2.1)$$

where $\mu_B$ and $\mu_N$ are Bohr and nuclear magnetons, $S = 1/2$ is the electron spin quantum number, $H_0 \,//\, z$ is the magnetic field, $g_{ni}$, $I_i$, and $A_i$ are the $g$ value, the spin

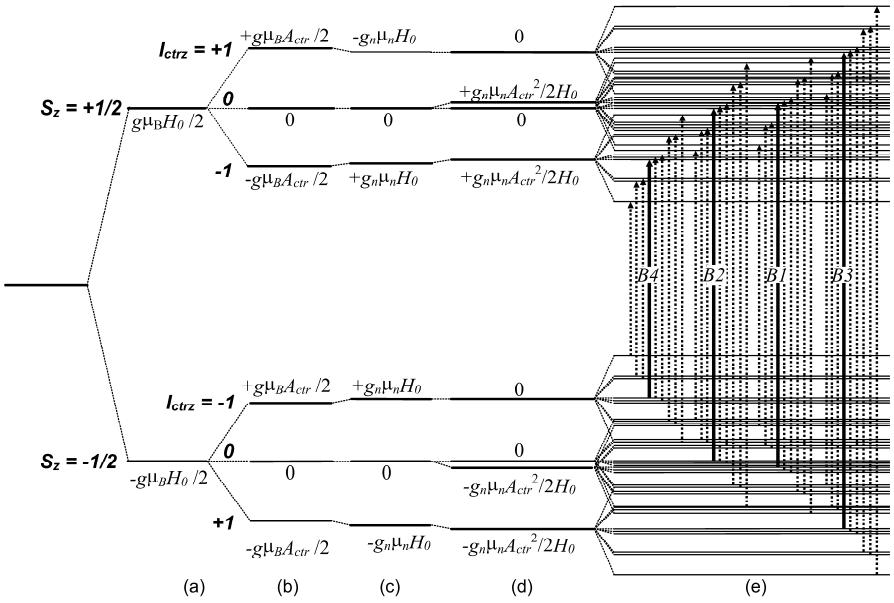


Figure 2.10. Spin energy levels of $[H_2(H_2)H_2]^+$ in magnetic field $H_0$: (a) Zeeman energy of unpaired electron; (b) First-order hyperfine interaction with $H_2^+$-core nuclei; (c) Nuclear Zeeman energy in $H_2^+$ core; (d) Second-order hyperfine interaction with $H_2^+$-core nuclei; (e) Sum of first- and second-order hyperfine interaction and nuclear Zeeman energies in two side-on $H_2$. Arrows show allowed ESR transition from [$S_z$ = - 1/2, $I_{12}$, $I_{12z}$, $I_{34}$, $I_{34z}$, $I_{56}$, $I_{56z}$] to [$S_z$ = +1/2, $I_{12}$, $I_{12z}$, $I_{34}$, $I_{34z}$, $I_{56}$, $I_{56z}$]. Solid arrows show the transitions between [±1/2, 1, 0, 0, 0, 0, 0] states for B1, [±1/2, 0, 0, 0, 0, 0, 0] for B2, [±1/2, 1, 1, 0, 0, 0, 0] for B3, and [±1/2, 1, - 1, 0, 0, 0, 0] for B4.

quantum number, and the hyperfine coupling constant of $i$th nucleus of $H_6^+$ in Figure 1.3(b), respectively. Because of $A_i << H_0$ in our experimental condition, the hyperfine terms can be referred as perturbation against the Zeeman term. Because of $D_{2d}$ symmetry with $A_{\mathrm{ctr}}(\mathrm{H}) = A_1 = A_2$ and $A_{\mathrm{sid}}(\mathrm{H}) = A_3 = A_4 = A_5 = A_6$, $I_{12} = I_1 + I_2$ and $I_{34} + I_{56} = I_3 + I_4 + I_5 + I_6$ should be the good quantum numbers for $H_6^+$. Energy levels $E_{\mathrm{tot}}$ are given by the summation of the Zeeman term $E_{\mathrm{Zee}}$, and hyperfine coupling terms for $H_2^+$ core $E_{\mathrm{ctr}}$, and side-on $H_2$, $E_{\mathrm{sid}}$,

$$E_{tot} = E_{Zee} + E_{ctr} + E_{sid}, \tag{2.2}$$

with

$$E_{Zee} = \mathrm{g}\,\mu_B S_z H_0 - \mathrm{g_n}\,\mu_N (I_{12z} + I_{3456z}) H_0, \tag{2.3}$$

$$E_{ctr} = g\mu_B A_{ctr}(H) I_{12z} S_z + \frac{g\mu_B A_{ctr}(H)^2}{4H_0} \begin{Bmatrix} \left(\frac{1}{2}+S_z\right)\left(\frac{3}{2}-S_z\right)(I_{12}-I_{12z})(I_{12}+I_{12z}+1) \\ -\left(\frac{1}{2}-S_z\right)\left(\frac{3}{2}+S_z\right)(I_{12}+I_{12z})(I_{12}-I_{12z}+1) \end{Bmatrix}, \quad (2.4)$$

and

$$E_{sid} = g\mu_B A_{sid}(H) I_{3456z} S_z + \frac{g\mu_B A_{sid}(H)^2}{4H_0} \begin{Bmatrix} \left(\frac{1}{2}+S_z\right)\left(\frac{3}{2}-S_z\right)(I_{3456}-I_{3456z})(I_{3456}+I_{3456z}+1) \\ -\left(\frac{1}{2}-S_z\right)\left(\frac{3}{2}+S_z\right)(I_{3456}+I_{3456z})(I_{3456}-I_{3456z}+1) \end{Bmatrix}. \quad (2.5)$$

$S = 1 / 2$ has already been substituted in Eqs. 2.4 and 2.5. The second term in Eqs. 2.4 and 2.5 are deduced from the second-order perturbation theory. Figure 2.10 shows 72 spin energy levels for $H_6^+$ obtained from Eqs. 2.2-2.5. Since ESR absorption takes place between energy levels with the same $I_i$ and $I_{iz}$, then the resonance conditions are given by

$$\frac{h\nu}{g\mu_B} = H_0 + A_{ctr}(H) I_{12z} + \frac{A_{ctr}(H)^2 \left\{ I_{12}(I_{12}+1) - {I_{12z}}^2 \right\}}{2H_0} + A_{sid}(H)(I_{34z}+I_{56z}) + \frac{A_{sid}(H)^2 \left\{ (I_{34}+I_{56})(I_{34}+I_{56}+1) - (I_{34z}+I_{56z})^2 \right\}}{2H_0}, \quad (2.6)$$

where $h$ is the Plank constant and $v$ is the microwave frequency. As shown by solid and dotted arrows in Figure 2.10, 36 ESR lines are expected from Eq. 2.6. However, only quartet lines shown by solid arrows should be observed at around 4 K.[11] Since the rotational constant for $H_2$ (~8 meV) is much larger than the rotational barrier for side-on $H_2$ along the main axis of $H_6^+$ calculated (1.4 meV) and thermal energy at 4.2 K (0.4 meV), almost all side-on $H_2$, which rotate nearly freely, should be at $J_{sid}(H_2) = 0$

Table 2.1. HFCC in mT of $H_2^+$-core $H_6^+$ calculated.

| | Level of Calculation | $A_{ctr}$(H) | | $A_{sid}$(H) | |
|---|---|---|---|---|---|
| | | *Iso.* | *Ani.* | *Iso.* | *Ani.* |
| Kurosaki and Takayanagi[10] | MP2/cc-pVTZ | 19.690 | | 8.745 | |
| Suter *et al.*[14] | MR-CISD | 20.397 | | | |
| Kumada *et al.*[11] | B3LYP/6-311++G(3df,3pd) | 20.079 | 1.17 | 10.263 | 0.51 |
| Shimizu *et al.*[16] | MP2/cc-pVQZ | 20.231 | 1.25 | 9.007 | 0.46 |

rotational state. Like a p-$H_2$ molecule, $H_6^+$ at $J_{sid}(H_2) = 0$ is exclusively at $I_{sid}(H_2) = I_{34} = I_{56} = 0$ state due to the parity conservation rule on exchanging fermion species of proton.[24, 25] In this case, the resonance condition reads

$$\frac{h\nu}{g\mu_B} = H_0 + A_{ctr}(H)I_{12z} + \frac{A_{ctr}(H)^2\left\{I_{12}(I_{12}+1) - I_{12z}{}^2\right\}}{2H_0}. \qquad (2.7)$$

Stick diagram in Figure 2.1 shows line positions obtained from Eq. 2.7 with $g$ = 2.00212, $I_{12}$ = 0 and 1, $I_{34} = I_{56} = 0$, and $A_{ctr}$(H) = 20.44 mT, which reproduce resonance fields of B1–B4 lines within an error of 0.01 mT. Table 2.1 lists $A_{ctr}$(H) and $A_{sid}$(H) of $H_6^+$ calculated.[11, 14] The $A_{ctr}$(H) value obtained experimentally is very close to that calculated. In this way, B1–B4 lines are assigned to $H_6^+$. The spectrum of $H_6^+$ has a characteristic shape of an ESR spectrum with uniaxial anisotropy of hyperfine interactions. It is obvious from Figure 2.1 that the anisotropic HFCC $A_{ctr}^{ani} = -0.06$ mT for $H_6^+$ defined as

$$\begin{aligned} A_{ctr} &= A_{ctr}^{iso} + A_{ctr}^{ani}(\Theta) \\ &= A_{ctr}^{iso} + A_{ctr}^{ani}(3\cos^2\Theta - 1) \end{aligned} \qquad (2.8)$$

(Θ: the angle between main axis of radicals and vector of magnetic field) is much smaller than the isotoropic Fermi contact term $A_{ctr}^{iso}$. In contrast to good agreement between experiments and theory for $A_{ctr}^{iso}$, $A_{ctr}^{ani}$ determined experimentally is −1/20 of that calculated. This result indicates that $H_6^+$ is in precession motion with the angle of Θ

≈ 60° in solid p-$H_2$.[11, 16] Hereafter, the superscript "iso" in $A_{ctr}^{iso}$ is abbreviated otherwise mentioned.

The same integrated intensities among B1($I_{12}$, $I_{12z}$ = 1, 0), B2($I_{12}$, $I_{12z}$ = 0, 0), B3($I_{12}$, $I_{12z}$ = 1, 1), and B4($I_{12}$, $I_{12z}$ = 1, −1)[9, 11] shows the para/ortho ratio for $H_2^+$-core of $H_6^+$ is 1/3 although the concentration of o-$H_2$ in p-$H_2$ sample is below 0.2%. We predict that the para-ortho conversion could proceed by the effects of unpaired electron of $H_6^+$ so that the para/ortho ratio of $H_2^+$-core obey the Boltzmann distribution as

$$\frac{para}{ortho} = \frac{\sum_{even}(2J+1)\exp\{-BJ(J+1)/T\}}{\sum_{odd}3(2J+1)\exp\{-BJ(J+1)/T\}}, \quad (2.9)$$

where $J$ and $B$ are the rotational quantum number and the rotational constants, respectively. The rotational constant of $H_6^+$ around vertical axis against main axis was calculated to be 1.97 K at MP2/cc-pVQZ level, which is lower than experimental temperature of 4.2 K. The para/ortho ratio of $H_2^+$-core by using Eq. 2.9 with the constants is calculated to 1/2.8 at 4.2 K, that is almost the same with the experimental ratio of 1/3.

### 2.4.2 C lines to $H_4D_2^+$

Since C lines are observed only in solid p-$H_2$–o-$D_2$ mixtures, they should be assigned to the species containing $D_2$ such as $[H_2(H_2)D_2]^+$. When protons of $H_6^+$ at positions 5 and 6 in Figure 1.3(b) are replaced by deuterons to obtain $[H_2(H_2)D_2]^+$, the resonance condition is expected to be

$$\frac{h\nu}{g\mu_B} = H_0 + A_{ctr}(H)I_{12z} + \frac{A_{ctr}(H)^2\left\{I_{12}(I_{12}+1) - {I_{12z}}^2\right\}}{2H_0} + A_{sid}(D)I_{56z} \tag{2.10}$$

based on the assumption of free rotation of side-on $H_2$ and $D_2$. The last term corresponds to the hyperfine interaction with side-on $D_2$. The second-order perturbation term for $A_{\mathrm{sid}}(\mathrm{D})$ ($\approx A_{\mathrm{sid}}(\mathrm{D})^2 / H_0$) is neglected because its magnitude ($\approx 0.01$ mT) is much smaller than the ESR linewidth ($\approx 0.1$ mT). Unlike $H_2$, $D_2$ in $J_{\mathrm{sid}}(\mathrm{D}_2) = 0$ is coupled to both $I_{\mathrm{sid}}(\mathrm{D}_2) = 0$ and 2; each of B1–B4 lines of $H_6^+$ should split into quintet lines corresponding to side-on $D_2$ at $I_{\mathrm{sid}z} = 2$, 1, 0, −1, and −2 with the ratio in intensity of 1:1:2:1:1. The doubled intensity at the center is due to the overlap of lines of [$I_{\mathrm{sid}}(\mathrm{D}_2)$, $I_{\mathrm{sid}z}(\mathrm{D}_2)$] = [2, 0] and [0, 0] states.

The stick diagram in Figure 2.3 (e) shows the resonance magnetic fields of $[\mathrm{H}_2(\mathrm{H}_2)\mathrm{D}_2]^+$ obtained by substituting ESR parameters $g = 2.0020$, $A_{\mathrm{ctr}}(\mathrm{H}) = 20.63$ mT, and $A_{\mathrm{sid}}(\mathrm{D}) = 1.44$ mT to Eq. 2.10. Resonance fields of C1–C5 and C13–C16 lines are reproduced, but C6–C12 lines are not. We suggest that the mismatch in C6–C12 is due to the lowering of $D_{2d}$ symmetry of the electronic wave function, such that $\Delta A(\mathrm{H}) = [A_1(\mathrm{H}) - A_2(\mathrm{H})] / 2 \neq 0$. In this case, the resonance condition is calculated using Eq. A17 in the appendix,

$$\frac{h\nu}{g\mu_B} = H_0 + A_{ctr}(H)\left(I_{1z} + I_{2z}\right) + \frac{A_{ctr}(H)^2}{2H_0} + \left(I_{1z} - I_{2z}\right)\sqrt{\Delta A(H)^2 + \left(\frac{A_{ctr}(H)^2}{2H_0}\right)^2} + A_{sid}(D)I_{56z}. \tag{2.11}$$

Eq. 2.10 coincides with Eq. 2.11 at the $\Delta A(\mathrm{H}) \rightarrow 0$ asymptotic limit. Stick diagram in Figure 2.3(f) shows resonance fields obtained by Eq. 2.11 with $g = 2.0020$,

Table 2.2. HFCC of $H_6^+$ and its isotope substituents in mT determined by the analysis of B-F lines. Italic values show HFCC for D atoms. Values in parentheses HFCC values for D atoms multiplied by $\gamma_p / \gamma_d = 6.514$. Anisotropy in $A_5$ and $A_6$ are too small to be determined experimentally.

| Lines | Species | g-value | $A_1$ | | $A_2$ | | $A_5$ | $A_6$ | Remarks |
|---|---|---|---|---|---|---|---|---|---|
| | | | *Iso.* | *Ani.* | *Iso.* | *Ani.* | | | |
| B | $[H_2(H_2)H_2]^+$ [9] | 2.00212 | 20.440 | -0.061 | 20.440 | 0.184 | | | |
| B | $[H_2(H_2)H_2]^+$ [11] | 2.002 0[a] | 20.42 | -0.06 | 20.42 | -0.06 | | | |
| C | $[H_2(H_2)D_2]^+$ | 2.002 0[a] | 21.83 | -0.08 | 19.43 | -0.16 | 1.44<br>(9.38) | 1.44<br>(9.38) | |
| D | $[D_2(H_2)D_2]^+$ | 2.002 0[a] | 21 | | 21 | | 1.44<br>(9.38) | 1.44<br>(9.38) | $A_3 = A_4$<br>$= A_5 = A_6$ |
| D | $[H_2(D_2)D_2]^+$ | 2.002 0[a] | 3.35<br>(21.8) | | 2.98<br>(19.4) | | 1.44<br>(9.38) | 1.44<br>(9.38) | |
| E | $[H_2(H_2)HD]^+$ | 2.002 0[a] | 21.24 | -0.10 | 19.86 | -0.40 | 9.58 | 1.40<br>(9.12) | |
| E | $[H_2(HD)H_2]^+$ | 2.002 0[a] | 21.02 | -0.12 | 3.02<br>(19.7) | -0.02<br>(-0.12) | | | |
| F | $[HD(H_2)HD]^+$ | 2.002 0[a] | 21 | | 21 | | 9.52 | 1.37<br>(8.92) | $A_3 = A_5$,<br>$A_4 = A_6$ |

[a] Accuracy of ± 0.0002.

$A_1(H) = A_{ctr}(H) + \Delta A(H) = 21.83$ mT, $A_2(H) = A_{ctr}(H) - \Delta A(H) = 19.43$ mT, and $A_{sid}(D) = A_{56}(D) = 1.44$ mT. Only three HFCCs and one $g$ value reproduce positions of all 16 C lines within an error of 0.03 mT, which is smaller than the linewidth of C lines (~0.1 mT). Not only $A_{ctr}(H)$ itself but also $A_{sid}(D)$ multiplied by the ratio in magnetomechanical ratio of proton to deuteron, $(\gamma_d / \gamma_p) A_{sid}(D)$, is very close to that of $H_6^+$ calculated.

The dotted lines in Figures 2.3(b) and 2.4(b) show spectra of $[H_2(H_2)D_2]^+$ fitted to C lines using a Lorentzian line shape function with full width at half maximum $\Delta H_{FWHM} = 0.12$ mT, and uniaxial anisotropy $A_1^{ani} = -0.08$ mT and $A_2^{ani} = -0.16$ mT. Not only line positions but also the line shapes of C lines are reproduced. That allows the unique assignment of the C lines to $[H_2(H_2)D_2]^+$.

The C lines in Figure 2.3(a) also show an evidence of free rotation of side-on $H_2$ in $H_6^+$. Figure 2.3(b) presents the simulated spectrum of $[H_2(H_2)D_2]^+$ where side-on $D_2$ rotates freely. Figure 2.3(c) also presents $[H_2(H_2)D_2]^+$, but rotation of side-on $D_2$ is strongly hindered. In the latter case, side-on $D_2$ should be populated in $I_{sid}(D_2) = 0$, 1, and 2 states in proportional to their spin degeneracy, $2I_{sid} + 1 = 1:3:5$, respectively, to split each of B1–B4 lines of $H_6^+$ to quintet lines with ratio in intensity of 1:2:3:2:1. C lines in the experimental data are found to be reproduced by Figure 2.3(b) rather than Figure 2.3(c), indicating the free rotation of side-on $D_2$. In a similar manner, side-on $H_2$ in $H_6^+$ and its isotopomer should freely rotate in solid hydrogen at 4 K.

Like B3 and B4 to B1 and B2 in the $H_6^+$ lines, ratio in peak height of C1–C5 and C13–C16 to C6–C12 lines in the experimental data is less than that in the simulated spectra, which could be due to the line broadening caused by inhomogeneity of cages. Small difference in the cages leads to small change in the precession motion and electronic wave function of $H_6^+$ and its isotopomers, causing distribution of HFCCs. The following arguments support the conclusion. First, as expected for $H_6^+$, the integrated intensity of B1–B4 lines in solid p-$H_2$ was found to be the same within errors, although it is difficult to measure the integrated intensity of C1–C5 and C13–C16 lines due to poor signal-to-noise ratio.[11] Second, linewidths for $H_6^+$ and its isotopomers at $I_{12z} \neq 0$ states such as B3, B4, C1–C5, and C13–C16 are much more sensitive to the inhomogeneity in $A_{ctr}$ than those at $I_{12z} = 0$ such as B1, B2, and C6–C12. Third, the $I_{12z} \neq 0$ lines are broadened by $A_{ctr}^{ani}$, which is very sensitive to the precession angle determined by the geometry of cages. The broadening of lines for $I_{12z} \neq 0$ states is common for all isotopomers of $H_6^+$ measured in this study.

### 2.4.3 D lines to $[D_2(H_2)D_2]^+$ and $[H_2(D_2)D_2]^+$

Since the ratio in intensity of D to C lines in solid p-$H_2$–$D_2$ (8 mol%) is higher than that in p-$H_2$–o-$D_2$ (1 mol%), D lines should be assigned to the species which contain larger number of $D_2$ than $[H_2(H_2)D_2]^+$. We simulated the ESR spectrum of $[D_2(H_2)D_2]^+$ and $[H_2(D_2)D_2]^+$ to compare it with the D lines. The resonance condition for $[D_2(H_2)D_2]^+$ is given by

$$\frac{h\nu}{g\mu_B} = H_0 + A_{ctr}(H)I_{12z} + \frac{A_{ctr}(H)^2\left\{I_{12}(I_{12}+1) - {I_{12z}}^2\right\}}{2H_0} + A_{sid}(D)(I_{34z} + I_{56z}), \tag{2.12}$$

with $I_{12} = 0, 1$, $I_{34}$, $I_{56} = 0, 2$, and that for $[H_2(D_2)D_2]^+$ is given by

$$\frac{h\nu}{g\mu_B} = H_0 + A_{ctr}(\mathrm{D})\left(I_{1z} + I_{2z}\right) + \frac{A_{ctr}(\mathrm{D})^2}{2H_0} + \left(I_{1z} - I_{2z}\right)\sqrt{\Delta A(\mathrm{D})^2 + \left(\frac{A_{ctr}(\mathrm{D})^2}{2H_0}\right)^2} + A_{sid}(\mathrm{D})I_{56z}. \tag{2.13}$$

with $I_1 = I_2 = 0, 1$, $I_{56} = 0, 2$. Figure 2.4(g) shows line positions of $[D_2(H_2)D_2]^+$ obtained by Eq. 2.12 with $g = 2.0020$, $A_{ctr}(H) = 21$ mT, and $A_{sid}(D) = 1.44$ mT. The positions of D lines are reproduced although the satellite lines around D5-D7 are not reproduced. It should be stressed that $A_1$ and $A_2$ are equivalent in $[D_2(H_2)D_2]^+$ because both side-on $H_2$'s are substituted for $D_2$. Figure 2.4(h) shows line positions of $[H_2(D_2)D_2]^+$ obtained by Eq. 2.13 with $g = 2.0020$, $A_1(D) = A_{ctr} + \Delta A(D) = 3.35$ mT, and $A_2(D) = A_{ctr} - \Delta A(D) = 2.98$ mT, and $A_{sid}(D) = 1.44$ mT. The positions of D lines are also reproduced. More over, the satellite lines around D5-D7 are reproduced. This results indicate that the D lines are the superposition of spectrum of $[D_2(H_2)D_2]^+$ and $[H_2(D_2)D_2]^+$. The dotted line in Figure 2.4(d), (e), and (f) shows the simulation spectrum of $[D_2(H_2)D_2]^+$, $[H_2(D_2)D_2]^+$,

and superposition of those ($[D_2(H_2)D_2]^+$: $[H_2(D_2)D_2]^+$ = 1: 1), respectively, with $\Delta H_{FWHM}$ = 0.24 mT. Although it is not clear in D3 and D4 due to the overlap with B1 and intense quartz line, not only line positions but also the ratio in intensity of lines in the simulated spectrum of (f) reproduce the D lines. These results strongly suggest that D lines should be assigned to $[D_2(H_2)D_2]^+$ and $[H_2(D_2)D_2]^+$.

### 2.4.4 E lines to $[H_2(H_2)HD]^+$ and $[H_2(HD)H_2]^+$

When proton of $H_6^+$ at position 6 in Figure 1.3(b) is replaced by D to form $[H_2(H_2)HD]^+$, the resonance condition is given by

$$\begin{aligned}\frac{h\nu}{g\mu_B} = {} & H_0 + A_{ctr}(H)\left(I_{1z} + I_{2z}\right) + \frac{A_{ctr}(H)^2}{2H_0} \\ & + \left(I_{1z} - I_{2z}\right)\sqrt{\Delta A(H)^2 + \left(\frac{A_{ctr}(H)^2}{2H_0}\right)^2} \\ & + A_{sid}(H)I_{5z} + \frac{A_{sid}(H)^2}{4H_0} + A_{sid}(D)I_{6z},\end{aligned} \tag{2.14}$$

where $I_5$ is the spin quantum number of proton and $I_6$ is that of deuteron in side-on HD. The second-order correction for $A_{sid}$(H) is kept in Eq. 2.14 since it is not negligible compared with the ESR linewidth of E lines. Each of B1–B4 lines of $H_6^+$ should split into six lines due to $A_{sid}$(H) and $A_{sid}$(D). The stick diagram in Figure 2.7(f) shows the resonance magnetic fields fitted to the E lines by substituting $g$ = 2.0020, $A_{ctr}$(H) = $A_1$(H) = $A_2$(H) = 20.55 mT, $\Delta A$(H) = 0 mT, $A_{sid}$(H) = 9.58 mT, and $A_{sid}$(D) = 1.40 mT to Eq. 2.14. Like the C lines of $[H_2(H_2)D_2]^+$, $[H_2(H_2)HD]^+$ at $I_{12z}$(H) = $I_{1z}$(H) + $I_{2z}$(H) = ±1 states (E1–E4, E22–E24) coincides in position with the E lines, but that at $I_{12z}$(H) = 0

(E7–E18) does not. Figure 2.7(g) shows the diagram fitted to the E lines with $A_1$(H) = $A_{ctr}$(H) + $\Delta A$(H) = 21.24 mT, and $A_2$(H) = $A_{ctr}$(H) − $\Delta A$(H) = 19.86 mT. The mismatch in position of E7–E18 lines is compensated. Figure 2.7(b) shows the simulated spectrum of $[H_2(H_2)HD]^+$ with $A_1^{ani}$(H) = $A_2^{ani}$(H) = −0.13 mT and $\Delta H_{FWHM}$ = 0.15 mT. The simulated spectrum reproduces both positions and shape of E1–E4, E7–E18, and E22–E24 lines. So that these lines are assigned to $[H_2(H_2)HD]^+$.

On the other hand, resonance fields of E5, E6, and E19–E21 lines are not reproduced. In addition, the integrated intensity of the E7 line is about twice larger than that of E8–E18 lines, whereas all the lines should have the same intensities in the case of the $[H_2(H_2)HD]^+$ radical. This result suggests that the rest of E lines, E5, E6, part of E7, and E19–E21, should be assigned to the species other than $[H_2(H_2)HD]^+$. As shown in Figure 2.9, the decay rate of all the E lines is the same. Then, the rest of E lines should be assigned to $[H_2(HD)H_2]^+$, which transforms into its isomer of $[H_2(H_2)HD]^+$ within the time scale of the decay. When the proton of $H_6^+$ at position 2 in Figure 1.3(b) is replaced by the deuteron to form $[H_2(HD)H_2]^+$, the resonance condition is given by

$$\frac{h\nu}{g\mu_B} = H_0 + A_{ctr}(H)I_{1z} + A_{ctr}(D)I_{2z} + \frac{A_{ctr}(H)^2/2 + A_{ctr}(D)^2\left\{2 - {I_{2z}}^2\right\}}{2H_0} \tag{2.15}$$

The dotted line in Figure 2.7(c) shows the simulated spectrum of $[H_2(HD)H_2]^+$ fitted to E lines with $A_{ctr}$(H) = 21.02 mT, $A_{ctr}$(D) = 3.02 mT, $A_1^{ani}$(H) = −0.12 mT, and $A_2^{ani}$(D) = −0.02 mT. Since the simulated spectrum reproduces both line positions and line shape, E5, E6, part of E7, and E19–E21 lines are assigned to $[H_2(HD)H_2]^+$.

### 2.4.5 F lines to $[HD(H_2)HD]^+$

Since the ratio in intensity of F to E lines in solid p-$H_2$–HD (8 mol%) is larger than that in p-$H_2$–HD (1 mol%), F lines should be assigned to the species containing larger number of HD molecules such as $[HD(H_2)HD]^+$. When protons of $H_6^+$ at positions 4 and 6 are replaced by deuterons to form $[HD(H_2)HD]^+$, the resonance condition is given by

$$\begin{aligned}\frac{h\nu}{g\mu_B} = {} & g\mu_B H_0 + A_{ctr}(H) I_{12z} \\ & + \frac{A_{ctr}(H)^2 \left\{ I_{12}(I_{12}+1) - {I_{12z}}^2 \right\}}{2H_0} \\ & + A_{sid}(H) I_{35z} + \frac{A_{sid}(H)^2 \left\{ I_{35}(I_{35}+1) - {I_{35z}}^2 \right\}}{2H_0} \\ & + A_{sid}(D) I_{46z},\end{aligned} \tag{2.16}$$

with $I_{35} = I_3 + I_5$, $I_{35z} = I_{3z} + I_{5z}$, $I_{46} = I_4 + I_6$, and $I_{46z} = I_{4z} + I_{6z}$. Since the main axis of $H_6^+$ does not rotate in solid hydrogens,[11] $I_{35}$ and $I_{46}$ are not coupled to the rotational states but have 0 and 1 for $I_{35}$ and 0, 1, and 2 for $I_{46}$ even at 4 K. The stick diagram in Figure 2.8 shows line positions of $[HD(H_2)HD]^+$ at $[I_{12}, I_{12z}] = [1, 0]$ and $[0, 0]$ with $g$ = 2.0020, $A_{ctr}(H)$ = 21 mT, $A_{sid}(H)$ = 9.52 mT, and $A_{sid}(D)$ = 1.37 mT. Since the positions of F lines are reproduced, they should be assigned to $[HD(H_2)HD]^+$. The other lines of $[HD(H_2)HD]^+$ at $I_{12z} = \pm 1$ are not observed. Probably, these lines are so broad that they are hidden.

HFCCs obtained by the fittings are summarized in Table 2.2. $A_{ctr}(H) \approx (\gamma_p / \gamma_d) A_{ctr}(D) \approx 20$ mT and $A$sid(H) $\approx (\gamma_p / \gamma_d) A_{sid}(D) \approx 9.5$ mT obtained for all series of lines, B–F, are very close to those of $H_6^+$ calculated in Table 2.1. This result indicates that totally more than 50 B–F lines observed in this study are uniquely assigned to $H_6^+$ and

its isotopomers. It should be noted that, although the sign of $\Delta A$ cannot be determined experimentally, $\Delta A > 0$ ($A_1 > A_2$) for $[H_2(H_2)D_2]^+$ and $[H_2(H_2)HD]^+$ is employed throughout the comparison with theoretical results (see below).

## 2.5 Asymmetric electron wave function in $[H_2(H_2)D_2]^+$ and $[H_2(H_2)HD]^+$

Optimized geometry of $H_6^+$ calculated has $D_{2d}$ symmetry, which should be common for all isotopomers $H_{6-n}D_n^+$. However, $A_1 > A_2$ is deduced from the analysis of $[H_2(H_2)D_2]^+$, $[H_2(D_2)D_2]^+$ and $[H_2(H_2)HD]^+$ signals. We suggest that the asymmetry between $A_1$ and $A_2$ in $[H_2(H_2)D_2]^+$, $[H_2(D_2)D_2]^+$ and $[H_2(H_2)HD]^+$ should be due to the kinetic term of the nuclei. The $D_{2d}$ symmetry is broken when differences in the nucleus masses leading to differences in the energy position of the vibrational levels and in the corresponding nuclei wave functions are taken into account. The asymmetry would be seen if one computes HFCCs averaged over the nuclei wave function (e.g., if one computes HFCCs for a given vibrational level). Here, we briefly discuss HFCCs on averaged nuclei distances instead of averaged HFCCs over nuclear wave function.

Since $H_2$ is lighter than $D_2$, amplitude of zero-point vibration near $H_2$ should be larger than that near $D_2$: the anharmonic term on vibrational levels near the $H_2$–$H_2^+$ bond should be larger than that near $H_2^+$–$D_2$ in $[H_2(H_2)D_2]^+$ even at ground vibrational state. Therefore, the averaged $H_2$–$H_2^+$ bond length in $[H_2(H_2)D_2]^+$ should be larger

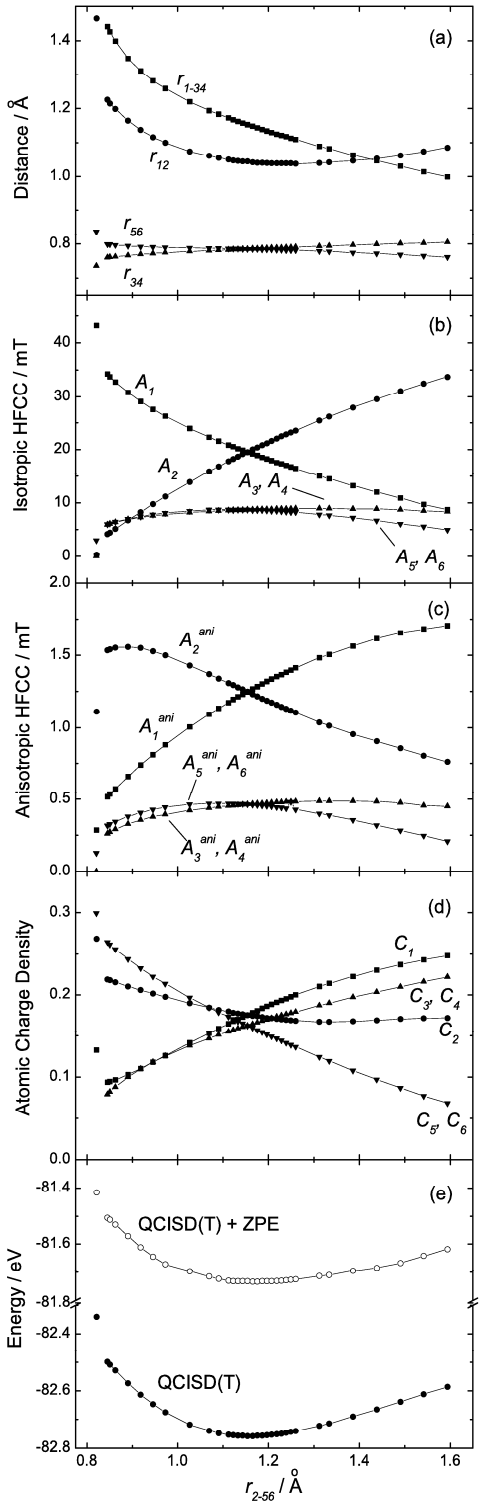


Figure 2.11. (a) Optimized bond length, (b) isotropic HFCC, (c) anisotropic HFCC, (d) charge density $C_i$, (e) expectation value of spin operator $\mathbf{S}^2$ $<\mathbf{S}^2>$, and (f) energy of $H_6^+$ calculated at the geometry of $C_{2v}$ symmetry optimized for each bond length $r_{2\text{-}56}$. The bond length, HFCCs, charge density, and $<\mathbf{S}^2>$ were calculated at the MP2/cc-pVQZ level. The energy was obtained at the MP2/cc-pVQZ and QCISD(T)/cc-pVQZ levels. The values plotted at $r_{2\text{-}56}$ = 0.821 Å are obtained for is for $r_{1\text{-}34} \rightarrow \infty$. $r_{2\text{-}56}$ = 0.821 Å corresponds to the optimized bond

than the $H_2^+$–$D_2$ one.

Figure 2.11 presents the potential energy profile, geometry, HFCC, and atomic charges $C_i$ of $i$th protons in $H_6^+$ with $C_{2v}$ symmetry calculated at a given bond length $r_{2–56}$. Here $r_{mn}$ is the distance between protons at $m$ and $n$ in Figure 1.3(b), and $r_{l\text{-}mn}$ ($l \in$ 1, 2; $m$, $n \in$ 3–6) is that between proton at $l$ in $H_2^+$ core and center of side-on $H_2$ at $m$ and $n$. $H_2^+$-core $H_6^+$ possesses $D_{2d}$ symmetry for $r_{1–34} = r_{2–56} = 1.15$ Å. As $r_{2–56}$ decreases, both $r_{12}$ and $r_{1–34}$ remarkably increase. The values plotted at $r_{2–56} = 0.821$ Å in Figure 2.11 are those calculated at $r_{1–34} \rightarrow \infty$ limit. ($r_{2–56} = 0.821$ Å corresponds to the optimized length at $r_{1–34} \rightarrow \infty$.) In this case, $H_6^+$ should decompose into isolated $H_2$ and H–$H_3^+$ complex, $H_2$ + H–$H_3^+$, where protons 3 and 4 are in $H_2$ and protons 1, 2, 5, and 6 are in the H–$H_3^+$ complex.[26] In fact, $A_1 = 43$ mT close to HFCC of isolated hydrogen atom of 50.8 mT, $A_2 \sim A_6 \rightarrow 0$ mT, and $C_2 + C_5 + C_6 \rightarrow 1$ with $C_2 \approx C_5 \approx C_6$ are calculated. Similarly, as $r_{2–56}$ increases, $H_6^+$ becomes the $H_3^+$–H + $H_2$ complex.

As $r_{2–56}$ decreases (and $r_{1–34}$ increases), most of the values for $H_6^+$ in Figure 2.11 approach those for $H_2$ + H–$H_3^+$. In particular, since the energy of $H_2$ + H–$H_3^+$ plotted at $r_{2–56} = 0.821$ Å lies on or above the energy curve of $H_6^+$ in (f), no activation barrier for the endothermic reaction,

$$[H_2(H_2)H_2]^+ \rightarrow H_2 + H–H_3^+ - 0.223 \text{ eV}, \qquad (2.17)$$

is expected. It means that $H_6^+$ is stabilized at the bottom of very shallow potential surface of $H_3^+$–H+$H_3^+$ ↔ $[H_2(H_2)H_2]^+$ ↔ $H_2$+H–$H_3^+$. Because the depth of this potential is comparable to the difference in zero point energy (ZPE) of $H_6^+$ and $H_4D_2^+$ (0.1 eV), the anharmonic term on vibrational levels can not be negligible. The anharmonic term on vibrational levels near the $H_2$–$H_2^+$ bond should be larger than that near $H_2^+$–$D_2$ in $[H_2(H_2)D_2]^+$ even at ground vibrational state. Therefore, the averaged $H_2$–$H_2^+$ bond

length in $[H_2(H_2)D_2]^+$ should be larger than the $H_2^+$–$D_2$ one. In another words, the structure of $[H_2(H_2)D_2]^+$ should slant to the $H_2$+H–$HD_2^+$.

As listed in Table 2.2, $A_1$ is larger than $A_2$ by 12% in $[H_2(H_2)D_2]^+$. Since $A_1$ = 1.12 $A_2$ is obtained for $r_{1-34}$ / $r_{2-56}$ = 1.04 in Figure 2.11, the averaged $H_2^+$–$D_2$ distance in $[H_2(H_2)D_2]^+$ is expected to be smaller than the $H_2^+$–$H_2$ one by ~4%. In a similar manner, $r_{1-34}$/ $r_{2-56}$ = 1.02 is expected for $[H_2(H_2)HD]^+$ and 1.03 for $[H_2(HD)H_2]^+$. On the other hand, $r_{34}$ and $r_{56}$ are less sensitive to $r_{2-56}$. H–H bonds in side-on $H_2$'s are so strong that the averaged lengths should be very close to the distance at minimum potential energy, less affected by the isotope substitution.

In contrast to $A_1$ and $A_2$, calculations predict that $|A_1^{ani}|$ should decrease and $|A_2^{ani}|$ should increase with the decrease in $r_{2-56}$ from the equilibrium position. These predictions are in agreement with the experimental result that $|A_1| > |A_2|$, but $|A_1^{ani}| < |A_2^{ani}|$ is obtained in $[H_2(H_2)D_2]^+$.

Kurosaki *et al*.[27] performed direct *ab initio* MD calculations for the $H_6^+$, $H_4D_2^+$, and $H_5D^+$ ions at the UMP2/cc-pVDZ level of theory with the total energy of the ZPE in the initial condition. The calculations predict that the average geometry becomes asymmetric in the deuterated clusters $H_4D_2^+$ and $H_5D^+$, causing disproportion in the spin density, which is well correspond to our experimental study.

## 2.6 Summary

We have reported totally more than 50 ESR lines assigned to $H_2^+$-core $H_6^+$ and its isotopomers such as $H_5D^+$, $H_4D_2^+$, and $H_2D_4^+$ in γ-ray irradiated solid para-$H_2$, para-$H_2$–ortho-$D_2$, and para-$H_2$–HD mixtures. ESR parameters, nuclear spin quantum numbers, and hyperfine coupling constants for these lines show a good agreement with theoretical results. The observation of $H_6^+$ denies the widely accepted idea that $H_n^+$ ion ($n \geq 3$) exclusively has $H_3^+$-cored structure.

The experimental results for $H_6^+$ and its isotopomers revealed that distribution of unpaired electron was distorted by substituting deuterons for protons, which is not expected by theoretical calculation under the Born-Oppenheimer approximation. We concluded that $H_6^+$ ions possess the $D_{2d}$ symmetry, whereas $H_4D_2^+$ and $H_5D^+$ in which one of the side-on $H_2$'s in $H_6^+$ is substituted by $D_2$ or HD, have $C_{2v}$ symmetry. This should be due to the difference in the effect of anharmonic term of electric wavefunction in $H_4D_2^+$ and $H_5D^+$. The averaged $H_2^+$-$D_2$ ($H_2^+$-HD) distance is estimated to be smaller than the $H_2^+$-$H_2$ one by 4% (2%) in $H_4D_2^+$ ($H_5D^+$) based on the comparison of hyperfine coupling constants on two protons in $H_2^+$ core experimentally determined with theoretically predicted parameters.[21]

# References


[1] M. Fushitani, N. Sogoshi, T. Wakabayashi, T. Momose, and T. Shida, J. Chem. Phys. **109**, 6346 (1998).

[2] T. Momose, H. Hoshina, N. Sogoshi, H. Katsuki, T. Wakabayashi, and T. Shida, J. Chem. Phys. **108**, 7334 (1998).

[3] N. Sogoshi, T. Wakabayashi, T. Momose, and T. Shida, J. Phys. Chem. A **105**, 3077 (2001).

[4] M. Fushitani and T. Momose, Low Temp. Phys. **29**, 740 (2003).

[5] H. Hoshina, M. Fushitani, T. Momose, and T. Shida, J. Chem. Phys. **120**, 3706 (2004).

[6] T. Momose, M. Fushitani, and H. Hoshina, Int. Rev. Phys. Chem. **24**, 533 (2005).

[7] S. Tam, M. Macler, and M. E. Fajardo, J. Chem. Phys. **106**, 8955 (1997).

[8] Y. Shimizu, M. Inagaki, T. Kumada, and J. Kumagai, J. Chem. Phys. **132** (2010).

[9] J. Kumagai, M. Hanabusa, H. Inagaki, and S. Kariya, Phys. Chem. Chem. Phys. **6**, 4363 (2004).

[10] Y. Kurosaki and T. Takayanagi, J. Chem. Phys. **109**, 4327 (1998).

[11] T. Kumada, H. Tachikawa, and T. Takayanagi, Phys. Chem. Chem. Phys. **7**, 776 (2005).

[12] T. Momose, C. M. Lindsay, Y. Zhang, and T. Oka, Phys. Rev. Lett. **86**, 4795 (2001).

[13] T. Momose, Y. Zhang, and T. Oka, Physica B **284**, 387 (2000).

[14] H. U. Suter, B. Engels, and S. Lunell, in *Advances in Quantum Chemistry, Vol 40: New Perspectives in Quantum Systems in Chemistry and Physics, Pt 2* (Academic Press Inc, San Diego, 2001), Vol. 40, p. 133.

[15] T. Miyazaki, K. Yamamoto, and Y. Aratono, Chem. Phys. Lett. **232**, 229 (1995).

[16] Y. Shimizu, T. Kumada, and J. Kumagai, J. Magn. Reson. **194**, 76 (2008).

[17] T. Kumada, H. Inagaki, T. Nagasawa, Y. Aratono, and T. Miyazaki, Chem. Phys. Lett. **251**, 219 (1996).

[18] A. Carrington, I. R. McNab, and C. A. Montgomerie, J. Phys. B-Atomic Molecular and Optical Physics **22**, 3551 (1989).

[19] T. Oka, Ann. Rev. Phys. Chem. **44**, 299 (1993).

[20] M. C. Chan, M. Okumura, and T. Oka, J. Phys. Chem. A **104**, 3775 (2000).

[21] J. Kumagai, H. Inagaki, S. Kariya, T. Ushida, Y. Shimizu, and T. Kumada, J. Chem. Phys. **127** (2007).

[22] M. C. R. Symons, Chem. Phys. Lett. **247**, 607 (1995).

[23] T. Kumada, N. Kitagawa, S. Mori, J. Kumagai, Y. Aratono, and T. Miyazaki, J. Low Temp. Phys. **114**, 413 (1999).

[24] P. C. Souers, *Hydrogen Properties for Fusion Energy* (University of California Press, Berkeley, 1986).

[25] I. F. Silvera, Rev. Mod. Phys. **52**, 393 (1980).

[26] Y. Kurosaki and T. Takayanagi, Chem. Phys. Lett. **293**, 59 (1998).

[27] Y. Kurosaki, Y. Shimizu, and J. Kumagai, Chem. Phys. Lett. **455**, 59 (2008).

# 3 Electron spin resonance spectroscopy of molecules in large precessional motion: A case of $H_6^+$ and $H_4D_2^+$ in solid parahydrogen

We have measured electron spin resonance (ESR) spectra of $H_6^+$ and $H_4D_2^+$ ions produced in γ-ray irradiated solid parahydrogen. Anisotropic hyperfine coupling constants for $H_6^+$ and $H_4D_2^+$ determined by the analysis of ESR lines at 4.2 K were −0.06 and −0.12 mT, respectively, which are opposite in sign to and much smaller than theoretical results of 1.25 mT. Although no change was observed in $H_6^+$, the constant for $H_4D_2^+$ increased to be 1.17 mT at 1.7 K, which is positive and very close to the theoretical value. We concluded that $H_6^+$ both at 4.2 and 1.7 K and $H_4D_2^+$ at 4.2 K should be in a large precessional motion with the angle of 57 ~ 59°, but the precession of $H_4D_2^+$ is stopped at 1.7 K.

## 3.1 Introduction

Study of rotational and librational motions of molecules trapped in cryocrystals has a long history.[1-14] These studies were mainly carried out by using infrared absorption spectroscopy (IR); however, electron spin resonance (ESR) spectroscopy is also useful.[9-11, 13, 14] Advantage of ESR over IR is that ESR measures pure rotational and librational motions, whereas IR excites ro-vibrational transitions. In order to study the rotational and librational motions by ESR spectroscopy, highly resolved lines are essential. Solid para-$H_2$ (p-$H_2$) is the ideal matrix for the spectroscopy[15-26] as is mentioned in Chapter 1.

ESR spectroscopic data of $H_6^+$ were firstly reported by our group by using highly resoluted ESR spectroscopy with p-$H_2$ matrices[20-23, 25, 26]. The $H_6^+$ ion has $H_2^+$ core on the main axis sandwiched between chemically bound two side-on $H_2$ groups (Figure 1.3(b)). Assignment of $H_6^+$ and its isotopomers was precisely confirmed in Chapter 2. Isotropic hyperfine-coupling constants (HFCCs) $A^{iso}$ obtained theoretically coincide with the experimental ones in excellent accuracy, indicating that the theoretical calculation properly optimized the geometry of $H_6^+$.[23]

Anisotropic HFCCs, $A^{ani}$, however, are quite different from the theoretical ones.[25] Recently, we have carried out ESR measurements of $H_6^+$ and $H_4D_2^+$ at 4.2 and 1.7 K and have concluded that the difference was derived from large precessional motion of the radical molecules. In this Chapter, we will present the ESR results and discuss possible precession modes in solid p-$H_2$.

## 3.2 Experiment

p-$H_2$ and ortho-$D_2$ (o-$D_2$) was obtained in the same manner with Chapter 1. The p-$H_2$ gas and p-$H_2$ containing o-$D_2$ at 1 mol % were sealed in a quartz ESR sample cell together with He (99.9999%; Taiyo Nippon Sanso Co.) at 0.1 mol %, introduced into a quartz ESR Dewar filled with liquid helium to produce solid p-$H_2$ at the bottom tip, and then irradiated with γ rays for ~1 h to a total dose of 2.88 kGy at the $^{60}$Co γ-ray irradiation facility at Nagoya University. The irradiated p-$H_2$ sample with the Dewar was used with a commercial *X*-band ESR spectrometer (JEOL JES-RE1X).

Temperatures were regulated by pumping liquid helium in the quartz Dewar as measured by a Au-Fe / Chromel thermo couple (The Nilaco Co.). Microwave frequency and magnetic field were monitored by the microwave frequency counter (Hewlett-Packard, 53150A) and NMR field meter (Echo Electronics Co. Ltd., EFM-2000AX), respectively.

## 3.3 Results

Figure 2.1(c) shows the quartet ESR lines (B1-B4) of $H_6^+$ ions in irradiated solid p-$H_2$. The splitting of $H_6^+$ lines is due to hyperfine interaction with the $H_2^+$-core nuclei.[21-23] The stick diagram shows resonance magnetic fields obtained by substituting the *g*-value $g = 2.002$, the isotropic HFCC for $H_2^+$-core $A^{iso} = 20.44$ mT, and a nuclear spin moment of $H_2^+$ core and its *z*-component $[I_{12}, I_{12z}] = [0, 0], [1, -1], [1, 0]$ and $[1, 1]$ in

Eq. 2.7 where suffixes of 1 and 2 express the positions of atoms in $H_6^+$ in Figure 1.3(b). The equation with these parameters completely reproduces the line positions. On the other hand, hyperfine splitting due to side-on $H_2$ groups was not observed, because the side-on $H_2$ groups near temperature 4 K are in the ground rotational state $J_{34} = J_{56} = 0$ around main axis of $H_6^+$, which is coupled to the $I_{34} = I_{56} = 0$ nuclear spin states.

Figure 3.1 shows ESR lines of $H_6^+$ at $I_{12z} = \pm 1$ named B3 and B4, respectively. The asymmetric lineshape in B3 and B4 is a typical powder-pattern shape with an uniaxial asymmetric hyperfine interaction. HFCC $A$ is composed of an isotropic Fermi contact term $A^{iso}$ and anisotropic dipolar-dipolar interaction one $A^{ani}$ (Eq. 2.8 in Chapter 2).[13, 14] $A^{iso}$ determines line positions, and $A^{ani}$ gives lineshape. The dotted lines in Figure 2.2 show the simulated powder-pattern spectrum of $H_6^+$ with $A^{ani} = -0.06$ mT. The B3 and B4 lines measured both at 4.2 and 1.7 K are completely reproduced. The larger peaks in B3 and B4 are of $H_6^+$ for $\Theta = 90°$ in Eq. 2.8, and smaller ones are for 0°. However, as shown in Table 2.1, theory has predicted $A^{ani} = 1.17 \sim 1.25$ mT, positive and much larger than that experimentally determined by a factor of −20.

Figure 2.3(a) shows ESR spectra of $H_2^+$-core $H_4D_2^+$ produced in irradiated solid p-$H_2$ containing ortho-$D_2$ (o-$D_2$) at 1 mol%. Each of B1-B4 lines of $H_6^+$ is split into quintets in the $H_4D_2^+$ spectra due to hyperfine interaction with side-on $D_2$, which has $I_{56} =$ 0 and 2 at $J_{56} = 0$.[23] The stick diagram in Fig. 2.3(f) shows resonance fields of $H_4D_2^+$ obtained by substituting $g = 2.002$, $A_{12}^{iso} = (A_1^{iso} + A_2^{iso}) / 2 = 20.63$ mT, $\Delta A_{12}^{iso} = (A_1^{iso} - A_2^{iso}) / 2 = 1.2$ mT, isotropic HFCC of side-on $D_2$, $A_D^{iso} = 1.44$ mT, and z-component of nuclear spin quantum numbers of nuclei 1 and 2 in $H_2^+$-core, and side-on $D_2$, $I_{1z} = \pm 1/2$, $I_{2z} = \pm 1/2$, $I_{56z} = \pm 2, \pm 1, 0$ in Eq. 2.10. The line positions are completely reproduced.[23] The small difference in HFCC between two protons in $H_2^+$-core, $A_1^{iso}$ and $A_2^{iso}$, is due to

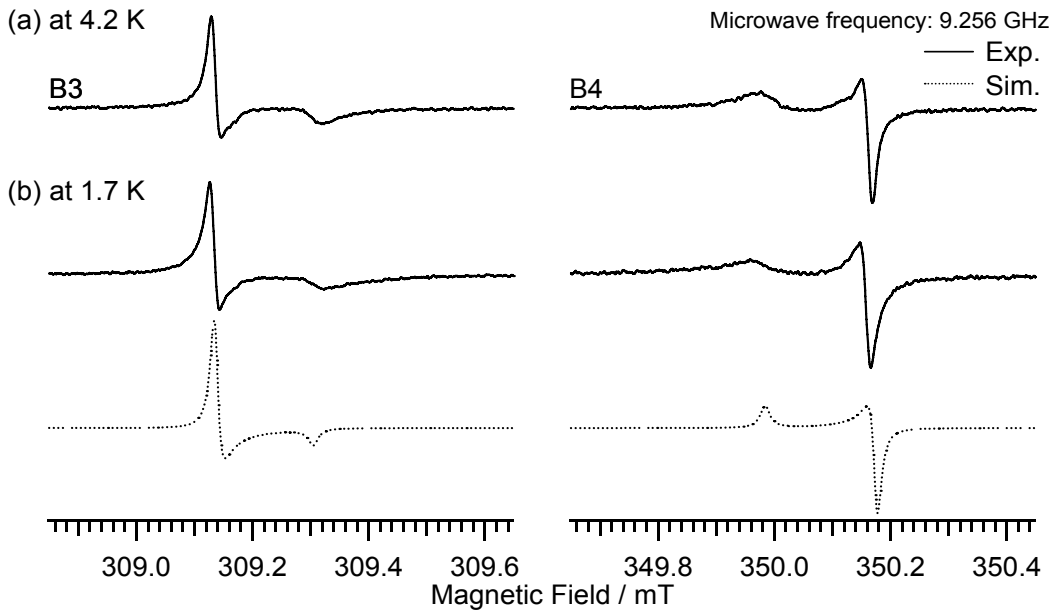


Figure 3.1. ESR lines of $H_6^+$ at $I_{12z} = \pm 1$ (B3 and B4) in γ-ray irradiated solid p-$H_2$ measured with field-modulation frequency of 50 kHz, its amplitude of 0.01 mT, and microwave power of 1 mW for (a) and 0.4 mT for (b). The dashed line is a simulated spectrum of $H_6^+$ with $A^{ani} = -0.06$ mT.

that in amplitude of zero-point motion between side-on $H_2$ and $D_2$ in $H_4D_2^+$.[27, 28]

Figure 3.2 shows C1-C5 and C13-C16 lines of $H_4D_2^+$ for $I_{12z} = I_{1z} + I_{2z} = \pm 1$. The C1-C5 and C13-C16 lines of $H_4D_2^+$ also look broadened by $A^{ani}$. The $H_4D_2^+$ lines at 4.2 K are reproduced by the simulated spectrum in Figure 3.2(b) with $A^{ani} = -0.12$ mT, which is twice that for $H_6^+$, but much less than the theoretical result by a factor of –10. Unlike $H_6^+$, $H_4D_2^+$ was remarkably changed both in line-positions and shapes by the decrease in temperature from 4.2 to 1.7 K. The C1-C5 (C13-C17) lines were shifted to upper (lower) fields by 1.2 mT. In addition, although upper (lower) peaks were more intense than the lower (upper) in the C1-C5 (C13-C17) lines at 4.2 K, the lower (upper) ones became more intense at 1.7 K.

The change in lineshape of C1-C5 and C13-C17 can be explained by the change in $A^{ani}$. The spectrum is reproduced by the simulated one in Figure 3.2(b) with $A^{ani} =$ 1.17 mT, which is positive and very close to the theoretical values. The smaller peaks of

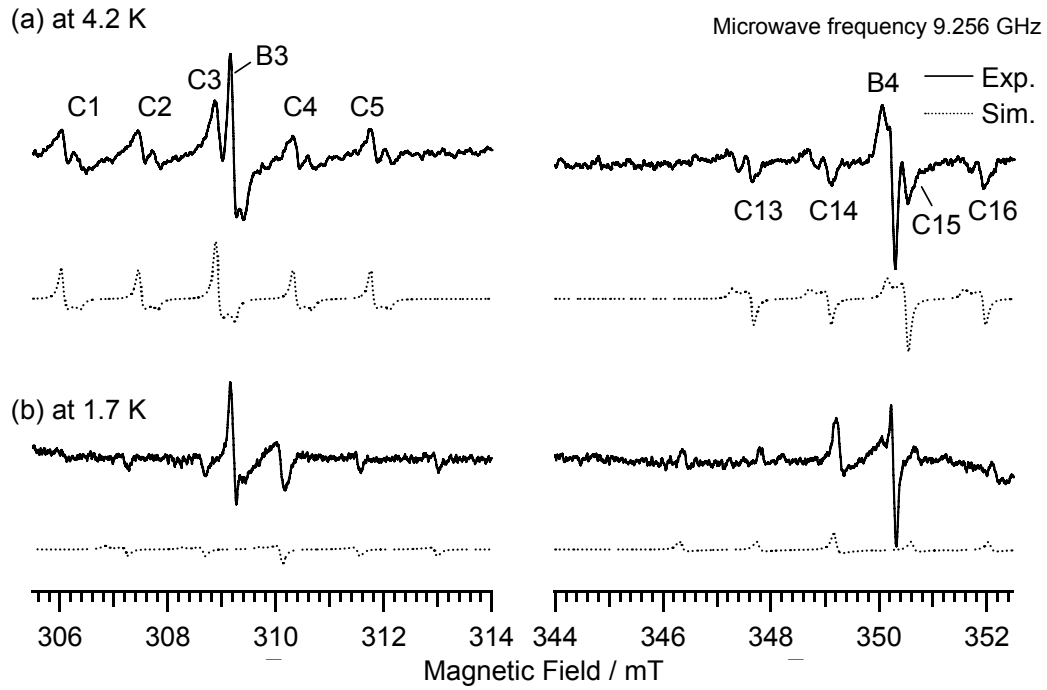


Figure 3.2. ESR lines of $H_4D_2^+$ at $I_{12z} = \pm 1$ (C1-C5 and C13-C17) in γ-ray irradiated solid p-$H_2$ containing o-$D_2$ at 1 mol % with field-modulation frequency of 50 kHz, its amplitude of 0.1 mT, and microwave power of 1 mW for (a) and 0.4 mT for (b). The dashed lines are simulated spectra of $H_4D_2^+$ with $A^{\mathrm{ani}} = -0.12$ mT for (a) and 1.17 mT for (b).

C1-C5 and C13-C17 lines of $H_4D_2^+$ for $\Theta = 0°$ in Eq. 2.8 disappeared at 1.7 K probably due to poor signal-to-noise ratio.

Note that we have not observed any feature due to anisotropic hyperfine interaction with side-on $D_2$ nuclei in $H_4D_2^+$, which causes difference in lineshape and width among C1-C5 and C13-C17. Theory also predicted that the anisotropic HFCC of side-on $D_2$ should be much less than that of $H_2^+$-core by a factor of ~10.[23] Therefore, we ignored it in the analysis of $H_4D_2^+$ lines.

## 3.4 Discussion

We propose that the discrepancy in $A^{ani}$ between experiment and theory is due to the local motion of $H_6^+$ and $H_4D_2^+$ in each cage of solid p-$H_2$. Although theory calculates $A_0^{ani}$, (the anisotropic HFCC) against the molecular axes, $A^{ani}$ determined by ESR is the projection of $A_0^{ani}$ on crystalline axes. Theoretical values of $A_0^{ani}$ can be compared with experimental ones only when radicals are completely fixed in the solids. The $A^{ani}$ values should decrease with the increase in amplitude of libration or rotation due to the motional narrowing effect.

As shown in Figure 3.3a, suppose that a radical has a precessional motion around a crystalline axis of a solid with the precession angle $\theta$, where the unit vector $r$ of the main axis of radical is given by

$$\begin{aligned} r(\theta,\varphi,\Theta) &= \begin{pmatrix} r_x \\ r_y \\ r_z \end{pmatrix} = \begin{pmatrix} 1 & 0 & 0 \\ 0 & \cos\Theta & -\sin\Theta \\ 0 & \sin\Theta & \cos\Theta \end{pmatrix} \begin{pmatrix} \cos\varphi\sin\theta \\ \sin\varphi\sin\theta \\ \cos\theta \end{pmatrix} \\ &= \begin{pmatrix} \cos\varphi\sin\theta \\ \cos\Theta\sin\varphi\sin\theta - \sin\Theta\cos\theta \\ \sin\Theta\sin\varphi\sin\theta + \cos\Theta\cos\theta \end{pmatrix}, \end{aligned} \tag{3.1}$$

with the phase of precession $\varphi$. $A^{ani}(\theta,\varphi,\Theta)$, anisotropic HFCC at $\Theta$, $\theta$, and phase $\varphi$, are related by

$$A^{ani}(\theta,\varphi,\Theta) = (3r_z^{\,2} - 1)A_0^{\,ani}, \tag{3.2}$$

where $A_0^{ani}$ is the value when the $H_6^+$ completely stop($\theta$ = 0° and $\varphi$ = 0°). $A_0^{ani}$ is calculated to be 1.25 mT at MP2/cc-pVQZ level as listed in Table 2.1. The expected value for $A^{ani}(\theta,\varphi,\Theta)$ in the precessional motion, is given by averaging $A^{ani}(\theta,\varphi,\Theta)$ around $\varphi$ as,

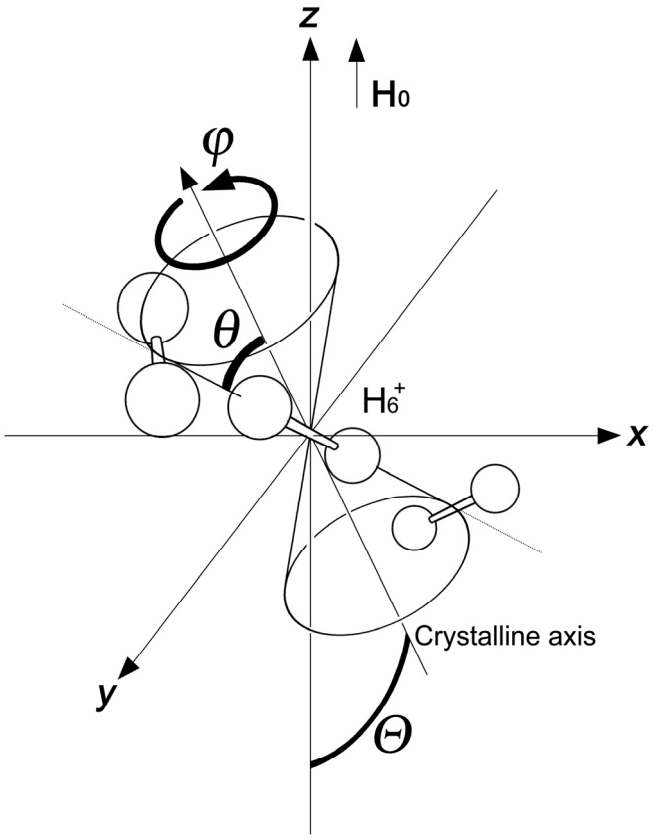


Figure 3.3. Schematic representation of $H_6^+$ in a precession motion against crystalline axis. $\theta$ is the angle between the main axis of $H_6^+$ and crystalline axis, and $\Theta$ the angle between the crystalline axis and vector of static magnetic field ($\mathbf{H_0}$).

$$A_{pre}^{\mathrm{ani}}(\theta,\Theta) = \frac{\int_0^{2\pi}(3r_z^{\,2}-1)A^{\mathrm{ani}}(\theta,\varphi,\Theta)d\varphi}{\int_0^{2\pi}d\varphi}$$
$$= \frac{3\cos^2\theta-1}{2}(3\cos^2\Theta-1)A_0^{\mathrm{ani}} \qquad (3.3)$$
$$\equiv (3\cos^2\Theta-1)A_{pre}^{\mathrm{ani}}(\theta),$$

In Eq. 3.3, $\theta = 0°$ corresponds to the situation that radicals are completely fixed to crystalline axes, and $\theta = 90°$ corresponds to the situation that each radical rotates in a plane. The anisotropy measured by ESR is $A_{pre}{}^{\mathrm{ani}}(\theta)$ derived from $A_0{}^{\mathrm{ani}}$ by

$$A_{\mathrm{pre}}^{\mathrm{ani}}(\theta) = \frac{3\cos^2\theta-1}{2}A_0^{\mathrm{ani}}. \qquad (3.3')$$

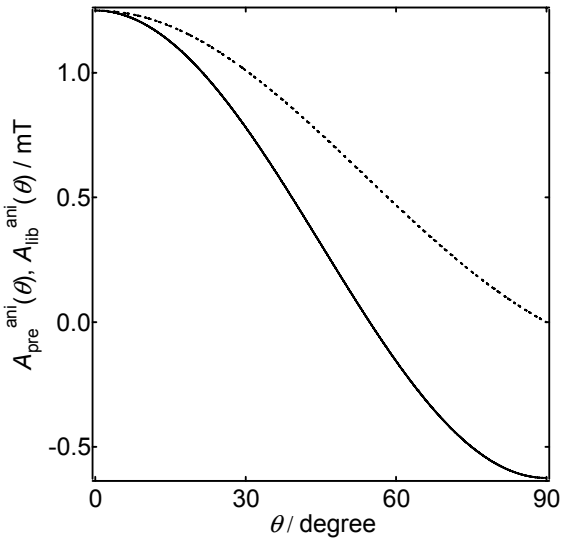


Figure 3.4. $A_{pre}^{ani}(\theta)$ and $A_{lib}^{ani}(\theta)$ plotted against θ. Solid line and doted line shows $A_{pre}^{ani}(\theta)/ A_0^{ani}$ and $A_{lib}^{ani}(\theta)/ A_0^{ani}$, respectively.

$A_{pre}^{ani}(\theta)$ decreases with increasing $\theta$ from 0°, crosses 0 at the magic angle of 54.74°, and then reach to $-A_0^{ani} / 2$ at $\theta = 90°$ as shown in Figure 3.4. The sign of $A_{pre}^{ani}(\theta)$ inverses at the magic angle.

On the other hand, when the radical is in librational motion with the maximum libration angle $\theta$, the expected value, $A_{lib}^{ani}(\theta, \Theta)$, is given by,

$$
\begin{aligned}
A_{lib}^{ani}(\theta,\Theta) &= \frac{\int_0^{\theta}\int_0^{2\pi} A^{ani}(3r_z^{\,2}-1)d\varphi\sin\theta d\theta}{\int_0^{\theta}\int_0^{2\pi} d\varphi\sin\theta d\theta} \\
&= A_0^{ani}\,\frac{\cos\theta(1+\cos\theta)}{2}(3\cos^2\Theta-1). \qquad (3.4)\\
&\equiv A_{lib}^{ani}(\theta)(3\cos^2\Theta-1)
\end{aligned}
$$

$A_{lib}^{ani}(\theta)$ decreases with increasing $\theta$ from 0° to 90°. The radicals are in free rotational state at $\theta = 0°$. Unlike $A_{pre}^{ani}(\theta)$, the sign of $A_{lib}^{ani}(\theta)$ cannot be negative for $0° \le \theta \le 90°$ as shown in Figure 3.4.

Figure 3.5 shows simulated ESR spectra of B3 and B4 lines depending on the

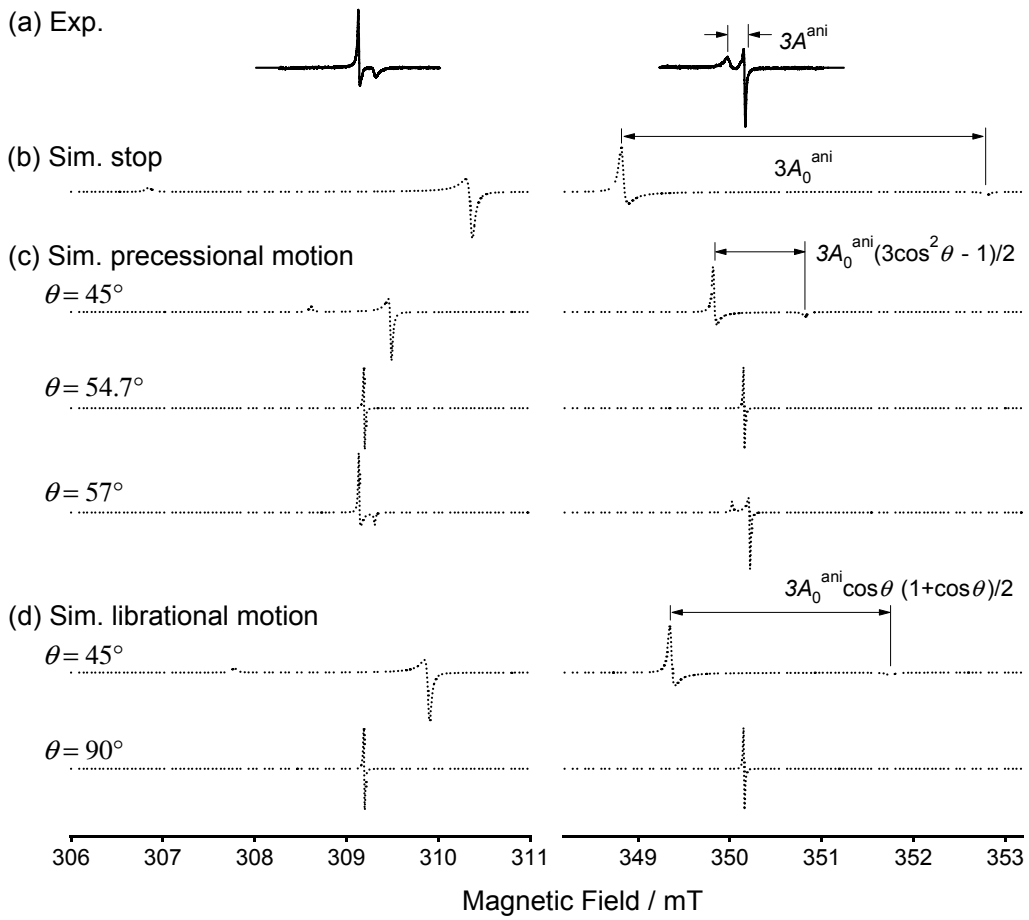


Figure 3.5. Simulated B3 and B4 lines according to the pressesional and librational models written in Eqs. 3.3 and 3.4, respectively, as a function of $A^{ani}(\theta,\varphi,\Theta)$ (b-d) with theoretical $A_0^{ani}$ value of 1.25 mT by MP2/cc-pVQZ. The simulations correspond to the motions of $H_6^+$ as (a) B3 and B4 lines in experiment; (b) stopped ($\theta$ = 0 in Eq. 3.3'); (c) in precessional motion (Eq. 3.3') (d) in librational motion (Eq. 3.4).

rotational motions of $H_6^+$ as a function of $A^{ani}(\theta,\varphi,\Theta)$ with experimental ones. We use theoretical $A^{ani}$ value of 1.25 mT (MP2/cc-pVQZ) as $A_0^{ani}$. Outer peaks of B3 and B4 lines observed by the experiments were more intense than inner peaks of them. The splitting of the outer and the inner peaks is 0.018 mT, which corresponds to 3 × $A^{ani}$. However, simulated lines of stopped $H_6^+$ have completely opposite symmetry as the inner peaks were more intense than the outer peaks. In addition the splitting was 3 × $A_0^{ani}$ = 3.75 mT, which was 20 times larger than that of experimental one. As is

Table 3.1. $A^{ani}$ of $H_2^+$-core of $H_6^+$ and $H_4D_2^+$ determined by the analysis of ESR lineshape of $H_6^+$ and $H_4D_2^+$.

| | Temperature / K | $A^{ani}$ / mT | precession angle $\theta$ [b] / degree |
|---|---|---|---|
| $H_6^+$ | 4.2 | −0.06 | 57 |
| | 1.7 | −0.06 | 57 |
| $H_4D_2^+$ | 4.2 | −0.12 | 59 |
| | 1.7 | 1.17 | - |
| Theory[a] | | 1.25 | - |

[a] Theoretical value is obtained at the MP2/cc-pVQZ level of calculation.
[b] Precession angle $\theta$ obtained by substituting experimental value in $A_{pre}^{ani}$, and theoretical one in $A_0^{ani}$ of Eq. 3.3' (see text).

mentioned above, the expected value for $A^{ani}(\theta,\varphi,\Theta)$ in the precessional motion is given by averaging $A^{ani}(\theta,\varphi,\Theta)$ around $\varphi$, and that in the librational motion by averaging $A^{ani}(\theta,\varphi,\Theta)$ around $\theta$ and $\varphi$. These averaging can be observed by ESR when the precessional or librational frequency is faster than ~100 MHz because the splitting due to $A_0^{ani}$ is 3.75 mT (~100 MHz).

When $H_6^+$ is in precessional motion at $\theta < 54.7°$, the symmetry of simulated lines was opposite from experimental ones. When $H_6^+$ is in precessional motion at $\theta > 54.7°$, the symmetry of simulated lines can be reproduced to that of experimental ones. The splitting width increased with increasing $\theta$ over 54.7° and was agree with experimental one at $\theta = 57°$.

When $H_6^+$ is assumed to be in libration motion, the symmetry is opposite from experimental one at the all range of $\theta$. It can be concluded that $H_6^+$ are not in libration motion. A negative value of experimental $A^{ani}$ in $H_6^+$ at 4.2 and 1.7 K, and $H_4D_2^+$ at 4.2 K should be due to a large precessional motion of them with $\theta > 54.74°$.

We determined $\theta$ in Table 3.1 by substituting the experimental value of $A^{ani}$ to

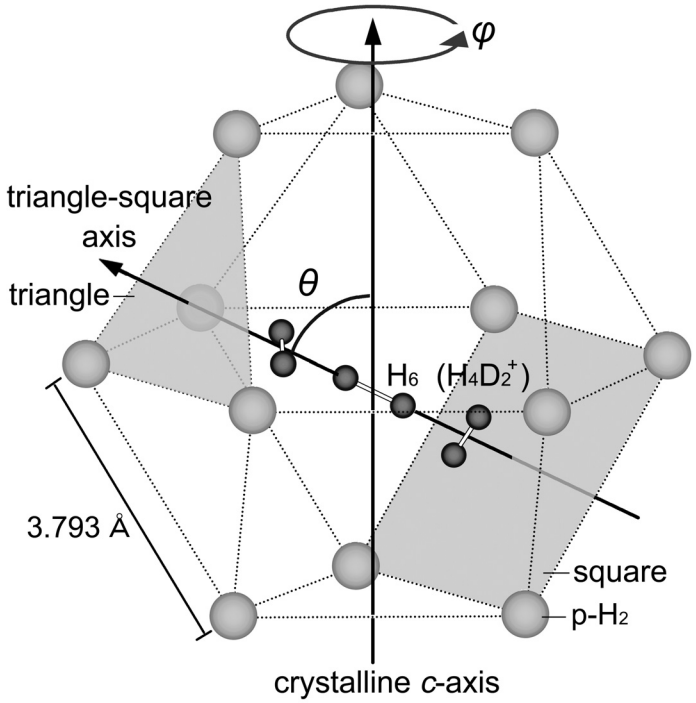


Figure 3.6 Schematic representation of $H_6^+$ in a precession motion against crystalline axis. $\theta$ is the angle between the main axis of $H_6^+$ and crystalline axis.

$A_{pre}^{ani}(\theta)$, and the theoretical one to $A_0^{ani}$ in Eq. 3.3', respectively. $\theta = 57°$ is obtained for $H_6^+$ at 4.2 and 1.7 K, and 59° for $H_4D_2^+$ at 4.2 K, indicating that $H_6^+$ at 4.2 and 1.7 K and $H_4D_2^+$ at 4.2 K are in a large precessional motion faster than 100 MHz. Positive and large $A^{ani}$ for $H_4D_2^+$ (1.17 mT) at 1.7 K, which is close to theoretical value, indicate that the precessional motion of $H_4D_2^+$ at 1.7 K should be stopped or much slower than 100 MHz.

Let's consider possible precession mode of $H_6^+$ and $H_4D_2^+$ in solid p-$H_2$. Figure 1.3(c) shows the optimized geometry of $H_{14}^+$.[29] as a model of $H_{14}^+$ is composed of $H_6^+$ and physically bound four $H_2$s. The equilibrium $H_6^+$-$H_2$ distance was estimated to be 3.2 Å for $H_{14}^+$, which is close to the intermolecular distance of solid p-$H_2$ (3.793 Å[30]). Therefore, $H_6^+$ can be assumed to be trapped in a single substitutional cage of solid p-$H_2$.

Figure 3.6 shows a model of $H_6^+$ trapped in a single substitutional *hcp* cage of

solid p-$H_2$. The cage has 8 trianglar and 6 square planes. All trianglar planes at the side diagonally face to the square ones, but the trianglar plane at the top faces to the trianglar one at the bottom. We propose that the main axis of $H_6^+$ should be along the axis passing through centers of a pair of diagonally faced square and triangle planes (triangle-square axis) in order to avoid overlap of electronic orbital between $H_6^+$ and p-$H_2$s. When $H_6^+$ in the axis is off-centered from the center of cages to the square by 0.3 Å, the distances between side-on $H_2$ of $H_6^+$ to each p-$H_2$ molecule at the apexes of triangle and square are calculated to be 2.8 Å. This value is very close to the distance between a side-on $H_2$ of $H_6^+$ and an outer $H_2$ in Figure 1.3(c) of 2.6 Å. Eventually, these values should be closer to each other when the effect of nuclear quantum fluctuation is taken into account on the calculation of $H_6^+$ and $H_{14}^+$.[27, 28] This result indicates that $H_6^+$ should be trapped along the triangle-square axis with little distortion of the *hcp* cage of solid p-$H_2$.

On the other hand, when $H_6^+$ is aligned along the *c*-axis of solid p-$H_2$, the distance between side-on $H_2$ and p-$H_2$ molecules at the apexes of upper and lower triangles is 2.6 Å, being a little shorter than the equilibrium distance expected when taking into account the fluctuation. Therefore, $H_6^+$ should prefer the triangle-square axes rather than *c*-axis.

We suggest that the $H_6^+$ ions are in precessional motion along *c*-axis by jumping among the six equivalent triangle-square axes in solid p-$H_2$. When the cage is not distorted, the angle between c-axis and triangle-square axis in the *hcp* cage is calculated to be $\theta_{min} = 63.2°$, which is very close to the precession angle of $H_6^+$ at 4.2 K and 1.7 K (57°), and $H_4D_2^+$ at 4.2 K (59°).

The similar values of $A^{ani}$ between experiment and theory in $H_4D_2^+$ at 1.7 K

indicate that the precessional motion is stopped. Why is the precessional motion stopped in $H_4D_2^+$ but not in $H_6^+$? We propose two possible reasons as follows: First, the moment of inertia for $H_4D_2^+$ is larger than that for $H_6^+$. $H_4D_2^+$ is heavier than $H_6^+$, and, unlike $H_6^+$, the center of mass does not coincide with the center of geometry in $H_4D_2^+$. Second, not only the nuclear configuration but also the electronic wave function of $H_4D_2^+$ no longer has $D_{2d}$ symmetry but has $C_{2v}$.[23] This means that the energy $E(\theta_{min}, \varphi)$ of $H_4D_2^+$ in the *hcp* cage of solid p-$H_2$ does not have 6-fold but has 3-fold symmetry around $\varphi$. $H_4D_2^+$ should be localized in one of three deeper potential wells at 1.7 K.

We have no idea whether the precession of $H_6^+$ is due to quantum mechanical tunneling or classical thermal hopping. Small mass and matching in energy levels between neighboring wells are essential for quantum tunneling. Because of the small moment of inertia and high symmetry, $H_6^+$ may keep the precession via the tunneling down to 0 K. On the other hand, the rate for the tunneling precession should be much less in $H_4D_2^+$, because of larger moment of inertia and lower symmetry in potential for precession.

## 3.5 Summary

In conclusion, we have compared anisotropic HFCC of $H_6^+$ and $H_4D_2^+$ in solid p-$H_2$ determined by the analysis of ESR lines with theoretical calculation to find the results as follows: $H_6^+$ is in precessional motion at precession angle of 57° along the c-axis of substitutional *hcp* cage in solid p-$H_2$ both at 4.2 and 1.7 K. Although $H_4D_2^+$ is also in the precessional motion at 4.2 K, the precession is stopped at 1.7 K. The difference should be due to larger moment of inertia and lower molecular symmetry in $H_4D_2^+$.

Local environment of cages around guest molecules and their local motions should be determined in order to study solid-phase chemical reaction between guest and host molecules. Recently, we have observed the reactions related to $H_6^+$ such as $H_6^+ + H_2 \rightarrow H_2 + H_6^+$ and $H_6^+ + e^- \rightarrow 3H_2$ in solid p-$H_2$. We hope that the mechanism of solid-phase reactions related to $H_6^+$ can be clarified through this study.

# References


1 V. A. Apkarian and N. Schwentner, Chem. Rev. **99**, 1481 (1999).

2 V. E. Bondybey, A. M. Smith, and J. Agreiter, Chem. Rev. **96**, 2113 (1996).

3 G. Schallmoser, A. Thoma, B. E. Wurfel, and V. E. Bondybey, Chem. Phys. Lett. **219**, 101 (1994).

4 W. H. Flygare, J. Chem. Phys. **39**, 2263 (1963).

5 Friedman.H and S. Kimel, J. Chem. Phys. **43**, 3925 (1965).

6 T. Oka, Annual Review of Physical Chemistry **44**, 299 (1993).

7 S. Tam, M. E. Fajardo, H. Katsuki, H. Hoshina, T. Wakabayashi, and T. Momose, J. Chem. Phys. **111**, 4191 (1999).

8 H. Hoshina, T. Wakabayashi, T. Momose, and T. Shida, J. Chem. Phys. **110**, 5728 (1999).

9 T. Yamada, K. Komaguchi, M. Shiotani, N. P. Benetis, and A. R. Sornes, J. Phys. Chem. A **103**, 4823 (1999).

10 K. Komaguchi, T. Kumada, T. Takayanagi, Y. Aratono, M. Shiotani, and T. Miyazaki, Chem. Phys. Lett. **300**, 257 (1999).

11 T. Kumada, J. Chem. Phys. **117**, 10133 (2002).

12 Z. Li and V. A. Apkarian, J. Chem. Phys. **107**, 1544 (1997).

13 C. P. P. Jr., *Electron Spin Resonance* (Dover, Mineola, 1983).

14 A.Abragam, (Oxford University Press, Oxford, 1961).

15 T. Kumada, N. Kitagawa, T. Noda, J. Kumagai, Y. Aratono, and T. Miyazaki, Chem. Phys. Lett. **288**, 755 (1998).

16 T. Kumada, M. Sakakibara, T. Nagasaka, H. Fukuta, J. Kumagai, and T. Miyazaki, J. Chem. Phys. **116**, 1109 (2002).

17 T. Kumada, J. Kumagai, and T. Miyazaki, J. Chem. Phys. **114**, 10024 (2001).

18 T. Miyazaki, K. Yamamoto, and J. Arai, Chem. Phys. Lett. **219**, 405 (1994).

19 T. Kumada, S. Mori, J. Kumagai, Y. Aratono, and T. Miyazaki, J. Phys. Chem. A **103**, 8966 (1999).

20 T. Kumada, Y. Shimizu, T. Ushida, and J. Kumagai, Rad. Phys. Chem. **77**, 1318 (2008).

21 T. Kumada, H. Tachikawa, and T. Takayanagi, Phys. Chem. Chem. Phys. **7**, 776 (2005).

22 T. Kumada, T. Takayanagi, and J. Kumagai, J. Mol. Struct. **786**, 130 (2006).

23 J. Kumagai, H. Inagaki, S. Kariya, T. Ushida, Y. Shimizu, and T. Kumada, J. Chem. Phys. **127** (2007).

24 J. Kumagai, M. Hanabusa, H. Inagaki, and S. Kariya, Phys. Chem. Chem. Phys. **6**, 4363 (2004).

25 Y. Shimizu, T. Kumada, and J. Kumagai, J. Magn. Reson. **194**, 76 (2008).

26 Y. Shimizu, M. Inagaki, T. Kumada, and J. Kumagai, J. Chem. Phys. **132** (2010).

27 A. Kakizaki, T. Takayanagi, and M. Shiga, Chem. Phys. Lett. **449**, 28 (2007).

28 Y. Kurosaki, Y. Shimizu, and J. Kumagai, Chem. Phys. Lett. **455**, 59 (2008).

29 Y. Kurosaki and T. Takayanagi, J. Chem. Phys. **109**, 4327 (1998).

30 I. F. Silvera, Rev. Mod. Phys. **52**, 393 (1980).

# 4 Negative and positive ion trapping by isotopic molecules in cryocrystals in case of solid parahydrogen containing electrons and $H_6^+$ radical cations

We performed electron spin resonance studies of trapped electrons and $H_6^+$ radical cations produced by radiolysis of solid parahydrogen (p-$H_2$), p-$H_2$–ortho-$D_2$, and p-$H_2$–HD mixtures. Yields of trapped electrons, $H_6^+$ radical cations, and its isotopomers $H_{6-n}D_n^+$ ($4 \geq n \geq 1$) increased with increasing ortho-$D_2$ (o-$D_2$) and HD concentrations in solid p-$H_2$. Electrons were found trapped near an o-$D_2$ or an HD in solid p-$H_2$ due to the long-range charge-induced dipole and quadrupole interactions between electrons and isotopic hydrogen molecules. $H_6^+$ radical cations diffuse in solid p-$H_2$ by repetition of $H_6^+ + H_2 \rightarrow H_2 + H_6^+$ and are trapped by ortho-$D_2$ or HD to form $H_{6-n}D_n^+$ ($4 \geq n \geq 1$) as isotope condensation reactions. Decay behaviors of these cations by the repetition, isotope condensation, and geminate recombination between electrons and $H_{6-n}D_n^+$ ($4 \geq n \geq 0$) were reproduced by determining the corresponding reaction rate constants $k_1$, $k_2$, and $k_3$. Values of 0.045 and 0.0015 L $mol^{-1}$ $min^{-1}$ were obtained for $k_1$ ($H_6^+ + D_2 \rightarrow H_2 + H_4D_2^+$) and $k_2$ ($H_4D_2^+ + D_2 \rightarrow H_2 + H_2D_4^+$), respectively, and the value was quasi-null for $k_3$ ($H_2D_4^+ + D_2 \rightarrow H_2 + D_6^+$). These rate constants suggest that hole mobility drastically decreased in the repetition reaction when $H_6^+$ radical cations acting as hole carriers formed $H_4D_2^+$ or $H_2D_4^+$. HD and $D_2$ molecules, therefore, act as electron and hole acceptors in irradiated solid p-$H_2$–o-$D_2$ and p-$H_2$–HD mixtures.

## 4.1 Introduction

Electrons trapped in solids at cryogenic temperature have been extensively studied since four decades in the field of radiation chemistry for aqueous matrices,[1-6] alcohols,[7-16] hydrocarbons,[11, 17-20] and hetero compounds.[9, 12-14, 21-27] Although most electrons produced by the radiolysis of solid matter recombine with the parent cations, some of them are trapped in local potential minima like defects, cracks, and distortions to form trapped electrons ($e_t^-$)[28-30]. Yields of $e_t^-$ in solids usually depend on solid crystallinity and polarity. Electrons in glassy solids can be stabilized as $e_t^-$ by local rearrangement of surrounding molecules to produce larger free volumes for reducing kinetic energy.[29-32] Polar molecules in solids assist in reducing the potential energy of electron by charge polarization[8]. On the other hand, no electron can be trapped in irradiated molecular crystals, except in irradiated single crystals of $D_2O$,[33] trehalose[34], and crystals of diols.[7] Large crystallization energy hinders the local rearrangements of molecules in crystals.[28]

Ten years ago, the yields of $e_t^-$ produced by radiolysis of solid parahydrogen (p-$H_2$) were found to significantly increase with increasing $D_2$ or HD concentrations, whereas no $e_t^-$ could be detected in their absence by electron spin resonance (ESR) spectroscopy.[35] Recently, we succeeded in detecting $e_t^-$ in pure p-$H_2$ and found that the isotope effect on $e_t^-$ yields was 10–24-fold with increasing $D_2$ and HD concentrations (~ 1–8 mol%) in solid p-$H_2$. This experimental result addresses the following outstanding issues. First, the isotope effect on $e_t^-$ yields is observed for small concentrations of isotopic hydrogen molecules in irradiated solid p-$H_2$. Isotope effects on $e_t^-$ yields in condensed matter have been studied by several researchers.[33, 36, 37] Wang and Willard

have reported that $e_t^-$ yields produced in fully deuterated saturated hydrocarbons like 3-methylpentane-$d_{14}$, methylcyclohexane-$d_{14}$, and 3-methylheptane-$d_{18}$ glasses irradiated using γ-rays at 77 K were around 1.5 times larger than in protiated hydrocarbons.[36] Regarding liquid phases, the survival probability of $e_t^-$ in liquid $D_2O$ has been reported to be about 1.1 times higher than in liquid $H_2O$.[37, 38] Hase and Kawabata have detected $e_t^-$ in irradiated crystalline $D_2O$ at 4 K using electron spin resonance and photo absorption spectroscopy, in particular, when $H_2O$ contents in $D_2O$ were below 3% in volume.[33] Because isotope effects on $e_t^-$ yields in fully deuterated irradiated solvents were below twofold increases in these reports, except for crystalline $D_2O$, 10–24-fold increases obtained by increasing $D_2$ and HD concentrations (~1–8 mol%) in solid p-$H_2$ were astonishingly large. In addition, significant amounts of $e_t^-$ have been yielded in irradiated solid hydrogens that are not in amorphous but crystalline phase. The detection of $e_t^-$ in solid p-$H_2$ crystals containing small amounts of isotopic hydrogen molecules is unusual. Solid hydrogen crystals must be perfect for the following reasons. Hydrogen molecules in solid hydrogen have large zero-point motions, which repair cracks, distortions, and imperfections maintaining high homogeneity of solid without annealing.[39-43] These occur because molecular hydrogen is light and undergoes small intermolecular interactions. In particular, p-$H_2$ molecules exclusively have a $J = 0$ rotational quantum state with no electric quadrupole moment. Therefore, solid p-$H_2$ is free from inhomogeneous electric quadrupole–quadrupole interactions between neighboring p-$H_2$ molecules. Neither an $H_2$ nor a $D_2$ has dipole moment and an HD has a negligible dipole moment.[44-46] The present model of electron trapping cannot account for this isotope effect as the trapping depends on inhomogeneity and polarity in solids.[28-31, 44-46]

Similar to the $e_t^-$ yields, the total yields of $H_6^+$ and $H_{6-n}D_n^+$ ($4 \geq n \geq 1$) increased with increasing ortho-$D_2$ (o-$D_2$) or HD concentrations. However, these increases have only been investigated by qualitative analysis. In this study, we performed a quantitative decay analysis for the concentrations of $H_6^+$ and $H_{6-n}D_n^+$ ($4 \geq n \geq 1$) in irradiated solid p-$H_2$ at 4.2 K and performed a kinetic analysis for isotope condensation reactions between $H_6^+$ and hydrogen isotopic molecules. In other words, $H_6^+$ ions were trapped by o-$D_2$ and/or HD molecules in solid p-$H_2$. Therefore, isotopic hydrogen molecules in solid p-$H_2$ play an important role in trapping $H_6^+$ and electrons. This Chapter reports isotope effects on the yields and decays of $e_t^-$ and $H_6^+$ in solid p-$H_2$, p-$H_2$–o-$D_2$, and p-$H_2$–HD and discusses the trapping mechanisms. We propose new trapping mechanisms of electron and cation by hydrogen isotopic molecules, which have not been accurately considered in the history of radiation chemistry.

## 4.2 Experiment

p-$H_2$ and o-$D_2$ molecules were obtained by the same in the same manner with Chapter 1. All hydrogen gases, p-$H_2$, o-$D_2$, and HD (96%; Isotec Inc.) were purified as mentioned in Chapter 1. Five p-$H_2$ samples, namely, p-$H_2$, p-$H_2$–o-$D_2$ (1 and 8 mol%), and p-$H_2$–HD (1 and 8 mol%) were prepared using different isotopic hydrogen molecule contents. All samples contained 0.1 mol% of He gas (99.9999%; Taiyo Nippon Sanso Co.) for thermal contact. The samples were sealed in quartz cells and immersed in a quartz Dewar filled with liquid He to prepare the solids. Solid samples were irradiated

with γ-rays for ~1 h to the total dose of 2.88 kGy at the $^{60}$Co γ-ray irradiation facility at Nagoya University. The irradiated samples were placed in an *X*-band ESR spectrometer (JEOL JES-RE1X) to measure the time course of ESR lines at 4.2 K. Microwave frequency and magnetic field of the spectrometer were monitored using a microwave frequency counter (Hewlett-Packard, 53150A) and an NMR field meter (Echo Electronics Co. Ltd., EFM-2000AX), respectively. Microwave powers of 1.0 mW and 0.1–1 nW were used to measure the $H_6^+$ and $e_t^-$ lines, respectively. $H_6^+$ and $e_t^-$ yields were determined by double integration of the ESR lines using hexyl radicals in γ-ray irradiated *n*-hexane (>97%; Kanto Chemical Co., Inc.) as a reference. The *G*-value, which corresponds to the number of products per 100 eV energy absorbed, has been reported as 4.7, on average, for hexyl radicals under γ- or X-ray irradiation.[28]

## 4.3 Results

Figure 4.1 shows the ESR spectra of $e_t^-$ produced in solid p-$H_2$, p-$H_2$–o-$D_2$, and p-$H_2$–HD mixtures. The lines at 331.38 mT ($g$ = 2.0023) were attributed to $e_t^-$. Peak intensity of $e_t^-$ significantly increased with increasing o-$D_2$ or HD concentrations in p-$H_2$. The isotope effect on $e_t^-$ yields was more significant for o-$D_2$ than for HD. Figure 4.2 shows the ESR spectra of $H_6^+$ [B lines: $I_{12}$(nuclear spin quantum number of $H_2^+$-core) = 0 and 1; $I_{34}$ = $I_{56}$ = 0; numbers in subscript corresponds to the atoms in Figure 1.3(b)] and $H_{6-n}D_n^+$ ($4 \geq n \geq 1$) produced in p-$H_2$, p-$H_2$–o-$D_2$, and p-$H_2$–HD. In these isotopomers, the $H_2^+$-core and side-on $H_2$ molecules present in $H_6^+$ are replaced by $D_2$ or HD molecules. In this Chapter, singly $D_2$-substituted $H_4D_2^+$ is denoted as

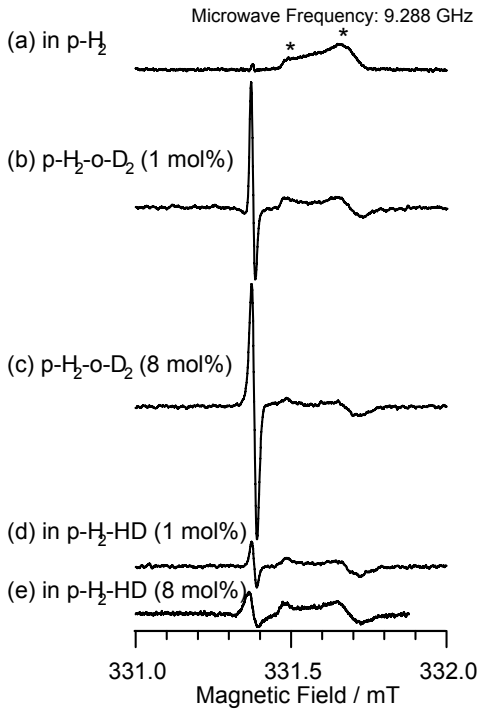


Figure 4.1. ESR spectra of $e_t^-$ produced in γ-ray irradiated solids at 4.2 K. (a) p-$H_2$, (b) p-$H_2$–o-$D_2$ (1 mol%), (c) p-$H_2$–o-$D_2$ (8 mol%), (d) p-$H_2$–HD (1 mol%), and (e) p-$H_2$–HD (8 mol%). Peaks denoted by asterisks were from ESR tubes and Dewar made by radiolysis of quartz. ESR field-modulation frequency, amplitude, and microwave power were 50 kHz, 0.005 mT, and 1 nW, respectively, for p-$H_2$ and, 50 kHz, 0.01 mT, and 0.1 nW, respectively, for p-$H_2$–o-$D_2$ and p-$H_2$–HD mixtures. Peak heights were normalized using field-modulation and the square root of microwave power.

"$H_4D_2^+$" and its doubly HD-substituted counterpart is denoted as "HD-sub. $H_4D_2^+$". Note that $D_2$-core $H_4D_2^+$ has been not detected to this date. In addition to B lines, ESR lines were observed for $H_4D_2^+$ [C lines: $I_1 = I_2 = 1/2$; $I_{34} = 0$; $I_{56}$(o-$D_2$) = 0 and 2] and $H_2D_4^+$ [D lines: $I_{12}$ =0 and 1; $I_{34}$(o-$D_2$) = $I_{56}$(o-$D_2$) = 0 and 2 for $H_2^+$-core $H_2D_4^+$ and $I_{12}$(o-$D_2$) =0 and 2; $I_{34}$ = 0; $I_{56}$(o-$D_2$) = 0 and 2 for $D_2^+$-core $H_2D_4^+$] in irradiated solid p-$H_2$–o-$D_2$ mixtures. Similarly, ESR lines were also observed for $H_5D^+$ [E lines: $I_1$(H) = 1/2; $I_2$(D) = 1; $I_{34} = I_{56} = 0$ for $HD^+$-core $H_5D^+$ and $I_1 = I_2 = 1/2$; $I_{34} = 0$; $I_5$(H) = 1/2; $I_6$(D) = 1 for $H_2^+$-core $H_5D^+$] and HD-sub.$H_4D_2^+$ [F lines: $I_1 = I_2 = 1/2$; $I_3$(H) = $I_5$(H) = 1/2; $I_4$(D) = $I_6$(D) = 1] in irradiated solid p-$H_2$–HD mixtures. The HFCCs for these

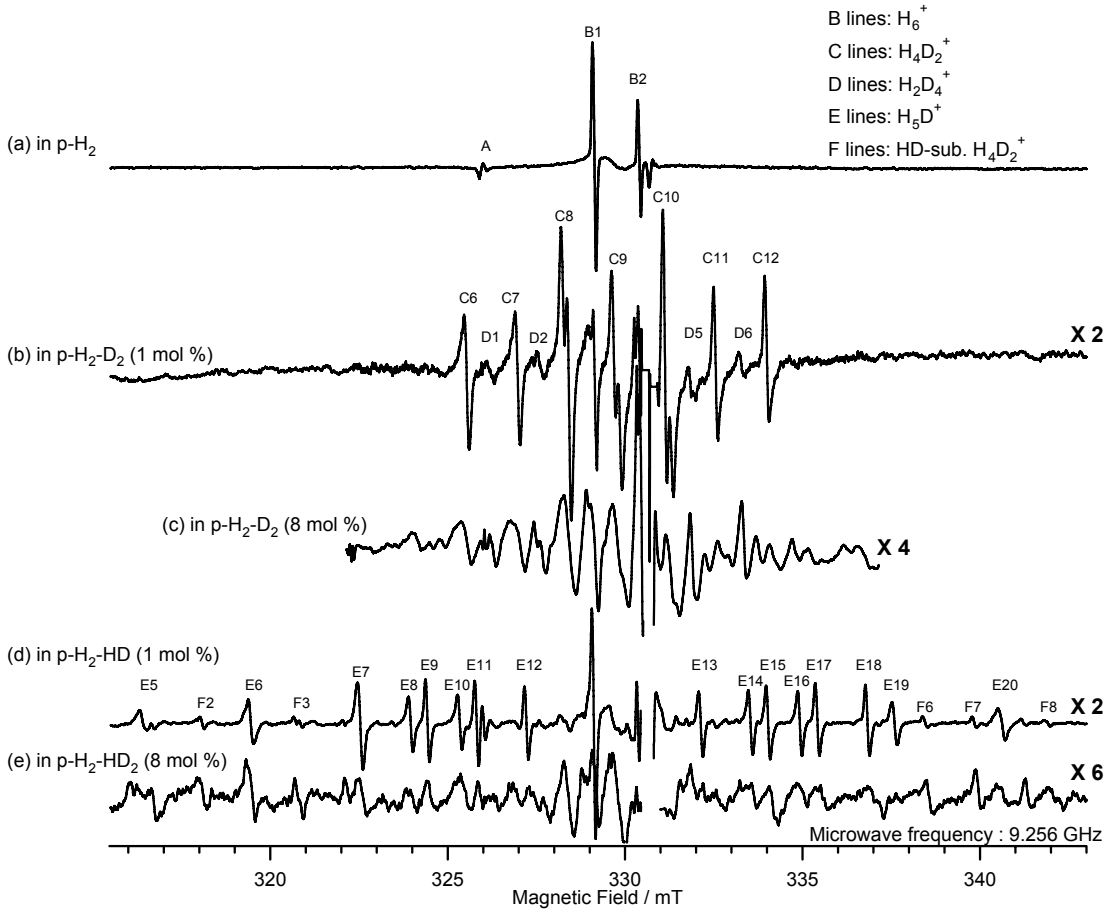


Figure 4.2. ESR spectra of γ-ray irradiated solid (a) p-$H_2$, [(b) and (c)] p-$H_2$–o-$D_2$ mixtures, and [(d) and (e)] p-$H_2$–HD mixtures measured with a field-modulation frequency of 50 kHz, an amplitude of 0.1 mT, and a microwave power of 1 mW. ESR lines marked as B, C, D, E, and F correspond to $H_6^+$, $H_4D_2^+$, $H_2D_4^+$, $H_5D^+$,and HD-sub. $H_4D_2^+$, respectively. The singlet peak marked as A in (a) results form a forbidden transition of H atom radicals.

radical cations are listed in Table 2.2. The precise assignments were discussed in Chapter 2. Although only 1 mol% of o-$D_2$ or HD was added to p-$H_2$, $H_4D_2^+$ and $H_5D^+$ ESR intensities were found to be much higher than for $H_6^+$ in solid p-$H_2$–o-$D_2$ [Figure 4.2(b)] and p-$H_2$–HD [Figure 4.2(d)], respectively. The B lines were not visible in p-$H_2$–o-$D_2$ [Figure 4.2(c)] and p-$H_2$–HD [Figure 4.2(e)] for o-$D_2$ and HD concentrations of 8 mol%.

Table 4.1 shows the relative yields of radical ions detected 30 min after irradiation in p-$H_2$, p-$H_2$-o-$D_2$, and p-$H_2$-HD mixtures. The yields were obtained by

Table 4.1. Relative yields of $e_t^-$, $H_6^+$, $H_4D_2^+$, $H_2D_4^+$, $H_5D^+$, HD-sub. $H_4D_2^+$, and H atom radicals produced in p-$H_2$, p-$H_2$–o-$D_2$, and p-$H_2$–HD mixtures measured 30 min after irradiation.

| | Negative | Positive | | | | | | Neutral |
|---|---|---|---|---|---|---|---|---|
| | $e_t^-$ | $H_6^+$ | $H_4D_2^+$ | $H_2D_4^+$ | $H_5D^+$ | HD-sub. $H_4D_2^+$ | Total* | H atom radicals |
| p-$H_2$ | ~7 | 1 | - | - | - | - | 1 | $6 \pm 1 \times 10^3$ |
| p-$H_2$-$D_2$ (1 mol%) | 70 | 0.5 | 1.9 | 0.4 | - | - | 2.8 | $6 \pm 1 \times 10^3$ |
| p-$H_2$-$D_2$ (8 mol%) | 170 | - | 4 ± 1 | 5 ± 2 | - | - | 9 ± 3 | n.d. |
| p-$H_2$-HD (1 mol%) | 20 | 0.6 | - | - | 1.2 | 0.2 | 2.0 | $5 \pm 1 \times 10^3$ |
| p-$H_2$-HD (8 mol%) | 70 | - | - | - | 1.7 | 0.9 | 2.6 | n.d. |

* The total yield of $H_6^+$ and $H_{6-n}D_n^+$ ($4 \geq n \geq 1$).

double integration of the corresponding ESR lines. Compared to the $H_6^+$ yield in p-$H_2$, the total yields of $H_6^+$, $H_4D_2^+$, and $H_2D_4^+$ displayed 2.8- and 9-fold increases upon addition of 1 and 8 mol% o-$D_2$ to p-$H_2$, respectively. The total yields of $H_6^+$, $H_5D^+$, and HD-sub. $H_4D_2^+$ increased 2- and 2.6-folds upon addition of 1 and 8 mol% HD to p-$H_2$, respectively. These increases in total yields of $H_6^+$ and $H_{6-n}D_n^+$ ($4 \geq n \geq 1$) caused by adding HD were less significant than that caused by adding o-$D_2$ at the same concentration. The ratios of the $H_6^+$:$H_4D_2^+$:$H_2D_4^+$ yields would be 97:3:0.03 for p-$H_2$–o-$D_2$ (1 mol%) and 74:23:1.9 for p-$H_2$–o-$D_2$ (8 mol%) if $H_6^+$, $H_4D_2^+$, and $H_2D_4^+$ were produced statistically with respect to p-$H_2$ and o-$D_2$ concentrations. However, the experimental ratios were 18:68:14 and 0:44:56, respectively. Similarly, the ratios of the $H_6^+$: $H_5D^+$: HD-sub. $H_4D_2^+$ yields were 30:60:10 for p-$H_2$–HD (1 mol%) and 0:65:35 for p-$H_2$–HD (8 mol%). These results clearly show that the $H_{6-n}D_n^+$ ($4 \geq n \geq 1$) species were preferentially produced in solid p-$H_2$. The yield of H atom radicals was ~6000 times greater than that of $H_6^+$ and was independent from o-$D_2$ and HD concentrations.

Figure 4.3 shows the decay behavior of $e_t^-$, $H_6^+$, $H_4D_2^+$, $H_2D_4^+$, and H atom radicals produced in p-$H_2$ and p-$H_2$–o-$D_2$ mixtures. The decay behavior of $e_t^-$ in

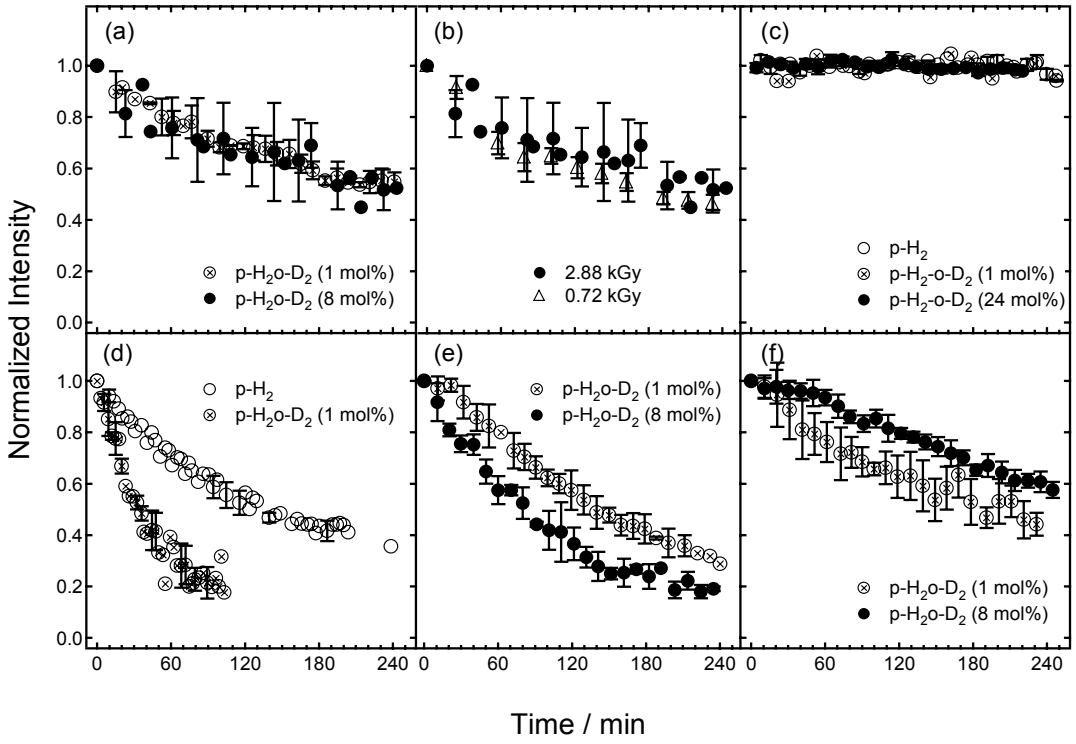


Figure 4.3. Decay behaviors of (a) $e_t^-$, (b) $e_t^-$ at different γ-ray irradiation doses, (c) H atom radicals (d) $H_6^+$, (e) $H_4D_2^+$, and (f) $H_2D_4^+$ in p-$H_2$ and p-$H_2$–o-$D_2$ mixtures. Decay of $e_t^-$ in (b) were measured in a p-$H_2$–o-$D_2$ (8 mol%) mixture.

p-$H_2$-o-$D_2$ mixtures was found to be independent of o-$D_2$ concentration and γ-ray dose [Figure 4.3(a) and 4.3(b)]. $H_6^+$ decayed much faster in p-$H_2$–o-$D_2$ (1 mol%) than that in p-$H_2$. On the other hand, $H_4D_2^+$ and $H_2D_4^+$ decayed in a similar manner in both p-$H_2$–o-$D_2$ mixtures [Figures 4.3(d)–(f)]. H atom radicals did not decay in p-$H_2$[39] and p-$H_2$–o-$D_2$ mixtures [Figure 4.3(c)]. The absolute yields of $e_t^-$, $H_5D^+$, and HD-sub. $H_4D_2^+$ in p-$H_2$–HD were lower than those of $e_t^-$, $H_4D_2^+$, and $H_2D_4^+$ in p-$H_2$–o-$D_2$, respectively. However, the decay behavior of the corresponding species were almost the same.

Figure 4.4 shows the decay rates determined using the inverse lifetimes ($1/\tau_{1/e}$) of $e_t^-$ and $H_{6-n}D_n^+(4 \geq n \geq 1)$. $H_6^+$ decayed significantly faster than $H_4D_2^+$, which decayed a little faster than $H_2D_4^+$. The decay rate of $H_2D_4^+$ was very close to that of $e_t^-$.

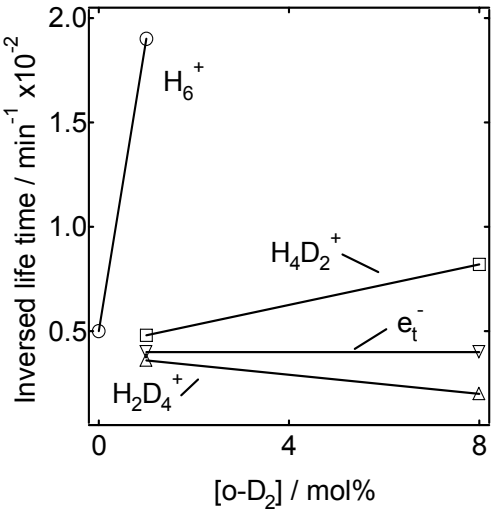


Figure 4.4. Decay rates of $e_t^-$, $H_6^+$, $H_4D_2^+$, and $H_2D_4^+$ as a function of o-$D_2$concentration. Decay rates are shown as inverse life times.

## 4.4 Discussion

We would like to describe the radiation chemical reactions of hydrogens before discussing the trapping mechanisms of $e_t^-$ and $H_6^+$. When gaseous $H_2$ molecules are subjected to ionizing radiation,[28, 47] the ionization of $H_2$ molecules initially produce $H_2^+$ as:

$$H_2 \xrightarrow{\gamma\text{-ray}} e^- + H_2^+ . \qquad (4.1)$$

The $H_2^+$ ions disappear immediately by reacting with neighboring $H_2$ molecules to form $H_3^+$ as:

$$H_2^+ + H_2 \rightarrow H_3^+ + H . \qquad (4.2)$$

The $H_3^+$ ions recombine with electrons to produce H atom radicals under irradiation:

$$H_3^+ + e^- \rightarrow H_3^* \rightarrow 3H \text{ or } H_2 + H . \qquad (4.3)$$

H atom radicals are also generated by dissociation of $H_2$ in an excited state:

$$H_2 \xrightarrow{\gamma\text{-ray}} H_2^* \rightarrow 2H . \qquad (4.4)$$

These ions and H atom radicals are expected to be produced in irradiated solid hydrogen. Although electrons produced in irradiated gaseous $H_2$ immediately recombine with the cations, very small portions of $e^-$ can be trapped in the solid phase to form $e_t^-$ without undergoing recombination. The yield of $e_t^-$ was about seven times higher than for $H_6^+$ in solid p-$H_2$ (cf. Table 4.1). The charge balance suggests a presence of other positive ions beside $H_6^+$ in irradiated solid p-$H_2$. Gas phase results indicate that $H_3^+$ may be the main cationic products in irradiated solid p-$H_2$. Yields of the other positive ions may be larger when hydrides ($H^-$) are produced in irradiated solid p-$H_2$.

### 4.4.1 Trapping mechanism of free electrons by heavier hydrogen isotope molecules

Large increases in $e_t^-$ yields caused by increases in o-$D_2$ and HD concentrations in irradiated solid p-$H_2$ strongly suggest that isotopic hydrogen molecules play an important role in trapping electrons in p-$H_2$ crystals. We would like to propose the new trapping mechanism of o-$D_2$ and HD-mediated electron. The isotope effect on electron trapping was derived from the difference in rotational constants between these isotopes as follows. Long-range charge-induced dipole and quadrupole interactions between $e_t^-$ with $H_2$ or with $D_2$ were calculated by assuming a point-charge model.[48] Hamiltonian ($H_s$) of the interactions are thus given by:

$$H_s = -\alpha e^2/2R^4 + (eQ/R^3 - \gamma e^2/3R^4)P_2(\cos\theta), \qquad (4.5)$$

where $R$ is the separation between a point charge and $H_2$ or $D_2$. $\theta$ denotes the orientation of the hydrogen molecule with respect to $R$ and $P_2$ (cos $\theta$) is the Legendre polynomial. $\alpha$

and $\gamma$ are the mean polarizability and its corresponding anisotropy, respectively. $Q$ is the quadrupole moment of the hydrogen molecule in a molecule-fixed frame. The first and third terms in Eq. 4.1 describe the charge-induced dipole interaction, while the second term shows the charge-induced quadrupole interactions. Because both p-$H_2$ and o-$D_2$ exclusively have a $J = 0$ rotational state at about 4.2 K, the interaction ($W_{J=0}$) is given by

$$\begin{aligned} W_{J=0} &= \langle \psi_{J=0} | H_s | \psi_{J=0} \rangle + \frac{\left| \langle \psi_{J=0} | H_s | \psi_{J=2} \rangle \right|^2}{E_0 - E_2} \\ &= -\alpha e^2 / 2R^4 + \frac{M \left| eQ / R^3 - \gamma e^2 / 3R^4 \right|^2}{15\hbar^2}. \end{aligned} \tag{4.6}$$

Here, $\Psi_J$ and $E_J$ are the rotational wave function of hydrogen nuclei and the rotational energy for $J$, respectively. $M$ is the moment of inertia of the molecule. Although the first term in Eq. 4.2 is common to o-$D_2$ and p-$H_2$, the second term for o-$D_2$ is twice as much as that for p-$H_2$ due to a difference in $M$.

Brooks *et al.*[49] calculated that electrons produced in solid hydrogen were stabilized to form trapped electrons called electron bubbles having a radius of 5 Å because of the zero-point energy. At $R$ = 5 Å, $|W_{J=0}|$ was 1.4 meV higher for o-$D_2$ (12.3 meV) than for p-$H_2$ (10.9 meV). Miller *et al.*[50] also found that $|W_{J=0}|$ for heteronuclear HD molecules (11.5 meV) was 0.6 meV larger than for p-$H_2$. These differences are larger than the thermal energy at 4.2 K as 0.4 meV. Relative $e_t^-$ yields in irradiated p-$H_2$, p-$H_2$-HD (1 mol%) and p-$H_2$-o-$D_2$ (1 mol%) as 1:3:10, respectively, are in the same order of the $|W_{J=0}|$ for $e^-$-p-$H_2$, $e^-$-HD, and $e^-$-o-$D_2$, respectively. These results strongly suggest that existence of HD or o-$D_2$ molecules assisted to trapping electrons qualitatively at 4.2 K.

Assuming a binominal distribution for HD or o-$D_2$ molecules in solid p-$H_2$, probability to have one HD or o-$D_2$ molecule in a first layer composed of twelve p-$H_2$ molecules is estimated to be 0.107 and 0.384 for the 1 and 8% samples, respectively. Probability to have two these molecules in a first layer is estimated to be 0.006 and 0.183 for the 1 and 8 mol% samples, respectively. For the 1 mol% samples, it is expected that one $e_t^-$ mostly interacts with one HD or o-$D_2$ molecule if one $e_t^-$ occupies a substitutional site of an *hcp* structure in solid p-$H_2$. Yields of $e_t^-$ for the 8 mol% samples including HD or o-$D_2$ molecules increased 3.5 or 2.4 times larger than those of the 1 mol% samples, respectively. The Probability to have one HD or o-$D_2$ molecule in a first layer in the 8% samples is estimated 3.8 times larger than those of the 1 mol% samples, which is in agreement with the experimental increases. More than two HD or o-$D_2$ molecules may interact with one $e_t^-$ especially in the 8 mol% sample but probability to have not less than two HD or o-$D_2$ molecules in the first layer is 0.249, which is smaller than that to have one molecule as 0.384. We speculate that the experimental increases in the $e_t^-$ yields in the 8 mol% samples mainly reflect the pairwise trapping structure. We would like to propose that long-range charge-induced dipole and quadrupole interactions between $e^-$ and HD or o-$D_2$, that are larger than $H_2$, play an important role in trapping electron in solid p-$H_2$.

This model, which proposes that isotopic hydrogen molecules trap electrons, may explain the results by Hase and Kawabata who detected $e_t^-$ in an irradiated $D_2O$ single crystal, but not in a $H_2O$ crystal.[33] Because the strong crystallization energy prevents the local rearrangement of molecules in crystals, no $e_t^-$ was detected in irradiated $H_2O$ crystals despite the strong polarizability of $H_2O$.[28] Stronger charge-induced dipole and quadrupole interactions with $e^-$ and D atoms in $D_2O$ may,

therefore, stabilize electrons as $e_t^-$ in $D_2O$ single crystals.

Let us estimate the probability to form $e_t^-$ from $e^-$ generated by radiolysis. It is reported that five H atom radicals are generated per ionization event through reactions (4.1–4.4) in the gas phase on average.[47] Assuming that H atom radicals do not undergo recombination during and after irradiation [cf. Figure 4.3(c)], the probability was roughly estimated as ~1/170, 1/17, and 1/7 in solid p-$H_2$, p-$H_2$-o-$D_2$ (1 mol%), and p-$H_2$–o-$D_2$ (8 mol%), respectively, using the ratio of the $e_t^-$ and H atom radical yields.

### 4.4.2 Decay mechanisms of trapped electrons

Electrons trapped in irradiated solid p-$H_2$ may decay according to the following reactions. One reaction is the attachment of $e_t^-$ to H atom radicals to produce $H^-$ (Eq. 4.7), and others are recombinations with $H_3^+$ (Eq. 4.8) and $H_6^+$ (Eq. 4.9).

$$e_t^- + H \rightarrow H^- \tag{4.7}$$

$$e_t^- + H_3^+ \rightarrow 3H \text{ or } H_2 + H \tag{4.8}$$

$$e_t^- + H_6^+ \rightarrow 6H, \text{ or } 4H + H_2, 2H + 2H_2, 3H_2 \tag{4.9}$$

Because the yield of H atom radicals in p-$H_2$ was ~860 times larger than for $e_t^-$ (Table 4.1), the decay rate of $e_t^-$ should increase with increasing H atom radical concentrations if reaction (4.7) was the dominant decay process. Note that H atom radicals are homogeneously distributed in solid p-$H_2$ as a result of diffusion, which occurs through repetitions of the tunneling reaction ($H + H_2 \rightarrow H_2 + H$).[39, 51, 52] As shown in Figure 4.3(b), the decay rates of $e_t^-$ were dose independent but the yield of H atom radicals

produced by radiolysis at a dose of 2.88 kGy was about 3–4 times higher than at 0.72 kGy.[53] These results indicate that instead of reaction (4.7), reactions (4.8) and (4.9) are the dominant processes for the decay of $e_t^-$.

The concentration of $e_t^-$ ($[e_t^-]$) may depend on the doses. If the decay processes of $e_t^-$ are dominantly governed by reactions (4.8) and (4.9), such as $H_3^+$ and $H_6^+$ concentrations, the decay rate should increase with increasing doses. As mentioned above, no difference was observed for the decay rate of $e_t^-$ at varying doses. We propose that these constant decay rates may be explained by geminate recombination processes with $H_3^+$ and $H_6^+$. Although no experimental evidence for the formation mechanisms of $H_3^+$ and $H_6^+$ is available, the formation of $H_2^+$ by ionization of $H_2$ molecules is most likely to be the first step in their production. $H_3^+$ may be produced by reaction (4.2) immediately after the ionization.[47] Theoretical studies have proposed that $H_6^+$ is produced by rearrangement reaction between H, $H_3^+$, and $H_2$.[54,55] Therefore, we may assume that reactions between $e_t^-$ and $H_3^+$ or $H_6^+$ as shown in reactions (4.8) and (4.9) correspond to the geminate recombination between parent $H_2^+$ and $e_t^-$.

The decay rate constant $K_e$ was estimated by fitting the exponential decay function,

$$-\frac{d[e_t^-]}{dt} = K_e[e_t^-], \tag{4.10}$$

using experimental results measured for 0 min $\leq t \leq$ 240 min. The $K_e$ value was determined to be 0.004 ± 0.002 $min^{-1}$ for p-$H_2$–o-$D_2$ (1 and 8 mol%). In general, $[e_t^-]$ follows a non-exponential decay function for geminate recombination in condensed matter due to the inhomogeneous distribution of cations and electrons,[56] but our method almost satisfies the fit.

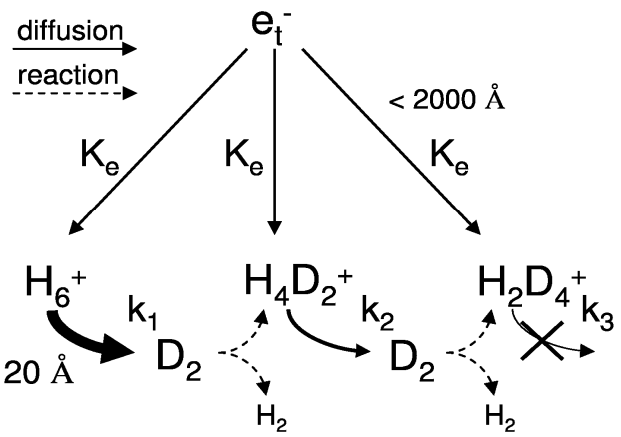


Figure 4.5. Schematic diagram representing the reactions of $e_t^-$, $H_6^+$, $H_4D_2^+$, and $H_2D_4^+$ in solid p-$H_2$–o-$D_2$ mixtures. Rate constants $K_e$, $k_1$, $k_2$, $k_3$ correspond to reactions (4.9) and (4.11)–(4.13), respectively.

### 4.4.3 Isotope condensation reactions of $H_6^+$

Figure 4.5 shows schematic diagrams for reactions involving $e_t^-$, $H_6^+$, $H_4D_2^+$, and $H_2D_4^+$ in solid p-$H_2$–o-$D_2$ mixtures. If $H_6^+$, $H_4D_2^+$, and $H_2D_4^+$ only decayed via geminate recombination with $e_t^-$, their decay rates would be the same as for $e_t^-$. However, while $H_2D_4^+$ decayed similarly to $e_t^-$, decay rates of $H_6^+$ and $H_4D_2^+$ were 6 and 1.5–3 times faster than that for $e_t^-$ in p-$H_2$–o-$D_2$ (1 mol%) (Figure 4.4). To explain these results, the isotope condensation reactions in solid p-$H_2$–o-$D_2$ mixtures were assumed to occur as,

$$H_6^+ + D_2 \xrightarrow{k_1} H_2 + H_4D_2^+ + 17\,\text{meV}, \tag{4.11}$$

$$H_4D_2^+ + D_2 \xrightarrow{k_2} H_2 + H_2D_4^+ + 18\,\text{meV}, \tag{4.12}$$

and

$$H_2D_4^+ + D_2 \xrightarrow{k_3} H_2 + D_6^+ + 19\,\text{meV}. \tag{4.13}.$$

Table 4.2. Zero-point vibrational energy (ZPE) in eV for $H_6^+$, $H_2$, and their isotopes calculate by using Gaussian09 program.

| Species | ZPE (eV)* | | |
|---|---|---|---|
| | MP2/6-311++G(3df, 3pd) Harmonic | MP2(full)/cc-pVQZ Harmonic | MP2(full)/cc-pVQZ Anharmonic |
| $H_6^+$ | 1.025 | 1.024 | 0.998 |
| $[H_2(H_2)HD]^+$ | 0.979 | 0.978 | 0.947 |
| $[H_2(HD)H_2]^+$ | 0.978 | 0.977 | 0.947 |
| $[HD(H_2)HD]^+$ | 0.932 | 0.931 | 0.900 |
| $[H_2(HD)HD]^+$ | 0.930 | 0.929 | 0.893 |
| $[HD(HD)HD]^+$ | 0.883 | 0.882 | 0.853 |
| $[H_2(H_2)D_2]^+$ | 0.926 | 0.925 | 0.894 |
| $[H_2(D_2)H_2]^+$ | 0.928 | 0.927 | 0.897 |
| $[D_2(H_2)D_2]^+$ | 0.826 | 0.826 | 0.810 |
| $[H_2(D_2)D_2]^+$ | 0.827 | 0.826 | 0.799 |
| $D_6^+$ | 0.725 | 0.725 | 0.715 |
| $H_2$ | 0.280 | 0.280 | - |
| HD | 0.243 | 0.243 | - |
| $D_2$ | 0.198 | 0.198 | - |

* Radical cations and neutral species were calculated by UHF (Unrestricted Hartree-Fock) and RHF (Restricted Hartree-Fock) methods, respectively, followed by a 2nd Møller-Plesset correlation energy correction truncated at second-order.

Note that the recombination reactions between $e_t^-$ and cations are also accompanied by the above reactions. The exothermic energies in reactions (4.11)–(4.13) were calculated from differences in zero-point energy (ZPE) at MP2/6-311++G(3df, 3pd) level using harmonic approximation between a reactant and a product listed in Table 4.2. Both MP2/6-311++G(3df, 3pd) and MP2(full)/cc-pVQZ methods have provided almost the same ZPEs with harmonic approximation. The energy differences in reactions (4.11)–(4.13), ranged from 17 to 19 meV, were much larger than the thermal energy at 4.2 K (0.4 meV), suggesting that reverse reactions cannot proceed. ZPEs treated with anharmonic vibration for these species also support the isotope condensation reactions

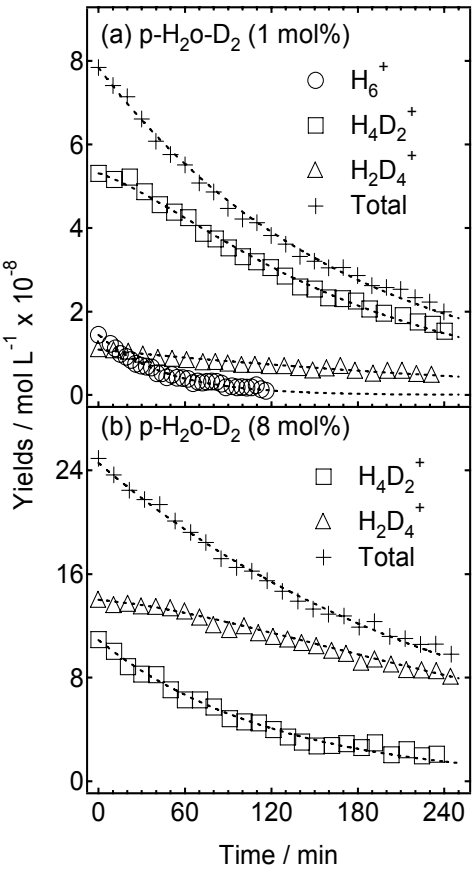


Figure 4.6. Time course of the yields of $H_6^+$ (open circles), $H_4D_2^+$ (open squares), and $H_2D_4^+$ (open triangles) and the total yield (crosses) in p-$H_2$–o-$D_2$ (a) 1 mol%, (b) 8 mol%. Broken lines are simulated decays obtained using $K_e$, $k_1$, $k_2$, and $k_3$ in Eqs. 4.14–4.16.

as shown in right column of Table 4.2.

To examine the quantitative validity of the proposed condensation reactions, we performed chemical kinetic analysis. The rate equations for $H_6^+$, $H_4D_2^+$, and $H_2D_4^+$ can be described as:

$$-\frac{d[\mathrm{H}_6^+]}{dt} = k_1[\mathrm{D}_2][\mathrm{H}_6^+] + K_\mathrm{e}'[\mathrm{H}_6^+], \tag{4.14}$$

$$-\frac{d[\mathrm{H}_4\mathrm{D}_2^+]}{dt} = -k_1[\mathrm{D}_2][\mathrm{H}_6^+] + k_2[\mathrm{D}_2][\mathrm{H}_4\mathrm{D}_2^+] + K_\mathrm{e}'[\mathrm{H}_4\mathrm{D}_2^+], \tag{4.15}$$

$$-\frac{d[\mathrm{H}_2\mathrm{D}_4^+]}{dt} = -k_2[\mathrm{D}_2][\mathrm{H}_4\mathrm{D}_2^+] + k_3[\mathrm{D}_2][\mathrm{H}_2\mathrm{D}_4^+] + K_\mathrm{e}'[\mathrm{H}_4\mathrm{D}_2^+], \tag{4.16}$$

where $k_1$, $k_2$, and $k_3$ are the rate constants for reactions (4.11)–(4.13), respectively, and

$K_e$' is the rate constant for the recombination involving $e_t^-$. Figure 4.6 shows the experimental decay curves of $H_6^+$ (open circles), $H_4D_2^+$ (open squares), and $H_2D_4^+$ (open triangles) in p-$H_2$–o-$D_2$ mixtures, along with the total decay curve (crosses). The simulated decay curves (broken lines) were found to coincide with experimental curves using $k_1$ of 0.045 L mol$^{-1}$ min$^{-1}$, $k_2$ of 0.0015 L mol$^{-1}$ min$^{-1}$, and $k_3$ of 0 L mol$^{-1}$ min$^{-1}$ for both p-$H_2$–o-$D_2$ samples (1 and 8 mol%). $K_e$' was determined to be 0.0058 min$^{-1}$ for p-$H_2$–o-$D_2$ (1 mol%) and 0.0039 min$^{-1}$ for p-$H_2$–o-$D_2$ (8 mol%) from the total decay curves, in close agreement with the $K_e$ value obtained in the previous section (0.004 ± 0.002 min$^{-1}$).

The rate-determining steps for reactions (4.11)–(4.13) may be the diffusion of $H_6^+$, $H_4D_2^+$, and $H_2D_4^+$ in solid p-$H_2$. Noticeable differences between $k_1$, $k_2$, and $k_3$ thus reflect differences in mobility between $H_6^+$, $H_4D_2^+$, and $H_2D_4^+$. $H_6^+$, $H_4D_2^+$, and $H_2D_4^+$ may diffuse via repeated hole hopping reactions as:

$$H_6^+ + H_2 \rightarrow H_2 + H_6^+, \tag{4.17}$$

$$H_4D_2^+ + H_2 \rightarrow H_2 + H_4D_2^+, \tag{4.18}$$

and

$$H_2D_4^+ + H_2 \rightarrow H_2 + H_2D_4^+. \tag{4.19}$$

The mobility of $H_6^+$ may drastically decrease with increasing number of deuterium atoms in $H_6^+$. Our hole hopping diffusion model described by the isotope condensation of $H_6^+$ is also sufficient to explain results observed for $H_5D^+$ and HD-sub. $H_4D_2^+$ was produced preferentially and decayed slower than $H_6^+$ in p-$H_2$–HD mixtures.[57]

## 4.5 Summary

We found that the yields of $e_t^-$ and $H_{6-n}D_n^+$ ($4 \geq n \geq 1$) increased significantly with increasing o-$D_2$ or HD concentrations in irradiated solid p-$H_2$, suggesting that both $e_t^-$ and $H_6^+$ are trapped by isotopic hydrogen molecules. Previous general methods, used to trap ionic species in local potential energy minima produced by cracks, distortions, and imperfections in the solids, could not be applied to electron and ion trapping in solid p-$H_2$ because of its self-annealing property. Isotope effects on induced dipole and quadrupole moments are proposed to generate local minima, allowing ionic species to be trapped in solid p-$H_2$. Electrons produced in solid p-$H_2$ were stabilized by neighboring o-$D_2$ and HD because the interaction energy between electrons and o-$D_2$ or HD was greater than with p-$H_2$. Previous reports[33, 36-38] on the enhancement of yields or electron lifetimes in several irradiated deuterated molecular crystals may be partly explained by our proposed mechanisms.

The chemical dynamics were elucidated quantitatively for the isotope condensation of $H_6^+$ to form $H_{6-n}D_n^+$ ($4 \geq n \geq 1$). $H_6^+$ diffused via repeated hole hopping in solid p-$H_2$ and reacted with o-$D_2$ or HD to produce $H_{6-n}D_n^+$ ($4 \geq n \geq 1$). The diffusion rates of $H_{6-n}D_n^+$ ($4 \geq n \geq 1$) by hole hopping were extremely slower than for $H_6^+$.

# References


[1] B. G. Ershov and A. K. Pikaev, Adv. Chem. Series, 1 (1968).
[2] B. G. Ershov, Khodzhae.Of, and A. K. Pikaev, Doklady Akademii Nauk Sssr **179**, 911 (1968).
[3] J. Zimbrick and L. Kevan, J. Chem. Phys. **47**, 2364 (1967).
[4] B. G. Ershov and A. K. Pikaev, Russ. J. Phys. Chem. **41**, 1394 (1967).
[5] L. Kevan, J. Am. Chem. Soc. **87**, 1481 (1965).
[6] M. J. Blandamer, M. C. R. Symons, and L. Shields, J. Chem. Soc., 4352 (1964).
[7] M. Ogasawara, M. Lindgren, A. Lund, and G. Nilsson, Chem. Phys. Lett. **117**, 254 (1985).
[8] T. Sasaki, Kawatsur.K, and S. Ohno, Chem. Lett., 91 (1972).
[9] L. Kevan and D. H. Chen, J. Chem. Phys. **49**, 1970 (1968).
[10] Habersbe.A, Collect. Czechoslovak Chem. Commun. **33**, 1925 (1968).
[11] A. Ekstrom and J. E. Willard, J. Phys. Chem. **72**, 4599 (1968).
[12] C. Chachaty, J. Chimi. Phys. **64**, 614 (1967).
[13] L. Shields, J. Phys. Chem. **69**, 3186 (1965).
[14] Blandame.Mj, L. Shields, and M. C. R. Symons, J. Chem. Soc., 1127 (1965).
[15] C. Chachaty and E. Hayon, J. Chimi. Phys. **61**, 1115 (1964).
[16] C. Chachaty, Comptes Rendus Hebdomadaires Des Seances De L Academie Des Sciences **259**, 2219 (1964).
[17] J. Lin, K. Tsuji, and F. Williams, J. Am. Chem. Soc. **90**, 2766 (1968).
[18] K. Tsuji, H. Yoshida, and K. Hayashi, J. Chem. Phys. **46**, 810 (1967).
[19] K. Tsuji and F. Williams, J. Am. Chem. Soc. **89**, 1526 (1967).
[20] D. R. Smith, F. Okenka, and J. J. Pieroni, Can. J. Chem. **45**, 833 (1967).
[21] A. D. Grishina, A. V. Vannikov, and N. M. Alpatova, Radiat. Phys. Chem. **11**, 289 (1978).
[22] H. Yoshida, D. Feng, and L. Kevan, J. Chem. Phys. **58**, 4924 (1973).
[23] H. Yoshida, M. Ogasawara, T. Warashina, and T. Higashimura, J. Chem. Phys. **56**, 4238 (1972).
[24] H. Yoshida, L. Kevan, and D. F. Feng, J. Am. Chem. Soc. **94**, 8922 (1972).
[25] S. Noda, K. Fueki, and Z. Kuri, Chem. Phys. Lett. **8**, 407 (1971).
[26] K. Tsuji and F. Williams, J. Phys. Chem. **73**, 4017 (1969).
[27] Cronenwe.W and M. C. R. Symons, J. Chem. Soc., 2991 (1968).
[28] Y. Tabata, Y. Ito, and S. Tagawa, *CRC handbook of radiation chemistry* (CRC Press, Boca Raton, 1991).
[29] A. Lund and M. Shiotani, *Radical Ionic Systems* (Kluwer Academic Publishers, Boston, 1991).
[30] L. Kevan, J. Phys. Chem. **84**, 1232 (1980).
[31] L. Kevan, J. Phys. Chem. **82**, 1144 (1978).
[32] D. C. Walker, J. Phys. Chem. **84**, 1140 (1980).
[33] H. Hase and K. Kawabata, J. Chem. Phys. **65**, 64 (1976).
[34] P. O. Samskog, L. D. Kispert, and A. Lund, J. Chem. Phys. **78**, 5790 (1983).
[35] T. Kumada, S. Mori, J. Kumagai, Y. Aratono, and T. Miyazaki, J. Phys. Chem. A **103**, 8966 (1999).
[36] H. Y. Wang and J. E. Willard, J. Chem. Phys. **69**, 2964 (1978).
[37] Y. Gauduel, S. Pommeret, A. Migus, and A. Antonetti, J. Phys. Chem. **95**, 533 (1991).
[38] R. A. Crowell and D. M. Bartels, J. Phys. Chem. **100**, 17713 (1996).
[39] T. Kumada, M. Sakakibara, T. Nagasaka, H. Fukuta, J. Kumagai, and T. Miyazaki, J. Chem. Phys. **116**, 1109 (2002).
[40] T. Kumada, J. Kumagai, and T. Miyazaki, J. Chem. Phys. **114**, 10024 (2001).
[41] S. Tam, M. E. Fajardo, H. Katsuki, H. Hoshina, T. Wakabayashi, and T. Momose, J. Chem. Phys. **111**, 4191 (1999).
[42] T. Kumada, N. Kitagawa, T. Noda, J. Kumagai, Y. Aratono, and T. Miyazaki, Chem. Phys. Lett. **288**, 755 (1998).
[43] T. Oka, Ann. Rev. Phys. Chem. **44**, 299 (1993).
[44] S. M. Blinder, J. Chem. Phys. **35**, 974 (1961).
[45] S. M. Blinder, J. Chem. Phys. **32**, 582 (1960).
[46] S. M. Blinder, J. Chem. Phys. **32**, 105 (1960).
[47] P. C. Souers, *Hydrogen Properties for Fusion Energy* (University of California Press, Berkeley, 1986).
[48] J. D. Poll and J. L. Hunt, Can. J. Phys. **63**, 84 (1985).
[49] R. L. Brooks, S. K. Bose, J. L. Hunt, J. R. Macdonald, J. D. Poll, and J. C. Waddington, Phys. Rev. B **32**, 2478 (1985).

[50] J. J. Miller, J. D. Poll, and J. L. Hunt, Can. J. Phys. **69**, 606 (1991).
[51] T. Miyazaki, *Atom Tunneling Phenomena in Physics, Chemistry and Biology* (Springer, Berlin, 2004).
[52] T. Kumada, Phys. Rev. B **68** (2003).
[53] T. Miyazaki, M. Kato, and K. Fueki, Radiat. Phys. Chem. **36**, 501 (1990).
[54] Y. Kurosaki and T. Takayanagi, J. Chem. Phys. **109**, 4327 (1998).
[55] Y. Kurosaki and T. Takayanagi, Chem. Phys. Lett. **293**, 59 (1998).
[56] G. R. Freeman, *Kinetics of Nonhomogeneous processes* (John Wiley & Sons, New York, 1987).
[57] J. Kumagai, H. Inagaki, S. Kariya, T. Ushida, Y. Shimizu, and T. Kumada, J. Chem. Phys. **127** (2007).

# 5 Conclusion

## 5.1 Summary

We have reported totally more than 50 ESR lines in γ-ray irradiated solid p-$H_2$, p-$H_2$-ortho-$D_2$ (o-$D_2$), and p-$H_2$-HD mixtures.[1, 2] The lines were assigned to $H_2^+$-core $H_6^+$ and its isotopomers such as $H_5D^+$, $H_4D_2^+$, $H_2D_4^+$. All experimental ESR spectra were reproduced by small number of parameters as a nuclear spin quantum numbers, isotropic hyperfine coupling constants (HFCCs), and *g*-value for these lines. Theoretical calculation of the HFCC and *g*-value of $H_6^+$ show a good agreement with the experimental ones.[3, 4] The observation of $H_2^+$-core $H_6^+$ denies the widely accepted idea that even membered $H_n^+$ ions ($n \geq 6$) exclusively have $H_3^+$-cored structure.

The experimental results for $H_6^+$ and its isotopomers revealed that distribution of unpaired electron was distorted by substituting deuterons for protons, which is not expected by theoretical calculation under the Born-Oppenheimer approximation.[1, 5] We concluded that $H_6^+$ ions possess the $D_{2d}$ symmetry, whereas $H_4D_2^+$ and $H_5D^+$ in which one of the side-on $H_2$'s in $H_6^+$ is substituted by $D_2$ or HD, have $C_{2v}$ symmetry. This should be due to the difference in the effect of anharmonic term of electric wavefunction in $H_4D_2^+$ and $H_5D^+$. The averaged $H_2^+$-$D_2$ ($H_2^+$-HD) distance is estimated to be smaller than the $H_2^+$-$H_2$ one by 4% (2%) in $H_4D_2^+$ ($H_5D^+$) based on the comparison of hyperfine coupling constants on two protons in $H_2^+$ core experimentally determined with theoretically predicted parameters.[1]

In spite of the good agreement of isotropic HFCCs with theoretical predictions,

anisotropic HFCC differ greatly from the theoretical ones.[6] We carried out ESR measurements on $H_6^+$ and $H_4D_2^+$, both at 4.2 K and 1.7 K to compared anisotropic HFCCs with theoretical calculation. We concluded that $H_6^+$ is in precessional motion at precessional angle of 57° along the *c*-axis of substitutional *hcp* cage in solid p-$H_2$ both at 4.2 and 1.7 K. Although $H_4D_2^+$ is also in the precessional motion at 4.2 K, the precession is stopped at 1.7 K. The deference should be due to lager moment of inertia and lower molecular symmetry in $H_4D_2^+$.[6]

We have found that isotope condensation reactions of $H_6^+$ such as $H_6^+ + D_2 \rightarrow H_2 + H_4D_2^+$ in solid p-$H_2$.[1, 7] The chemical dynamics of the reactions in the solid were elucidated quantitatively with only three reaction rate constants. $H_6^+$ diffused via repeated hole hopping in solid p-$H_2$ and reacted with $D_2$ or HD to produce $H_{6-n}D_n^+$ ($4 \geq n$). The diffusion rates for $H_6^+$ drastically decreased with increasing number of deuterium atoms in $H_6^+$ and that for $H_2D_4^+$ was quasi zero. The total yield of $H_6^+$ and its isotopomers increased significantly with increasing $D_2$ or HD concentrations in irradiated solid p-$H_2$. These results indicate that $H_6^+$ is stabilized by the condensation reactions with $D_2$ and HD.[7]

Similar to $H_6^+$, the $e_t^-$ yield was drastically increased with increasing $D_2$ or HD concentrations in irradiated solid p-$H_2$.[7, 8] In general trapped electrons cannot be detected in crystalline phase but were observed in the solid p-$H_2$ crystal related with the concentration of $D_2$ or HD. This new isotope effect is probably due to induced dipole and quadrupole moments between the trapped electrons acting as making local potential minima, allowing electrons to be trapped in solid p-$H_2$. Electrons produced in solid p-$H_2$ were stabilized by neighboring $D_2$ and HD because the interaction energy between electrons and $D_2$ or HD was greater than that with p-$H_2$. Previous reports on the

enhancement of yields or electron lifetime in several irradiated deuterated molecular crystals may be partly explained by our proposed mechanisms.[7]

Owing to the homogeneous property of solid p-$H_2$ and the low temperature, we can reveal a lot of physical and chemical properties on $H_6^+$, which are behind in complicated interactions at room temperature. The direct detection and assignment of $H_2^+$-core $H_6^+$ ($D_{2d}$) and its isotopomers boosted up variety of fields of study.[5, 9, 10] Hao *et al*.[10] employed *ab initio* molecular electronic structure theory in order to systematically investigate six isomers of the $H_6^+$ ions. They concluded that the $H_2^+$-core cluster with $D_{2d}$ symmetry has been confirmed to be the global minimum on the $H_6^+$ potential energy surface. Not only theoretical studies, but also experimental studies were affected by our results. Jaksch *et al*.[11] reported that the large even-numbered $H_n^+$ can be formed by electron-impact ionization of hydrogen clusters embedded in helium nanodroplets. They suggested that these clusters should have a $H_6^+$ core.

## 5.2 Prospect of future study

Studies of chemical reactions in solid hydrogen are definite and potential method for the understanding of nature of low-temperature chemistry as well as molecular evolution in interstellar space. Recently, it is becoming increasingly clear that chemical reactions on cosmic dust in dense clouds, which are characterized by very low temperature (~10 K) and high densities ($10^4$ – $10^8$ $cm^{-3}$), play an important role rather than in gas-phase ion-molecule reactions.[12] In 2010, Kaneda *et al*. obtain clear evidence that emissions of the polycyclic aromatic hydrocarbons come predominantly from the

dust lane of the galaxy. They also detect molecular hydrogen line emissions from the dust lane. Hydrogen is the most abundant molecule in the space so that it is possible that solid hydrogen is major molecules on cosmic dust surface.[13]

In this thesis, we revealed that the diffusion and isotope condensation reactions of $H_6^+$ in solid p-$H_2$, which are very similar to that of $H_3^+$ in dark nebulae. These isotope condensations are in good agreement with the extremely high deuterium fractionation in the cold cores of dark clouds, where multiply deuterated molecules such as $D_2CO$, $ND_3$, and $CD_3OH$ have been discovered.[14] $H_6^+$ may play an important role of chemical reactions in solid p-$H_2$ because of its mobility and oxidation activity.

Not only $H_6^+$ but also H atom, which is also detected in irradiated solid hydrogen by ESR measurement,[15-21] should play important role in chemical reactions because the yield of H atom is ~5000 times larger than that of $H_6^+$.[7] Very recently, we perform ESR study on H atoms and $CH_3$ radicals produced in solid hydrogen, and found highly selective radical - radical reactions not governed by diffusion rate. Figure 5.1 shows the time course of H atoms and $CH_3$ radicals produced in solid hydrogen. $CH_3$ radicals did not decay although H atoms decay with a half-life of 600 min. H atom produced in solid $H_2$ can not react with $CH_3$ radical as $CH_3 + H \rightarrow CH_4$ having no or quite small reaction barrier height although H atoms diffused in solid hydrogen to recombine with other H atoms as $H + H \rightarrow H_2$. We have concluded that H diffuse in solid hydrogen eliminating $CH_3$. We also found that H atoms left from $D_2$ molecules although $H_6^+$ ions were trapped by $D_2$ molecules. These results may suggest the reactions in solid hydrogen are partly dominated by long-range interactions such as dipole-dipole interactions, although further experimental data and theoretical treatment for solid phase reactions are essential for developing this study.

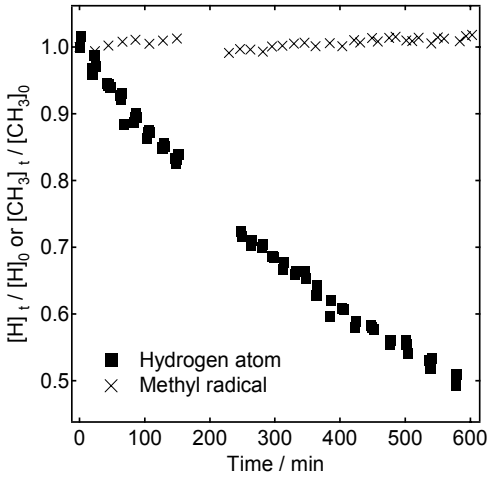


Figure 5.1. Time course of the yields of H atoms and $CH_3$ radicals in solid hydrogen at 4.2 K.

In order to study the chemical reactions in solid hydrogen, porous silica such as silica aero gel or silica gel as substrates of solid hydrogen is useful for two reasons. First, abundant solute molecules can be introduced into solid hydrogen by adsorbing the molecules to the gel. Second, silica aero gel or silica gel may be assumed to the core of the cosmic dust whose component is silicates. I hope the thesis of $H_6^+$ in solid hydrogen will become a “Rosetta stone” of low temperature chemistry and physics, as well as molecular evolution in interstellar space.

# References


[1] J. Kumagai, H. Inagaki, S. Kariya, T. Ushida, Y. Shimizu, and T. Kumada, J. Chem. Phys. **127** (2007).

[2] T. Kumada, Y. Shimizu, T. Ushida, and J. Kumagai, Rad. Phys. Chem. **77**, 1318 (2008).

[3] Y. Kurosaki and T. Takayanagi, Chem. Phys. Lett. **293**, 59 (1998).

[4] Y. Kurosaki and T. Takayanagi, J. Chem. Phys. **109**, 4327 (1998).

[5] Y. Kurosaki, Y. Shimizu, and J. Kumagai, Chem. Phys. Lett. **455**, 59 (2008).

[6] Y. Shimizu, T. Kumada, and J. Kumagai, J. Magn. Reson. **194**, 76 (2008).

[7] Y. Shimizu, M. Inagaki, T. Kumada, and J. Kumagai, J. Chem. Phys. **132** (2010).

[8] T. Kumada, S. Mori, J. Kumagai, Y. Aratono, and T. Miyazaki, J. Phys. Chem. A **103**, 8966 (1999).

[9] A. Kakizaki, T. Takayanagi, and M. Shiga, Chem. Phys. Lett. **449**, 28 (2007).

[10] Q. Hao, A. C. Simmonett, Y. Yamaguchi, D. C. Fang, and H. F. Schaefer, J. Phys. Chem. A **113**, 13608 (2009).

[11] S. Jaksch, et al., J. Chem. Phys. **129** (2008).

[12] T. J. Millar and D. A. Williams, *Dust and chemistry in astronomy* (Institute of Physics Pub., Bristol; Philadelphia, 1993).

[13] H. Kaneda, T. Onaka, I. Sakon, T. Kitayama, Y. Okada, T. Suzuki, D. Ishihara, and M. Yamagishi, Astrophys. J. Lett. **716**, L161 (2010).

[14] T. R. Geballe and T. Oka, Science **312**, 1610 (2006).

[15] T. Kumada, M. Sakakibara, T. Nagasaka, H. Fukuta, J. Kumagai, and T. Miyazaki, J. Chem. Phys. **116**, 1109 (2002).

[16] T. Miyazaki, H. Tsuruta, and K. Fuekl, J. Phys. Chem. **87**, 1611 (1983).

[17] T. Miyazaki, Bull. Chem. Soc. Jpn. **58**, 2413 (1985).

[18] T. Miyazaki and K. P. Lee, J. Phys. Chem. **90**, 400 (1986).

[19] T. Miyazaki, N. Iwata, K. P. Lee, and K. Fueki, J. Phys. Chem. **93**, 3352 (1989).

[20] T. Miyazaki, N. Iwata, K. Fueki, and H. Hase, J. Phys. Chem. **94**, 1702 (1990).

[21] T. Miyazaki, S. Mori, T. Nagasaka, J. Kumagai, Y. Aratono, and T. Kumada, J. Phys. Chem. A **104**, 9403 (2000).

# Appendix

## A. Energy levels and resonance condition for one unpaired electron and two-proton system

Spin Hamiltonian for one unpaired electron and two proton system in magnetic field $H_0$ // z is given by

$$\mathrm{H} = g\mu_B S_z H_0 - g_n \mu_N (I_{1z} + I_{2z}) H_0 + g\mu_B (A_1 I_1 + A_2 I_2) S \equiv \mathrm{H}_0 + \mathrm{H}'. \qquad \text{(A1)}$$

The third them H' = g $\mu_B$ ($A_1$ $I_1$ + $A_2$ $I_2$)$S$ is referred as a perturbation against the main term $\mathrm{H}_0 = g\mu_B S_z H_0 - g_n \mu_N (I_{1z} + I_{2z}) H_0$. Eigenvalues and corresponding eigenstates at $A_1 > A_2$ are obtained using a second-order perturbation theory on non-degenerate states.

$$E_0(+,+,+) = \frac{g\mu_B}{4}(2H_0 + A_1 + A_2) - g_n \mu_N H_0$$

$$\text{for } \left| S_z = \frac{1}{2}, I_{1z} = \frac{1}{2}, I_{2z} = \frac{1}{2} \right\rangle, \qquad \text{(A2)}$$

$$E_0(+,-,+) = \frac{g\mu_B}{4}\left(2H_0 - A_1 + A_2 + \frac{{A_1}^2}{H_0}\right)$$

$$\text{for } \left| \frac{1}{2}, -\frac{1}{2}, \frac{1}{2} \right\rangle + \varepsilon_1 \left| -\frac{1}{2}, \frac{1}{2}, \frac{1}{2} \right\rangle, \qquad \text{(A3)}$$

$$E_0(+,+,-) = \frac{g\mu_B}{4}\left(2H_0 + A_1 - A_2 + \frac{{A_2}^2}{H_0}\right)$$

$$\text{for } \left| \frac{1}{2}, \frac{1}{2}, -\frac{1}{2} \right\rangle + \varepsilon_2 \left| -\frac{1}{2}, \frac{1}{2}, \frac{1}{2} \right\rangle, \qquad \text{(A4)}$$

$$E_0(+,-,-) = \frac{g\mu_B}{4}\left(2H_0 - A_1 - A_2 + \frac{{A_1}^2 + {A_2}^2}{H_0}\right) + g_n \mu_N H_0$$

$$\text{for } \left|\frac{1}{2},-\frac{1}{2},-\frac{1}{2}\right\rangle+\varepsilon_1\left|-\frac{1}{2},\frac{1}{2},-\frac{1}{2}\right\rangle+\varepsilon_2\left|-\frac{1}{2},-\frac{1}{2},\frac{1}{2}\right\rangle, \quad \text{(A5)}$$

$$E_0(-,+,+)=\frac{g\mu_B}{4}\left(-2H_0+A_1+A_2-\frac{{A_1}^2+{A_2}^2}{H_0}\right)-g_n\mu_N H_0$$

$$\text{for } \left|-\frac{1}{2},\frac{1}{2},\frac{1}{2}\right\rangle-\varepsilon_1\left|\frac{1}{2},-\frac{1}{2},\frac{1}{2}\right\rangle-\varepsilon_2\left|\frac{1}{2},\frac{1}{2},-\frac{1}{2}\right\rangle, \quad \text{(A6)}$$

$$E_0(-,-,+)=\frac{g\mu_B}{4}(-2H_0+A_1-A_2-\frac{{A_2}^2}{H_0})$$

$$\text{for } \left|-\frac{1}{2},-\frac{1}{2},\frac{1}{2}\right\rangle+\varepsilon_2\left|\frac{1}{2},-\frac{1}{2},-\frac{1}{2}\right\rangle, \quad \text{(A7)}$$

$$E_0(-,+,-)=\frac{g\mu_B}{4}(-2H_0-A_1+A_2-\frac{{A_1}^2}{H_0})$$

$$\text{for } \left|-\frac{1}{2},\frac{1}{2},-\frac{1}{2}\right\rangle+\varepsilon_1\left|\frac{1}{2},-\frac{1}{2},-\frac{1}{2}\right\rangle, \quad \text{(A8)}$$

$$E_0(-,-,-)=\frac{g\mu_B}{4}(-2H_0+A_1+A_2)+g_n\mu_N H_0$$

$$\text{for } \left|-\frac{1}{2},-\frac{1}{2},-\frac{1}{2}\right\rangle, \quad \text{(A9)}$$

with

$$\varepsilon_1=\frac{{}_{\pm\mp+}V_{\mp\pm+}}{g\mu_B H_0}=\frac{{}_{\pm\mp-}V_{\mp\pm-}}{g\mu_B H_0}=\frac{A_1}{2g\mu_B H_0}, \quad \text{(A10)}$$

$$\varepsilon_2=\frac{{}_{\pm+\mp}V_{\mp+\pm}}{g\mu_B H_0}=\frac{{}_{\pm-\mp}V_{\mp-\pm}}{g\mu_B H_0}=\frac{A_2}{2g\mu_B H_0}, \quad \text{(A11)}$$

and

$${}_{\pm\pm\pm}V_{\pm\pm\pm}=\left\langle\pm\frac{1}{2},\pm\frac{1}{2},\pm\frac{1}{2}\middle|H'\middle|\pm\frac{1}{2},\pm\frac{1}{2},\pm\frac{1}{2}\right\rangle.$$

In case of $A_1 \approx A_2$, that is, $E(\pm - +) \approx E(\pm + -)$, these eigenstates mix each other to be,

$$E(+,\pm,\mp) = E_0(+,\pm,\mp) + \frac{1}{2}\left\{ \begin{array}{l} {}_{+\pm\mp}V_{+\pm\mp} + {}_{+\mp\pm}V_{+\mp\pm} \\ \pm\sqrt{\left({}_{+\pm\mp}V_{+\pm\mp} - {}_{+\mp\pm}V_{+\mp\pm}\right)^2 + 4\left|{}_{+\pm\mp}V_{+\mp\pm}\right|^2} \end{array} \right\}$$

$$= \frac{g\mu_B}{2}\left\{ \begin{array}{l} H_0 + \dfrac{A_1^{\,2} + A_2^{\,2}}{4H_0} \\ \pm\sqrt{\left(\dfrac{A_1 - A_2}{2} + \dfrac{-A_1^{\,2} + A_2^{\,2}}{4H_0}\right)^2 + 4\left(\dfrac{A_1 A_2}{4H_0}\right)^2} \end{array} \right\} \quad , \qquad \text{(A12)}$$

$$E(-,\pm,\mp) = E_0(-,\pm,\mp) + \frac{1}{2}\left\{ \begin{array}{l} {}_{-\pm\mp}V_{-\pm\mp} + {}_{-\mp\pm}V_{-\mp\pm} \\ \pm\sqrt{\left({}_{-\pm\mp}V_{-\pm\mp} - {}_{-\mp\pm}V_{-\mp\pm}\right)^2 + 4\left|{}_{-\pm\mp}V_{-\mp\pm}\right|^2} \end{array} \right\}$$

$$= -\frac{g\mu_B}{2}\left\{ \begin{array}{l} H_0 + \dfrac{A_1^{\,2} + A_2^{\,2}}{4H_0} \\ \pm\sqrt{\left(\dfrac{A_1 - A_2}{2} + \dfrac{A_1^{\,2} - A_2^{\,2}}{4H_0}\right)^2 + 4\left(\dfrac{A_1 A_2}{4H_0}\right)^2} \end{array} \right\} \quad , \qquad \text{(A13)}$$

and

$$E(\pm,\pm,\pm) = E_0(\pm,\pm,\pm)$$

$$E(\pm,\mp,\mp) = E_0(\pm,\mp,\mp)$$

Here, the second-order perturbation theory on nearly degenerate two states is employed on Equations (A12) and (A13). Since ESR absorption takes place between the levels $\{S_z, I_{1z}, I_{2z}\}$ and $\{S_z + 1, I_{1z}, I_{2z}\}$, the resonance conditions for ESR spectroscopy are given by

$$h\nu = \left\{ \begin{array}{l} E'(+,+,-) - E'(-,+,-), \\ E'(+,-,+) - E'(-,-,+), \\ E(+,+,+) - E(-,+,+), \\ E(+,-,-) - E(-,-,-). \end{array} \right. \qquad \text{(A14)}$$

By substituting Equations (A2), (A5), (A6), (A9), (A12), (A13) into (A14),

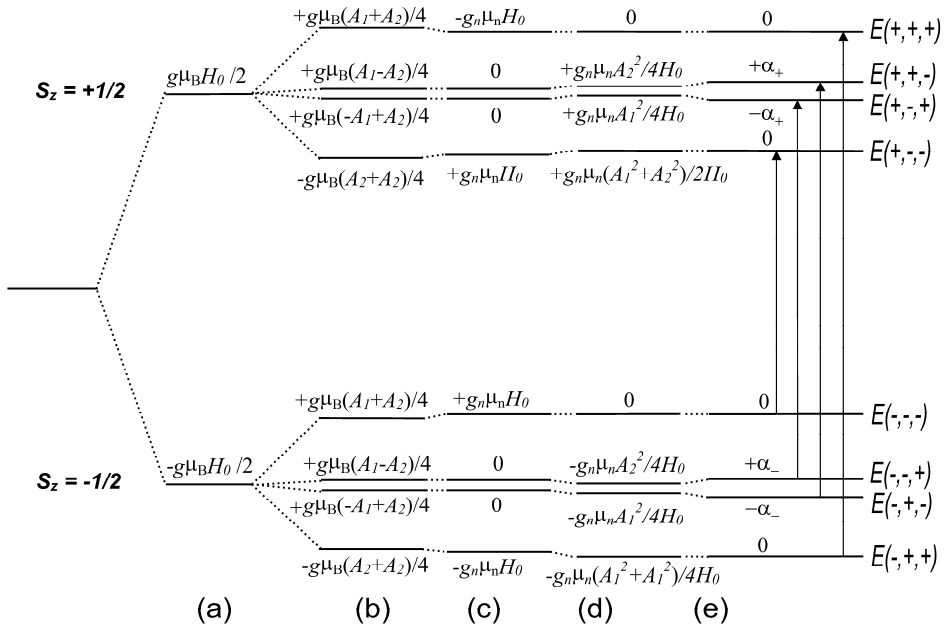


Figure A1. Spin energy levels of one unpaired electron and two-proton system: (a) Zeeman energy of unpaired electron; (b) First-order hyperfine interaction; (c) nuclear Zeeman energy; (d) Second-order hyperfine interaction between $S_z = \pm 1 / 2$ states obtained by second-order perturbation theory between non-degenerate states; (e) Same as (d) but between same $S_z$ states.

$$\alpha_+ = \sqrt{\left(\frac{A_1 - A_2}{2} + \frac{-A_1^2 + A_2^2}{4H_0}\right)^2 + 4\left(\frac{A_1 A_2}{4H_0}\right)^2} \approx \sqrt{\Delta A^2 + \left(\frac{A_{ctr}^2}{2H_0}\right)^2},$$

and

$$\alpha_- = \sqrt{\left(\frac{A_1 - A_2}{2} + \frac{A_1^2 - A_2^2}{4H_0}\right)^2 + 4\left(\frac{A_1 A_2}{4H_0}\right)^2} \approx \sqrt{\Delta A^2 + \left(\frac{A_{ctr}^2}{2H_0}\right)^2}.$$

Arrows show the allowed ESR transitions whose resonance conditions are given in Equation (A17).

$$\frac{h\nu}{g\mu_B} = H_0 + \frac{A_1 + A_2}{2}(I_{1z} + I_{2z}) + \frac{A_1^2 + A_2^2}{4H_0} + \frac{I_{1z} - I_{2z}}{2}\left\{\begin{array}{l}\sqrt{\left(\frac{A_1 - A_2}{2} + \frac{-A_1^2 + A_2^2}{4H_0}\right)^2 + \left(\frac{A_1 A_2}{2H_0}\right)^2}, \\ +\sqrt{\left(\frac{A_1 - A_2}{2} + \frac{A_1^2 - A_2^2}{4H_0}\right)^2 + \left(\frac{A_1 A_2}{2H_0}\right)^2}\end{array}\right\}, \quad \text{(A15)}$$

is obtained. This equation approaches

$$\frac{h\nu}{g\mu_B} = H_0 + A_1 I_{1z} + A_2 I_{2z} + \frac{A_1^2 + A_2^2}{4H_0}, \quad \text{(A16)}$$

at the $A_1 - A_2 >> A_1 A_2 / H_0$ asymptotic limit, where the mixing of $E(\pm, +,-)$ and $E(\pm, -, +)$ states is not taken into account. On the other hand, in case of $A_1 \approx A_2$, Equation (A15) is simplified using $\Delta A = (A_1 - A_2) / 2$, $A_{ctr} = (A_1 + A_2) / 2$ to be

$$\frac{h\nu}{g\mu_B} = H_0 + A_{ctr}\left(I_{1z} + I_{2z}\right) + \frac{{A_{ctr}}^2}{2H_0} + \left(I_{1z} - I_{2z}\right)\sqrt{\Delta A^2 + \left(\frac{{A_{ctr}}^2}{2H_0}\right)^2}\ , \qquad \text{(A17)}$$

which coincides with Equation (8) with $I_{12} = I_1 + I_2$ and $I_{12z} = I_{1z} + I_{2z}$ at $\Delta A \rightarrow 0$.

# B. Simulation programs for $H_6^+$ and its isotopomers

Computer programs for simulations of ESR spectra of $H_6^+$ and its isotopomres. These are written as the “Igor Procedures” for IGOR Pro 4.04J (WaveMetrics , Inc.). The numbers of the line head show the line numbers.

```
0001 #pragma rtGlobals=1 // Use modern global access
     method.
0002
0003 //Simulation ver.10//
0004
0005
0006 menu "simulation"
0007          "H2H2H2"
0008          "H2H2D2"
0009          "H2H2HD"
0010          "H2HDH2"
0011          "H2HDHD"
0012          "HDH2HD"
0013          "H2D2H2"
0014          "H2D2D2"
0015          "D2D2D2"
0016 end
0017
0018
0019 ////////////////////////////////////////////////////////////////////////////
0020 //
0021 // This is the function to get the solution to an equation
0022 //
0023 ////////////////////////////////////////////////////////////////////////////
0024
0025 function
     getH(hpoint,type,Aciso,dAciso,ani,dani,A5,A6,As,Iz12,I
     z1,Iz2,I5,I6,Iz5,Iz6,Iz56,I12,I1,I2,I56,H0,A1,A2)
0026 variable
     hpoint,type,Aciso,dAciso,ani,dani,A5,A6,As,Iz12,Iz1,Iz2
     ,I5,I6,Iz5,Iz6,Iz56,I12,I1,I2,I56,H0,A1,A2
0027 variable a,b,h,tmp
0028 a = 250
0029 b = 400
0030 do
0031 h = (a + b) / 2
0032 if(H0 >
     peak(type,Aciso,dAciso,ani,dani,A5,A6,As,Iz12,Iz1,Iz2,I
     5,I6,Iz5,Iz6,Iz56,I12,I1,I2,I56,H0,h,A1,A2))
0033 a = h
0034 elseif(H0 ==
     peak(type,Aciso,dAciso,ani,dani,A5,A6,As,Iz12,Iz1,Iz2,I
     5,I6,Iz5,Iz6,Iz56,I12,I1,I2,I56,H0,h,A1,A2))
0035 break
0036 else
0037 b = h
0038 endif
0039 while( (0.000000001 < (a-b)/2) || (-0.000000001 >
     (a-b)/2) ) // Get resonance field
0040 return h
0041 end
0042
0043
0044 ////////////////////////////////////////////////////////////////////////////
0045 //
0046 // This is the function to get the resonant magnetic fields
0047 //
0048 ////////////////////////////////////////////////////////////////////////////
0049
0050 function
     peak(type,Aciso,dAciso,ani,dani,A5,A6,As,Iz12,Iz1,Iz2,I
```

```
    5,I6,Iz5,Iz6,Iz56,I12,I1,I2,I56,H0,h,A1,A2) // Get
    resonance conditions
0051 variable
    type,Aciso,dAciso,ani,dani,A5,A6,As,Iz12,Iz1,Iz2,I5,I6,I
    z5,Iz6,Iz56,I12,I1,I2,I56,H0,h,A1,A2
0052 variable y
0053 if (type == 0)
0054 y =
    h+(Aciso+ani)*(Iz12)+(((Aciso-ani)^2)*(I12*(I12+1)-Iz1
    2^2)/(2*h)) // Equation of resonance condition of H6+
0055 return y
0056 endif
0057 if (type == 1)
0058 y = h+(Aciso+ani)*((Iz1)+(Iz2))+(((Aciso-ani)^2)/(2*h))
    +((Iz1)-(Iz2))*( ((dAciso+dani)^2)+(((Aciso-ani)^2)/(2*h
    ))^2)^(1/2) +As*Iz56 // Equation of resonance condition
    of H4D2+
0059 return y
0060 endif
0061 if (type == 2)
0062 y = h+(Aciso+ani)*(Iz1+Iz2)+(((Aciso-ani)^2)/2/h)
    +(Iz1-Iz2)*(((dAciso+dani)^2)+(((Aciso-ani)^2)/2/h)^2)^
    (1/2) +A5*Iz5+((As^2)/4/h)^2 +A6*Iz6
0063 return y
0064 endif
0065 if (type == 3)
0066 y = h+(A1+ani)*(Iz1)+(A2+ani/6.514)*(Iz2)+
    (((A1-ani)^2)/2+((A2-ani/6.514)^2)*(2-Iz2^2))/(2*h)
0067 return y
0068 endif
0069 if (type == 4)
0070 y = h+(A1)*(Iz1)+(A2)*(Iz2)+
    ((A1^2)/2+(A2^2)*(2-Iz2^2))/(2*h) +
    (Iz1-Iz2)*(((dAciso+dani)^2)+(((Aciso-ani)^2)/2/h)^2)^(
    1/2) +A5*Iz5+((As^2)/4/h)^2 +A6*Iz6
0071 return y
0072 endif
0073 if (type == 5)
0074 y =
    h+(Aciso)*(Iz12)+(((Aciso)^2)*(I12*(I12+1)-Iz12^2)/(2
    *h))+(A5)*(Iz5)+(((A5)^2)*(I5*(I5+1)-Iz5^2)/(2*h))+A6
    *Iz6 //HDH2HD
0075 return y
0076 endif
0077 if (type == 6)
0078 y = h+Aciso*Iz12 +
    ((Aciso^2)*(I12*(I12+1)-Iz12^2))/(2*h)    +
    A5*(Iz5+Iz6)
0079 return y
0080 endif
0081 if (type == 7)
0082 y =
    h+(Aciso+ani)*(Iz12)+(((Aciso-ani)^2)*(I12*(I12+1)-Iz1
    2^2)/(2*h)) // H2D2H2
0083 return y
0084 endif
0085 end
0086
0087
0088 ////////////////////////////////////////////////////////////////////////////
0089 //
0090 // These are the function to make line shapes
0091 //
0092 ////////////////////////////////////////////////////////////////////////////
0093
0094 function
    gau_f(lineshape,quality,hpoint,width,linefunction,laxis,ha
    xis,hpr,hpd)
0095
0096 wave lineshape
0097 variable
    quality,hpoint,width,linefunction,laxis,haxis,hpr,hpd
0098 variable dh =hpr-hpd
0099 variable boundary1 = width //mT
0100 Make/O/D/N=(hpoint) gx; SetScale x 0, 2*PI, gx;gx=0
0101 SetScale/I x laxis,haxis,"mT", gx
0102 variable k=0
0103 variable sigma = width
0104 variable C =0
0105 variable point
0106 if(linefunction==1)//gaussian
0107 if (dh>0)
0108 for (point=x2pnt(lineshape,hpd-quality*sigma);
    point<=x2pnt(lineshape,hpr+quality*sigma); point+=1)
0109 for (k=-x2pnt(lineshape,laxis+quality*sigma);
    k<=x2pnt(lineshape,laxis+quality*sigma); k+=1)
0110 gx[point]+=(exp( (-(pnt2x(lineshape, k)-laxis)^2)/
    (2*sigma^2)))*lineshape[point+k]
0111 C+=exp( (-(pnt2x(lineshape, k)-laxis)^2)/ (2*sigma^2))
0112 endfor
0113 gx[point]=gx/C
0114 C=0
0115 endfor
0116 lineshape=gx
0117 else
0118 for (point=x2pnt(lineshape,hpr-quality*sigma);
    point<=x2pnt(lineshape,hpd+quality*sigma); point+=1)
0119 for (k=-x2pnt(lineshape,laxis+quality*sigma);
    k<=x2pnt(lineshape,laxis+quality*sigma); k+=1)
0120 gx[point]+=(exp( -((pnt2x(lineshape,
    k)-laxis)^2)/(2*sigma^2)    ))*lineshape[point+k]
0121 C+=exp( (-(pnt2x(lineshape, k)-laxis)^2)/ (2*sigma^2))
0122 endfor
0123 gx[point]=gx/C
0124 C=0
0125 endfor
0126 lineshape=gx
0127 endif
0128 endif
0129 if(linefunction==0)//laurenz
0130 if (dh>0)
0131 for (point=x2pnt(lineshape,hpd-quality*sigma);
    point<=x2pnt(lineshape,hpr+quality*sigma); point+=1)
0132 for (k=-x2pnt(lineshape,laxis+quality*sigma);
    k<=x2pnt(lineshape,laxis+quality*sigma); k+=1)
0133
    gx[point]+=((1/3.141592654)*(sigma/( ((pnt2x(lineshape
    ,k)-laxis)^2)+sigma^2 )))*lineshape[point+k]
0134
    C+=((1/3.141592654)*(sigma/( ((pnt2x(lineshape,k)-laxi
    s)^2)+sigma^2 )))
0135 endfor
0136 gx[point]=gx/C
0137 C=0
0138 endfor
0139 lineshape=gx
0140 else
0141 for (point=x2pnt(lineshape,hpr-quality*sigma);
    point<=x2pnt(lineshape,hpd+quality*sigma); point+=1)
0142 for (k=-x2pnt(lineshape,laxis+quality*sigma);
    k<=x2pnt(lineshape,laxis+quality*sigma); k+=1)
0143
    gx[point]+=((1/3.141592654)*(sigma/( ((pnt2x(lineshape
    ,k)-laxis)^2)+sigma^2 )))*lineshape[point+k]
0144
    C+=((1/3.141592654)*(sigma/( ((pnt2x(lineshape,k)-laxi
    s)^2)+sigma^2 )))
0145 endfor
0146 gx[point]=gx/C
0147 C=0
0148 endfor
0149 lineshape=gx
0150 endif
0151 endif
0152 if (linefunction==5)//laurenzian
0153 if (dh>0)
0154 for (point=x2pnt(lineshape,hpd-quality*sigma);
    point<=x2pnt(lineshape,hpr+quality*sigma); point+=1)
0155 for (k=-x2pnt(lineshape,laxis+quality*sigma);
    k<=x2pnt(lineshape,laxis+quality*sigma); k+=1)
0156
    gx[point]+=((1/3.141592654)*(0.01/( ((pnt2x(lineshape,k
    ))^2)+0.01^2 )))*lineshape[point+k]
0157
    C+=((1/3.141592654)*(0.01/( ((pnt2x(lineshape,k))^2)+0
    .01^2 )))
0158 endfor
0159 C=0
0160 endfor
0161 else
0162 for (point=x2pnt(lineshape,hpr-quality*sigma);
    point<=x2pnt(lineshape,hpd+quality*sigma); point+=1)
0163 for (k=-x2pnt(lineshape,laxis+quality*sigma);
    k<=x2pnt(lineshape,laxis+quality*sigma); k+=1)
```

```
0164
      gx[point]+=((1/3.141592654)*(0.01/( ((pnt2x(lineshape,k
      ))^2)+0.01^2 )))*lineshape[point+k]
0165
      C+=((1/3.141592654)*(0.01/( ((pnt2x(lineshape,k))^2)+0
      .01^2 )))
0166 endfor
0167 C=0
0168 endfor
0169 lineshape=gx
0170 endif
0171 endif
0172 KILLWAVES GX
0173 end
0174
0175 function makeline(quality,linefunction,hpoint,lineshape,
      laxis, haxis, width, hpr, hpd)
0176 Wave lineshape
0177 variable quality,linefunction,hpoint, laxis, haxis
0178 variable width
0179 variable hpr,hpd
0180 variable T2, dW
0181 variable hmT,hp, S, S0, sumS
0182 variable dh=hpr-hpd
0183 variable point=hpoint-1
0184 variable boundary1 = width //mT
0185 variable boundary2 = 0.01
0186 if (dh < boundary1 && dh >-1*boundary1)
0187 if (linefunction == 0)
0188 T2=1/(width*    point/(haxis-laxis))
0189 lineshape = (T2/3.141592654)*(1+((T2)^2)*
      (p-(((hpr+hpd)/2-laxis)*point/(haxis-laxis)))^2)^(-1)
0190 endif
0191 if (linefunction == 1)
0192 T2=((3.141592654*ln(2))^0.5)/(width*
      point/(haxis-laxis))
0193 lineshape = (T2/3.141592654)*exp(-(T2^2)*
      ((p-(((hpr+hpd)/2-laxis)*point/(haxis-laxis)))^2)/3.14159
      2654 )
0194 endif
0195 if (linefunction == 2)
0196 T2=1/(width*    point/(haxis-laxis))
0197 lineshape = (T2/3.141592654)*(1+((T2)^2)*
      (p-(((hpr+hpd)/2-laxis)*point/(haxis-laxis)))^2)^(-1)
0198 T2=((3.141592654*ln(2))^0.5)/(width*
      point/(haxis-laxis))
0199 lineshape = lineshape*0.5 +
      (T2/3.141592654)*exp(-(T2^2)*
      ((p-(((hpr+hpd)/2-laxis)*point/(haxis-laxis)))^2)/3.14159
      2654 )*0.5
0200 endif
0201 duplicate lineshape lineshape_cp
0202 integrate lineshape_cp
0203 wavestats/Q lineshape_cp
0204 lineshape = (lineshape)/V_max
0205 killwaves lineshape_cp
0206 endif
0207 if (dh <= -1*boundary1)
0208 for(hp=x2pnt(lineshape, hpr); hp<x2pnt(lineshape,
      hpd);hp+=1)
0209 S = (hpr*(hpd^2)*((pnt2x(lineshape,
      hp))^(-2))*((hpd^2-hpr^2)*(hpd^2-(pnt2x(lineshape,
      hp))^2))^(-0.5))//*((haxis-laxis)/point)
0210 lineshape[hp] += S
0211 endfor
0212 duplicate lineshape lineshape_cp
0213 integrate lineshape_cp
0214 wavestats/Q lineshape_cp
0215 lineshape = (lineshape)/V_max
0216 killwaves lineshape_cp
0217 endif
0218 if (dh >= boundary1 )
0219 for(hp=x2pnt(lineshape, hpr); hp>x2pnt(lineshape,
      hpd);hp-=1)
0220 S = hpr*(hpd^2)*((pnt2x(lineshape,
      hp))^(-2))*((hpd^2-hpr^2)*(hpd^2-(pnt2x(lineshape,
      hp))^2))^(-0.5)
0221 lineshape[hp] += S
0222 endfor
0223 duplicate lineshape lineshape_cp
0224 integrate lineshape_cp
0225 wavestats/Q lineshape_cp
0226 lineshape = (lineshape)/V_max
0227 killwaves lineshape_cp
0228 endif
0229 end
0230
0231
0232 ////////////////////////////////////////////////////////////////////////////
0233 //
0234 // This is the function to make spectra of H6+
0235 //
0236 ////////////////////////////////////////////////////////////////////////////
0237
0238 function H2H2H2()
0239 variable type
0240 variable y
0241 variable laxis, haxis
0242 variable g, freq, width
0243 variable hpd,hpr,hpoint
0244 variable Aciso,Acani,dAciso,dAcani,A1,A2,As,A5,A6
0245 variable ani,dani
0246 variable Iz12,Iz1,Iz2,Iz5,Iz6,Iz56
0247 variable I1,I2,I12,I5,I6,I56
0248 variable H0,first,second
0249 variable LF, linefunction, quality
0250 type = 0
0251 laxis = 300
0252 haxis = 360
0253 g = 2.00212
0254 freq = 9.256
0255 Aciso = 20.441
0256 Acani = -0.061
0257 width = 0.01
0258 hpoint = 65536
0259 quality = 10
0260 prompt laxis, "enter start Magnetic Field: "
0261 prompt haxis, "enter end Magnetic Field: "
0262 prompt hpoint, "enter number of points: "
0263 DoPrompt "Enter magnetic field" ,laxis,haxis
0264 if (V_flag)
0265 return -1
0266 endif
0267 prompt LF, "Chose linefunction", popup "laurentian;
      gaussian; mix"
0268 prompt quality, "Smoothing width (peak width X )"
0269 DoPrompt "Chose line function" ,LF,quality
0270 if (V_flag)
0271 return -1
0272 endif
0273 if (LF==1)
0274 linefunction=0
0275 endif
0276 if (LF==2)
0277 linefunction=1
0278 endif
0279 if (LF==3)
0280 linefunction=2
0281 endif
0282 prompt g, "enter g-value: "
0283 prompt freq, "enter microwave frequency: "
0284 prompt Aciso, "enter isotropic Actr in mT: "
0285 prompt Acani, "enter anisotropic Actr in mT: "
0286 prompt width, "enter half width at half maximum in mT:
      "
0287 DoPrompt "Enter ESR
      Parameters" ,g,freq,Aciso,Acani,width
0288 if (V_flag)
0289 return -1
0290 endif
0291 printf "g = %g¥r",g
0292 printf "freq. = %g¥r",freq
0293 printf "Aciso = %g¥r",Aciso
0294 printf "Acani = %g¥r",Acani
0295 printf "width = %g¥r",width
0296 Make/O/N=(hpoint) sim1; SetScale x 0, 2*PI,
      sim1;sim1=0
0297 SetScale/I x laxis,haxis,"mT", sim1
0298 Make/O/N=(hpoint) sim2; SetScale x 0, 2*PI,
      sim2;sim2=0
0299 SetScale/I x laxis,haxis,"mT", sim2
0300 Make/O/N=(hpoint) simani; SetScale x 0, 2*PI,
      simani;simani=0
0301 SetScale/I x laxis,haxis,"mT", simani
```

```
0302 Make/O/N=(hpoint) simallH6; SetScale x 0, 2*PI,
     simallH6;simallH6=0
0303 SetScale/I x laxis,haxis,"mT", simallH6
0304 Make/O/N=(hpoint) lineshape; SetScale x 0, 2*PI,
     lineshape;lineshape=0
0305 SetScale/I x laxis,haxis,"mT", lineshape
0306 I12 = 1
0307 H0=(6.6260755*(10^-34) * freq *
     (10^9))*1000/(g*9.2740154*10^-24)
0308 variable cnt =0
0309 for(Iz12=I12;Iz12>=-I12;Iz12-=1)
0310 ani = -Acani
0311 hpd =
     getH(hpoint,type,Aciso,dAciso,ani,dani,A5,A6,As,Iz12,I
     z1,Iz2,I5,I6,Iz5,Iz6,Iz56,I12,I1,I2,I56,H0,A1,A2)
0312 ani = 2*Acani
0313 hpr =
     getH(hpoint,type,Aciso,dAciso,ani,dani,A5,A6,As,Iz12,I
     z1,Iz2,I5,I6,Iz5,Iz6,Iz56,I12,I1,I2,I56,H0,A1,A2)
0314 printf "%g¥r",hpd
0315 printf "%g¥r",hpr
0316 if (hpr < haxis && hpr > laxis)
0317 makeline(quality,linefunction,hpoint,lineshape, laxis,
     haxis, width, hpr, hpd)
0318 if (hpr-hpd > width || width <-1*(hpr-hpd))
0319
     gau_f(lineshape,quality,hpoint,width,linefunction,laxis,ha
     xis,hpr,hpd)
0320 endif
0321 sim1 += lineshape
0322 lineshape=0
0323 else
0324 sim1=sim1
0325 endif
0326 cnt+=1
0327 endfor
0328 I12 = 0
0329 Iz12 = 0
0330 ani = -Acani
0331 hpd =
     getH(hpoint,type,Aciso,dAciso,ani,dani,A5,A6,As,Iz12,I
     z1,Iz2,I5,I6,Iz5,Iz6,Iz56,I12,I1,I2,I56,H0,A1,A2)
0332 ani = 2*Acani
0333 hpr =
     getH(hpoint,type,Aciso,dAciso,ani,dani,A5,A6,As,Iz12,I
     z1,Iz2,I5,I6,Iz5,Iz6,Iz56,I12,I1,I2,I56,H0,A1,A2)
0334 if (hpr < haxis && hpr > laxis)
0335 makeline(quality,linefunction,hpoint,lineshape, laxis,
     haxis, width, hpr, hpd)
0336 if (hpr-hpd > width || width <-1*(hpr-hpd))
0337
     gau_f(lineshape,quality,hpoint,width,linefunction,laxis,ha
     xis,hpr,hpd)
0338 endif
0339 sim2 += lineshape
0340 else
0341 sim2=sim2
0342 endif
0343 cnt+=1
0344 simallH6=(sim1+sim2)/cnt
0345 Differentiate simallH6
0346 end
0347
0348
0349 ////////////////////////////////////////////////////////////////////////////
0350 //
0351 // This is the function to make spectra of H4D2+
0352 //
0353 ////////////////////////////////////////////////////////////////////////////
0354
0355 function H2H2D2()
0356 variable type
0357 variable y
0358 variable laxis, haxis
0359 variable g, freq, width,linefunction,quality,LF
0360 variable hpd,hpr,hpoint
0361 variable Aciso,Acani,dAciso,dAcani,A1,A2,As,A5,A6
0362 variable ani,dani
0363 variable Iz12,Iz1,Iz2,Iz5,Iz6,Iz56
0364 variable I1,I2,I12,I5,I6,I56
0365 variable H0,first,second
0366 type     = 1
0367 laxis    = 300
0368 haxis    = 360
0369 g        = 2.00212
0370 freq     = 9.256
0371 Aciso    = 20.65
0372 Acani    = -0.12
0373 dAciso = 1.2
0374 dAcani = 0.04
0375 As       = 1.44
0376 width    = 0.07
0377 hpoint=4096
0378 quality = 100
0379 prompt laxis, "enter start Magnetic Field: "
0380 prompt haxis, "enter end Magnetic Field: "
0381 prompt hpoint, "enter number of points: "
0382 DoPrompt "Enter magnetic field" ,laxis,haxis
0383 if (V_flag)
0384 return -1
0385 endif
0386 prompt LF, "Chose linefunction", popup "laurentian;
     gaussian"
0387 prompt quality, "Smoothing width (peak width X )"
0388 DoPrompt "Chose line function" ,LF,quality
0389 if (V_flag)
0390 return -1
0391 endif
0392 if (LF==1)
0393 linefunction=0
0394 endif
0395 if (LF==2)
0396 linefunction=1
0397 endif
0398 prompt g, "enter g-value: "
0399 prompt freq, "enter microwave frequency: "
0400 prompt Aciso, "enter isotropic Actr in mT: "
0401 prompt Acani, "enter anisotropic Actr in mT: "
0402 prompt dAciso, "enter (A1iso-A2iso)/2 in mT: "
0403 prompt dAcani, "enter (A1ani-A2ani)/2 in mT: "
0404 prompt As, "enter Asid in mT: "
0405 prompt width, "enter half width at half maximum in mT:
     "
0406 DoPrompt "Enter ESR
     Parameters" ,g,freq,Aciso,Acani,dAciso,dAcani,As,width
0407 if (V_flag)
0408 return -1
0409 endif
0410 printf "g = %g¥r",g
0411 printf "freq. = %g¥r",freq
0412 printf "Aciso = %g¥r",Aciso
0413 printf "Acani = %g¥r",Acani
0414 printf "dAciso = %g¥r",dAciso
0415 printf "dAcani = %g¥r",dAcani
0416 printf "As = %g¥r",As
0417 printf "width = %g¥r",width
0418 Make/O/D/N=(hpoint) sim1; SetScale x 0, 2*PI,
     sim1;sim1=0
0419 SetScale/I x laxis,haxis,"mT", sim1
0420 Make/O/D/N=(hpoint) sim2; SetScale x 0, 2*PI,
     sim2;sim2=0
0421 SetScale/I x laxis,haxis,"mT", sim2
0422 Make/O/D/N=(hpoint) simani; SetScale x 0, 2*PI,
     simani;simani=0
0423 SetScale/I x laxis,haxis,"mT", simani
0424 Make/O/D/N=(hpoint) simallH4D2; SetScale x 0, 2*PI,
     simallH4D2;simallH4D2=0
0425 SetScale/I x laxis,haxis,"mT", simallH4D2
0426 Make/O/D/N=(hpoint) lineshape; SetScale x 0, 2*PI,
     lineshape;lineshape=0
0427 SetScale/I x laxis,haxis,"mT", lineshape
0428 variable cnt =0
0429 I1=1/2
0430 I2=1/2
0431 I56=2
0432 H0=(6.626*(10^-34) * freq *
     (10^9))*1000/(g*9.274*10^-24)
0433 for(Iz1=I1;Iz1>=-I1;Iz1-=1)
0434 for(Iz2=I2;Iz2>=-I2;Iz2-=1)
0435 for(Iz56=I56;Iz56>=-I56;Iz56-=1)
0436 ani = -Acani
0437 dani = -dAcani
```

```
0438 hpd =
     getH(hpoint,type,Aciso,dAciso,ani,dani,A5,A6,As,Iz12,I
     z1,Iz2,I5,I6,Iz5,Iz6,Iz56,I12,I1,I2,I56,H0,A1,A2)
0439 ani = 2*Acani
0440 dani = 2*dAcani
0441 hpr =
     getH(hpoint,type,Aciso,dAciso,ani,dani,A5,A6,As,Iz12,I
     z1,Iz2,I5,I6,Iz5,Iz6,Iz56,I12,I1,I2,I56,H0,A1,A2)
0442 if (hpr < haxis && hpr > laxis)
0443 makeline(quality,linefunction,hpoint,lineshape, laxis,
     haxis, width, hpr, hpd)
0444 if (hpr-hpd > width || width <-1*(hpr-hpd))
0445
     gau_f(lineshape,quality,hpoint,width,linefunction,laxis,ha
     xis,hpr,hpd)
0446 endif
0447 sim1 += lineshape
0448 lineshape=0
0449 else
0450 sim1=sim1
0451 endif
0452 cnt+=1
0453 endfor
0454 endfor
0455 endfor
0456 lineshape=0
0457 for(Iz1=I1;Iz1>=-I1;Iz1-=1)
0458 for(Iz2=I2;Iz2>=-I2;Iz2-=1)
0459 Iz56=0
0460 I56=0
0461 ani = -Acani
0462 dani = -dAcani
0463 hpd =
     getH(hpoint,type,Aciso,dAciso,ani,dani,A5,A6,As,Iz12,I
     z1,Iz2,I5,I6,Iz5,Iz6,Iz56,I12,I1,I2,I56,H0,A1,A2)
0464 ani = 2*Acani
0465 dani = 2*dAcani
0466 hpr =
     getH(hpoint,type,Aciso,dAciso,ani,dani,A5,A6,As,Iz12,I
     z1,Iz2,I5,I6,Iz5,Iz6,Iz56,I12,I1,I2,I56,H0,A1,A2)
0467 if (hpr < haxis && hpr > laxis)
0468 makeline(quality,linefunction,hpoint,lineshape, laxis,
     haxis, width, hpr, hpd)
0469 if (hpr-hpd > width || width <-1*(hpr-hpd))
0470
     gau_f(lineshape,quality,hpoint,width,linefunction,laxis,ha
     xis,hpr,hpd)
0471 endif
0472 sim2 += lineshape
0473 lineshape=0
0474 else
0475 sim2=sim2
0476 endif
0477 cnt+=1
0478 endfor
0479 endfor
0480 lineshape=0
0481 simallH4D2=(sim1+sim2)/cnt
0482 Differentiate simallH4D2
0483 end
0484
0485
0486 ////////////////////////////////////////////////////////////////////////////
0487 //
0488 // This is the function to make spectra of H2H2HD+
0489 //
0490 ////////////////////////////////////////////////////////////////////////////
0491
0492 function H2H2HD()
0493 variable type
0494 variable y
0495 variable laxis, haxis
0496 variable g, freq, width,linefunction,quality,LF
0497 variable hpd,hpr,hpoint
0498 variable Aciso,Acani,dAciso,dAcani,A1,A2,As,A5,A6
0499 variable ani,dani
0500 variable Iz12,Iz1,Iz2,Iz5,Iz6,Iz56
0501 variable I1,I2,I12,I5,I6,I56
0502 variable H0,first,second
0503 type      = 2
0504 laxis    = 298
0505 haxis    = 362
0506 g          = 2.00212
0507 freq      = 9.256
0508 Aciso    = 20.55
0509 Acani    = -0.1
0510 dAciso = 0.69
0511 dAcani = 0.00
0512 A5         = 9.58
0513 A6         = 1.4
0514 width    = 0.07
0515 hpoint = 4096
0516 quality = 500
0517 variable cnt =0
0518 prompt laxis, "enter start Magnetic Field: "
0519 prompt haxis, "enter end Magnetic Field: "
0520 prompt hpoint, "enter number of points: "
0521 DoPrompt "Enter magnetic field" ,laxis,haxis
0522 if (V_flag)
0523 return -1
0524 endif
0525 prompt LF, "Chose linefunction", popup "laurentian;
     gaussian"
0526 prompt quality, "Enter the value of lineshape quality
     (1-5000)"
0527 DoPrompt "Chose line function" ,LF,quality
0528 if (V_flag)
0529 return -1
0530 endif
0531 if (LF==1)
0532 linefunction=0
0533 endif
0534 if (LF==2)
0535 linefunction=1
0536 endif
0537 prompt g, "enter g-value: "
0538 prompt freq, "enter microwave frequency: "
0539 prompt Aciso, "enter isotropic Actr in mT: "
0540 prompt Acani, "enter anisotropic Actr in mT: "
0541 prompt dAciso, "enter (A1iso-A2iso)/2 in mT: "
0542 prompt dAcani, "enter (A1ani-A2ani)/2 in mT: "
0543 prompt A5, "enter A5 in mT: "
0544 prompt A6, "enter A6 in mT: "
0545 prompt width, "enter half width at half maximum in mT:
     "
0546 DoPrompt "Enter ESR
     Parameters" ,g,freq,Aciso,Acani,dAciso,dAcani,A5,A6,w
     idth
0547 if (V_flag)
0548 return -1
0549 endif
0550 printf "g = %g¥r",g
0551 printf "freq. = %g¥r",freq
0552 printf "Aciso = %g¥r",Aciso
0553 printf "Acani = %g¥r",Acani
0554 printf "dAciso = %g¥r",dAciso
0555 printf "dAcani = %g¥r",dAcani
0556 printf "A5 = %g¥r",A5
0557 printf "A6 = %g¥r",A6
0558 printf "width = %g¥r",width
0559 Make/O/D/N=(hpoint) sim1; SetScale x 0, 2*PI,
     sim1;sim1=0
0560 SetScale/I x laxis,haxis,"mT", sim1
0561 Make/O/D/N=(hpoint) sim2; SetScale x 0, 2*PI,
     sim2;sim2=0
0562 SetScale/I x laxis,haxis,"mT", sim2
0563 Make/O/D/N=(hpoint) simani; SetScale x 0, 2*PI,
     simani;simani=0
0564 SetScale/I x laxis,haxis,"mT", simani
0565 Make/O/D/N=(hpoint) simallH2H2HD; SetScale x 0,
     2*PI, simallH2H2HD;simallH2H2HD=0
0566 SetScale/I x laxis,haxis,"mT", simallH2H2HD
0567 Make/O/D/N=(hpoint) lineshape; SetScale x 0, 2*PI,
     lineshape;lineshape=0
0568 SetScale/I x laxis,haxis,"mT", lineshape
0569 I1=1/2
0570 I2=1/2
0571 I5=1/2
0572 I6=1
0573 H0=(6.626*(10^-34) * freq *
     (10^9))*1000/(g*9.274*10^-24)
0574 for(Iz1=I1;Iz1>=-I1;Iz1-=1)
0575 for(Iz2=I2;Iz2>=-I2;Iz2-=1)
0576 for(Iz5=I5;Iz5>=-I5;Iz5-=1)
```

```
0577 for(Iz6=I6;Iz6>=-I6;Iz6-=1)
0578 ani = -Acani
0579 dani = -dAcani
0580 hpd =
     getH(hpoint,type,Aciso,dAciso,ani,dani,A5,A6,As,Iz12,I
     z1,Iz2,I5,I6,Iz5,Iz6,Iz56,I12,I1,I2,I56,H0,A1,A2)
0581 ani = 2*Acani
0582 dani = 2*dAcani
0583 hpr =
     getH(hpoint,type,Aciso,dAciso,ani,dani,A5,A6,As,Iz12,I
     z1,Iz2,I5,I6,Iz5,Iz6,Iz56,I12,I1,I2,I56,H0,A1,A2)
0584 if (hpr < haxis && hpr > laxis)
0585 makeline(quality,linefunction,hpoint,lineshape, laxis,
     haxis, width, hpr, hpd)
0586 if (hpr-hpd > width || width <-1*(hpr-hpd))
0587
     gau_f(lineshape,quality,hpoint,width,linefunction,laxis,ha
     xis,hpr,hpd)
0588 endif
0589 sim1 += lineshape
0590 lineshape=0
0591 else
0592 sim1=sim1
0593 endif
0594 cnt+=1
0595 endfor
0596 endfor
0597 endfor
0598 endfor
0599 lineshape=0
0600 simallH2H2HD=(sim1)/cnt
0601 Differentiate simallH2H2HD
0602 end
0603
0604
0605 ////////////////////////////////////////////////////////////////////////////
0606 //
0607 // This is the function to make spectra of H2HDHD+
0608 //
0609 ////////////////////////////////////////////////////////////////////////////
0610
0611 function H2HDHD()
0612 variable type
0613 variable y
0614 variable laxis, haxis
0615 variable g, freq, width,linefunction,quality,LF
0616 variable hpd,hpr,hpoint
0617 variable Aciso,Acani,dAciso,dAcani,A1,A2,As,A5,A6
0618 variable ani,dani
0619 variable Iz12,Iz1,Iz2,Iz5,Iz6,Iz56
0620 variable I1,I2,I12,I5,I6,I56
0621 variable H0,first,second
0622 type      = 4
0623 laxis    = 298
0624 haxis    = 362
0625 g           = 2.00212
0626 freq      = 9.256
0627 A1         = 20.6
0628 A2         = 3.12
0629 A5         = 9.55
0630 A6         = 1.39
0631 width    = 0.07
0632 hpoint = 4096
0633 quality = 100
0634 variable cnt =0
0635 prompt laxis, "enter start Magnetic Field: "
0636 prompt haxis, "enter end Magnetic Field: "
0637 prompt hpoint, "enter number of points: "
0638 DoPrompt "Enter magnetic field" ,laxis,haxis
0639 if (V_flag)
0640 return -1
0641 endif
0642 prompt g, "enter g-value: "
0643 prompt freq, "enter microwave frequency: "
0644 prompt A1, "enter isotropic A1 in mT: "
0645 prompt A2, "enter isotropic A2 in mT: "
0646 prompt A5, "enter isotropic A5 in mT: "
0647 prompt A6, "enter isotropic A6 in mT: "
0648 prompt width, "enter half width at half maximum in mT:
     "
0649 DoPrompt "Enter ESR
     Parameters" ,g,freq,A1,A2,A5,A6,width
0650 if (V_flag)
0651 return -1
0652 endif
0653 printf "g = %g¥r",g
0654 printf "freq. = %g¥r",freq
0655 printf "A1 = %g¥r",A1
0656 printf "A2 = %g¥r",A2
0657 printf "A5 = %g¥r",A5
0658 printf "A6 = %g¥r",A6
0659 printf "width = %g¥r",width
0660 Make/O/D/N=(hpoint) sim1; SetScale x 0, 2*PI,
     sim1;sim1=0
0661 SetScale/I x laxis,haxis,"mT", sim1
0662 Make/O/D/N=(hpoint) sim2; SetScale x 0, 2*PI,
     sim2;sim2=0
0663 SetScale/I x laxis,haxis,"mT", sim2
0664 Make/O/D/N=(hpoint) simani; SetScale x 0, 2*PI,
     simani;simani=0
0665 SetScale/I x laxis,haxis,"mT", simani
0666 Make/O/D/N=(hpoint) simallH2HDHD; SetScale x 0,
     2*PI, simallH2HDHD;simallH2HDHD=0
0667 SetScale/I x laxis,haxis,"mT", simallH2HDHD
0668 Make/O/D/N=(hpoint) lineshape; SetScale x 0, 2*PI,
     lineshape;lineshape=0
0669 SetScale/I x laxis,haxis,"mT", lineshape
0670 I1=1/2
0671 I2=1
0672 I5=1/2
0673 I6=1
0674 H0=(6.626*(10^-34) * freq *
     (10^9))*1000/(g*9.274*10^-24)
0675 for(Iz1=I1;Iz1>=-I1;Iz1-=1)
0676 for(Iz2=I2;Iz2>=-I2;Iz2-=1)
0677 for(Iz5=I5;Iz5>=-I5;Iz5-=1)
0678 for(Iz6=I6;Iz6>=-I6;Iz6-=1)
0679 hpd =
     getH(hpoint,type,Aciso,dAciso,ani,dani,A5,A6,As,Iz12,I
     z1,Iz2,I5,I6,Iz5,Iz6,Iz56,I12,I1,I2,I56,H0,A1,A2)
0680 hpr =
     getH(hpoint,type,Aciso,dAciso,ani,dani,A5,A6,As,Iz12,I
     z1,Iz2,I5,I6,Iz5,Iz6,Iz56,I12,I1,I2,I56,H0,A1,A2)
0681 makeline(quality,linefunction,hpoint,lineshape, laxis,
     haxis, width, hpr, hpd)
0682 if (hpr-hpd > width || width <-1*(hpr-hpd))
0683
     gau_f(lineshape,quality,hpoint,width,linefunction,laxis,ha
     xis,hpr,hpd)
0684 endif
0685 sim1 += lineshape
0686 lineshape=0
0687 cnt+=1
0688 endfor
0689 endfor
0690 endfor
0691 endfor
0692 lineshape=0
0693 simallH2HDHD=sim1/cnt
0694 Differentiate simallH2HDHD
0695 end
0696
0697
0698 ////////////////////////////////////////////////////////////////////////////
0699 //
0700 // This is the function to make spectra of H2HDH2+
0701 //
0702 ////////////////////////////////////////////////////////////////////////////
0703
0704 function H2HDH2()
0705 variable type
0706 variable y
0707 variable laxis, haxis
0708 variable g, freq, width,linefunction,quality,LF
0709 variable hpd,hpr,hpoint
0710 variable Aciso,Acani,dAciso,dAcani,A1,A2,As,A5,A6
0711 variable ani,dani
0712 variable Iz12,Iz1,Iz2,Iz5,Iz6,Iz56
0713 variable I1,I2,I12,I5,I6,I56
0714 variable H0,first,second
0715 type      = 3
0716 laxis    = 300
0717 haxis    = 360
0718 g           = 2.00212
```

```
0719 freq      = 9.256
0720 A1         = 21.02
0721 A2         = 3.02
0722 Acani    = -0.12
0723 width    = 0.07
0724 hpoint = 4096
0725 quality = 100
0726 VARIABLE CNT=0
0727 prompt laxis, "enter start Magnetic Field: "
0728 prompt haxis, "enter end Magnetic Field: "
0729 prompt hpoint, "enter number of points: "
0730 DoPrompt "Enter magnetic field" ,laxis,haxis
0731 if (V_flag)
0732 return -1
0733 endif
0734 prompt LF, "Chose linefunction", popup "laurentian;
     gaussian"
0735 prompt quality, "Enter the value of lineshape quality
     (1-5000)"
0736 DoPrompt "Chose line function" ,LF,quality
0737 if (V_flag)
0738 return -1
0739 endif
0740 if (LF==1)
0741 linefunction=0
0742 endif
0743 if (LF==2)
0744 linefunction=1
0745 endif
0746 prompt g, "enter g-value: "
0747 prompt freq, "enter microwave frequency: "
0748 prompt A1, "enter isotropic A1 in mT: "
0749 prompt A2, "enter isotropic A2 in mT: "
0750 prompt Acani, "enter anisotropic Actr in mT: "
0751 prompt width, "enter half width at half maximum in mT:
     "
0752 DoPrompt "Enter ESR
     Parameters" ,g,freq,A1,A2,Acani,width
0753 if (V_flag)
0754 return -1
0755 endif
0756 printf "g = %g¥r",g
0757 printf "freq. = %g¥r",freq
0758 printf "A1 = %g¥r",A1
0759 printf "A2 = %g¥r",A2
0760 printf "Acani = %g¥r",Acani
0761 printf "width = %g¥r",width
0762 Make/O/D/N=(hpoint) sim1; SetScale x 0, 2*PI,
     sim1;sim1=0
0763 SetScale/I x laxis,haxis,"mT", sim1
0764 Make/O/D/N=(hpoint) sim2; SetScale x 0, 2*PI,
     sim2;sim2=0
0765 SetScale/I x laxis,haxis,"mT", sim2
0766 Make/O/D/N=(hpoint) simani; SetScale x 0, 2*PI,
     simani;simani=0
0767 SetScale/I x laxis,haxis,"mT", simani
0768 Make/O/D/N=(hpoint) simallH2HDH2; SetScale x 0,
     2*PI, simallH2HDH2;simallH2HDH2=0
0769 SetScale/I x laxis,haxis,"mT", simallH2HDH2
0770 Make/O/D/N=(hpoint) lineshape; SetScale x 0, 2*PI,
     lineshape;lineshape=0
0771 SetScale/I x laxis,haxis,"mT", lineshape
0772 I1=1/2
0773 I2=1
0774 H0=(6.626*(10^-34) * freq *
     (10^9))*1000/(g*9.274*10^-24)
0775 for(Iz1=I1;Iz1>=-I1;Iz1-=1)
0776 for(Iz2=I2;Iz2>=-I2;Iz2-=1)
0777 ani = -Acani
0778 dani = -dAcani
0779 hpd =
     getH(hpoint,type,Aciso,dAciso,ani,dani,A5,A6,As,Iz12,I
     z1,Iz2,I5,I6,Iz5,Iz6,Iz56,I12,I1,I2,I56,H0,A1,A2)
0780 ani = 2*Acani
0781 dani = 2*dAcani
0782 hpr =
     getH(hpoint,type,Aciso,dAciso,ani,dani,A5,A6,As,Iz12,I
     z1,Iz2,I5,I6,Iz5,Iz6,Iz56,I12,I1,I2,I56,H0,A1,A2)
0783 if (hpr < haxis && hpr > laxis)
0784 makeline(quality,linefunction,hpoint,lineshape, laxis,
     haxis, width, hpr, hpd)
0785 if (hpr-hpd > width || width <-1*(hpr-hpd))
0786
     gau_f(lineshape,quality,hpoint,width,linefunction,laxis,ha
     xis,hpr,hpd)
0787 endif
0788 sim1 += lineshape
0789 lineshape=0
0790 else
0791 sim1=sim1
0792 endif
0793 cnt+=1
0794 endfor
0795 endfor
0796 lineshape=0
0797 simallH2HDH2=sim1/CNT
0798 Differentiate simallH2HDH2
0799 end
0800
0801
0802 ////////////////////////////////////////////////////////////////////////////
0803 //
0804 // This is the function to make spectra of HDH2HD+
0805 //
0806 ////////////////////////////////////////////////////////////////////////////
0807
0808 function HDH2HD()
0809 variable type
0810 variable y
0811 variable laxis, haxis
0812 variable g, freq, width,linefunction,quality,LF
0813 variable hpd,hpr,hpoint
0814 variable Aciso,Acani,dAciso,dAcani,A1,A2,As,A5,A6
0815 variable ani,dani
0816 variable Iz12,Iz1,Iz2,Iz5,Iz6,Iz56
0817 variable I1,I2,I12,I5,I6,I56
0818 variable H0,first,second
0819 type      = 5
0820 laxis    = 290
0821 haxis    = 370
0822 g           = 2.00212
0823 freq      = 9.256
0824 Aciso          = 21.2
0825 A5          = 9.52
0826 A6          = 1.37
0827 width    = 0.07
0828 hpoint = 4096
0829 quality = 100
0830 VARIABLE CNT=0
0831 prompt laxis, "enter start Magnetic Field: "
0832 prompt haxis, "enter end Magnetic Field: "
0833 prompt hpoint, "enter number of points: "
0834 DoPrompt "Enter magnetic field" ,laxis,haxis
0835 if (V_flag)
0836 return -1
0837 endif
0838 prompt g, "enter g-value: "
0839 prompt freq, "enter microwave frequency: "
0840 prompt Aciso, "enter isotropic Actr in mT: "
0841 prompt Acani, "enter anisotropic Actr in mT: "
0842 prompt A5, "enter A5 in mT: "
0843 prompt A6, "enter A6 in mT: "
0844 prompt width, "enter half width at half maximum in mT:
     "
0845 DoPrompt "Enter ESR
     Parameters" ,g,freq,Aciso,A5,A6,width
0846 if (V_flag)
0847 return -1
0848 endif
0849 printf "g = %g¥r",g
0850 printf "freq. = %g¥r",freq
0851 printf "Aciso = %g¥r",Aciso
0852 printf "A5 = %g¥r",A5
0853 printf "A6 = %g¥r",A6
0854 printf "width = %g¥r",width
0855 Make/O/D/N=(hpoint) sim1; SetScale x 0, 2*PI,
     sim1;sim1=0
0856 SetScale/I x laxis,haxis,"mT", sim1
0857 Make/O/D/N=(hpoint) sim2; SetScale x 0, 2*PI,
     sim2;sim2=0
0858 SetScale/I x laxis,haxis,"mT", sim2
0859 Make/O/D/N=(hpoint) sim3; SetScale x 0, 2*PI,
     sim3;sim3=0
0860 SetScale/I x laxis,haxis,"mT", sim3
```

```
0861 Make/O/D/N=(hpoint) sim4; SetScale x 0, 2*PI,
     sim4;sim4=0
0862 SetScale/I x laxis,haxis,"mT", sim4
0863 Make/O/D/N=(hpoint) sim5; SetScale x 0, 2*PI,
     sim5;sim5=0
0864 SetScale/I x laxis,haxis,"mT", sim5
0865 Make/O/D/N=(hpoint) sim6; SetScale x 0, 2*PI,
     sim6;sim6=0
0866 SetScale/I x laxis,haxis,"mT", sim6
0867 Make/O/D/N=(hpoint) sim7; SetScale x 0, 2*PI,
     sim7;sim7=0
0868 SetScale/I x laxis,haxis,"mT", sim7
0869 Make/O/D/N=(hpoint) sim8; SetScale x 0, 2*PI,
     sim8;sim8=0
0870 SetScale/I x laxis,haxis,"mT", sim8
0871 Make/O/D/N=(hpoint) sim9; SetScale x 0, 2*PI,
     sim9;sim9=0
0872 SetScale/I x laxis,haxis,"mT", sim9
0873 Make/O/D/N=(hpoint) sim10; SetScale x 0, 2*PI,
     sim10;sim10=0
0874 SetScale/I x laxis,haxis,"mT", sim10
0875 Make/O/D/N=(hpoint) sim11; SetScale x 0, 2*PI,
     sim11;sim11=0
0876 SetScale/I x laxis,haxis,"mT", sim11
0877 Make/O/D/N=(hpoint) sim12; SetScale x 0, 2*PI,
     sim12;sim12=0
0878 SetScale/I x laxis,haxis,"mT", sim12
0879 Make/O/D/N=(hpoint) simani; SetScale x 0, 2*PI,
     simani;simani=0
0880 SetScale/I x laxis,haxis,"mT", simani
0881 Make/O/D/N=(hpoint) simallHDH2HD; SetScale x 0,
     2*PI, simallHDH2HD;simallHDH2HD=0
0882 SetScale/I x laxis,haxis,"mT", simallHDH2HD
0883 Make/O/D/N=(hpoint) lineshape; SetScale x 0, 2*PI,
     lineshape;lineshape=0
0884 SetScale/I x laxis,haxis,"mT", lineshape
0885 I12=1
0886 I5=1
0887 I6=2
0888 H0=(6.626*(10^-34) * freq *
     (10^9))*1000/(g*9.274*10^-24)
0889 for(Iz12=I12;Iz12>=-I12;Iz12-=1)
0890 for(Iz5=I5;Iz5>=-I5;Iz5-=1)
0891 for(Iz6=I6;Iz6>=-I6;Iz6-=1)
0892 hpd =
     getH(hpoint,type,Aciso,dAciso,ani,dani,A5,A6,As,Iz12,I
     z1,Iz2,I5,I6,Iz5,Iz6,Iz56,I12,I1,I2,I56,H0,A1,A2)
0893 hpr =
     getH(hpoint,type,Aciso,dAciso,ani,dani,A5,A6,As,Iz12,I
     z1,Iz2,I5,I6,Iz5,Iz6,Iz56,I12,I1,I2,I56,H0,A1,A2)
0894 makeline(quality,linefunction,hpoint,lineshape, laxis,
     haxis, width, hpr, hpd)
0895 if (hpr-hpd > width || width <-1*(hpr-hpd))
0896
     gau_f(lineshape,quality,hpoint,width,linefunction,laxis,ha
     xis,hpr,hpd)
0897 endif
0898 sim1 += lineshape
0899 lineshape=0
0900 CNT+=1
0901 endfor
0902 endfor
0903 endfor
0904 lineshape=0
0905 I12=1
0906 I5=1
0907 I6=1
0908 H0=(6.626*(10^-34) * freq *
     (10^9))*1000/(g*9.274*10^-24)
0909 for(Iz12=I12;Iz12>=-I12;Iz12-=1)
0910 for(Iz5=I5;Iz5>=-I5;Iz5-=1)
0911 for(Iz6=I6;Iz6>=-I6;Iz6-=1)
0912 hpd =
     getH(hpoint,type,Aciso,dAciso,ani,dani,A5,A6,As,Iz12,I
     z1,Iz2,I5,I6,Iz5,Iz6,Iz56,I12,I1,I2,I56,H0,A1,A2)
0913 hpr =
     getH(hpoint,type,Aciso,dAciso,ani,dani,A5,A6,As,Iz12,I
     z1,Iz2,I5,I6,Iz5,Iz6,Iz56,I12,I1,I2,I56,H0,A1,A2)
0914 makeline(quality,linefunction,hpoint,lineshape, laxis,
     haxis, width, hpr, hpd)
0915 if (hpr-hpd > width || width <-1*(hpr-hpd))
0916
     gau_f(lineshape,quality,hpoint,width,linefunction,laxis,ha
     xis,hpr,hpd)
0917 endif
0918 sim2 += lineshape
0919 lineshape=0
0920 CNT+=1
0921 endfor
0922 endfor
0923 endfor
0924 lineshape=0
0925 I12=1
0926 I5=1
0927 I6=0
0928 H0=(6.626*(10^-34) * freq *
     (10^9))*1000/(g*9.274*10^-24)
0929 for(Iz12=I12;Iz12>=-I12;Iz12-=1)
0930 for(Iz5=I5;Iz5>=-I5;Iz5-=1)
0931 for(Iz6=I6;Iz6>=-I6;Iz6-=1)
0932 hpd =
     getH(hpoint,type,Aciso,dAciso,ani,dani,A5,A6,As,Iz12,I
     z1,Iz2,I5,I6,Iz5,Iz6,Iz56,I12,I1,I2,I56,H0,A1,A2)
0933 hpr =
     getH(hpoint,type,Aciso,dAciso,ani,dani,A5,A6,As,Iz12,I
     z1,Iz2,I5,I6,Iz5,Iz6,Iz56,I12,I1,I2,I56,H0,A1,A2)
0934 makeline(quality,linefunction,hpoint,lineshape, laxis,
     haxis, width, hpr, hpd)
0935 if (hpr-hpd > width || width <-1*(hpr-hpd))
0936
     gau_f(lineshape,quality,hpoint,width,linefunction,laxis,ha
     xis,hpr,hpd)
0937 endif
0938 sim3 += lineshape
0939 lineshape=0
0940 CNT+=1
0941 endfor
0942 endfor
0943 endfor
0944 lineshape=0
0945 I12=1
0946 I5=0
0947 I6=2
0948 H0=(6.626*(10^-34) * freq *
     (10^9))*1000/(g*9.274*10^-24)
0949 for(Iz12=I12;Iz12>=-I12;Iz12-=1)
0950 for(Iz5=I5;Iz5>=-I5;Iz5-=1)
0951 for(Iz6=I6;Iz6>=-I6;Iz6-=1)
0952 hpd =
     getH(hpoint,type,Aciso,dAciso,ani,dani,A5,A6,As,Iz12,I
     z1,Iz2,I5,I6,Iz5,Iz6,Iz56,I12,I1,I2,I56,H0,A1,A2)
0953 hpr =
     getH(hpoint,type,Aciso,dAciso,ani,dani,A5,A6,As,Iz12,I
     z1,Iz2,I5,I6,Iz5,Iz6,Iz56,I12,I1,I2,I56,H0,A1,A2)
0954 makeline(quality,linefunction,hpoint,lineshape, laxis,
     haxis, width, hpr, hpd)
0955 if (hpr-hpd > width || width <-1*(hpr-hpd))
0956
     gau_f(lineshape,quality,hpoint,width,linefunction,laxis,ha
     xis,hpr,hpd)
0957 endif
0958 sim4 += lineshape
0959 lineshape=0
0960 CNT+=1
0961 endfor
0962 endfor
0963 endfor
0964 lineshape=0
0965 I12=1
0966 I5=0
0967 I6=1
0968 H0=(6.626*(10^-34) * freq *
     (10^9))*1000/(g*9.274*10^-24)
0969 for(Iz12=I12;Iz12>=-I12;Iz12-=1)
0970 for(Iz5=I5;Iz5>=-I5;Iz5-=1)
0971 for(Iz6=I6;Iz6>=-I6;Iz6-=1)
0972 hpd =
     getH(hpoint,type,Aciso,dAciso,ani,dani,A5,A6,As,Iz12,I
     z1,Iz2,I5,I6,Iz5,Iz6,Iz56,I12,I1,I2,I56,H0,A1,A2)
0973 hpr =
     getH(hpoint,type,Aciso,dAciso,ani,dani,A5,A6,As,Iz12,I
     z1,Iz2,I5,I6,Iz5,Iz6,Iz56,I12,I1,I2,I56,H0,A1,A2)
```

```
0974 makeline(quality,linefunction,hpoint,lineshape, laxis,
     haxis, width, hpr, hpd)
0975 if (hpr-hpd > width || width <-1*(hpr-hpd))
0976
     gau_f(lineshape,quality,hpoint,width,linefunction,laxis,ha
     xis,hpr,hpd)
0977 endif
0978 sim5 += lineshape
0979 lineshape=0
0980 CNT+=1
0981 endfor
0982 endfor
0983 endfor
0984 lineshape=0
0985 I12=1
0986 I5=0
0987 I6=0
0988 H0=(6.626*(10^-34) * freq *
     (10^9))*1000/(g*9.274*10^-24)
0989 for(Iz12=I12;Iz12>=-I12;Iz12-=1)
0990 for(Iz5=I5;Iz5>=-I5;Iz5-=1)
0991 for(Iz6=I6;Iz6>=-I6;Iz6-=1)
0992 hpd =
     getH(hpoint,type,Aciso,dAciso,ani,dani,A5,A6,As,Iz12,I
     z1,Iz2,I5,I6,Iz5,Iz6,Iz56,I12,I1,I2,I56,H0,A1,A2)
0993 hpr =
     getH(hpoint,type,Aciso,dAciso,ani,dani,A5,A6,As,Iz12,I
     z1,Iz2,I5,I6,Iz5,Iz6,Iz56,I12,I1,I2,I56,H0,A1,A2)
0994 makeline(quality,linefunction,hpoint,lineshape, laxis,
     haxis, width, hpr, hpd)
0995 if (hpr-hpd > width || width <-1*(hpr-hpd))
0996
     gau_f(lineshape,quality,hpoint,width,linefunction,laxis,ha
     xis,hpr,hpd)
0997 endif
0998 sim6 += lineshape
0999 lineshape=0
1000 CNT+=1
1001 endfor
1002 endfor
1003 endfor
1004 lineshape=0
1005 I12=0
1006 I5=1
1007 I6=2
1008 H0=(6.626*(10^-34) * freq *
     (10^9))*1000/(g*9.274*10^-24)
1009 for(Iz12=I12;Iz12>=-I12;Iz12-=1)
1010 for(Iz5=I5;Iz5>=-I5;Iz5-=1)
1011 for(Iz6=I6;Iz6>=-I6;Iz6-=1)
1012 hpd =
     getH(hpoint,type,Aciso,dAciso,ani,dani,A5,A6,As,Iz12,I
     z1,Iz2,I5,I6,Iz5,Iz6,Iz56,I12,I1,I2,I56,H0,A1,A2)
1013 hpr =
     getH(hpoint,type,Aciso,dAciso,ani,dani,A5,A6,As,Iz12,I
     z1,Iz2,I5,I6,Iz5,Iz6,Iz56,I12,I1,I2,I56,H0,A1,A2)
1014 makeline(quality,linefunction,hpoint,lineshape, laxis,
     haxis, width, hpr, hpd)
1015 if (hpr-hpd > width || width <-1*(hpr-hpd))
1016
     gau_f(lineshape,quality,hpoint,width,linefunction,laxis,ha
     xis,hpr,hpd)
1017 endif
1018 sim7 += lineshape
1019 lineshape=0
1020 CNT+=1
1021 endfor
1022 endfor
1023 endfor
1024 lineshape=0
1025 I12=0
1026 I5=1
1027 I6=1
1028 H0=(6.626*(10^-34) * freq *
     (10^9))*1000/(g*9.274*10^-24)
1029 for(Iz12=I12;Iz12>=-I12;Iz12-=1)
1030 for(Iz5=I5;Iz5>=-I5;Iz5-=1)
1031 for(Iz6=I6;Iz6>=-I6;Iz6-=1)
1032 hpd =
     getH(hpoint,type,Aciso,dAciso,ani,dani,A5,A6,As,Iz12,I
     z1,Iz2,I5,I6,Iz5,Iz6,Iz56,I12,I1,I2,I56,H0,A1,A2)
1033 hpr =
     getH(hpoint,type,Aciso,dAciso,ani,dani,A5,A6,As,Iz12,I
     z1,Iz2,I5,I6,Iz5,Iz6,Iz56,I12,I1,I2,I56,H0,A1,A2)
1034 makeline(quality,linefunction,hpoint,lineshape, laxis,
     haxis, width, hpr, hpd)
1035 if (hpr-hpd > width || width <-1*(hpr-hpd))
1036
     gau_f(lineshape,quality,hpoint,width,linefunction,laxis,ha
     xis,hpr,hpd)
1037 endif
1038 sim8 += lineshape
1039 lineshape=0
1040 CNT+=1
1041 endfor
1042 endfor
1043 endfor
1044 lineshape=0
1045 I12=0
1046 I5=1
1047 I6=0
1048 H0=(6.626*(10^-34) * freq *
     (10^9))*1000/(g*9.274*10^-24)
1049 for(Iz12=I12;Iz12>=-I12;Iz12-=1)
1050 for(Iz5=I5;Iz5>=-I5;Iz5-=1)
1051 for(Iz6=I6;Iz6>=-I6;Iz6-=1)
1052 hpd =
     getH(hpoint,type,Aciso,dAciso,ani,dani,A5,A6,As,Iz12,I
     z1,Iz2,I5,I6,Iz5,Iz6,Iz56,I12,I1,I2,I56,H0,A1,A2)
1053 hpr =
     getH(hpoint,type,Aciso,dAciso,ani,dani,A5,A6,As,Iz12,I
     z1,Iz2,I5,I6,Iz5,Iz6,Iz56,I12,I1,I2,I56,H0,A1,A2)
1054 makeline(quality,linefunction,hpoint,lineshape, laxis,
     haxis, width, hpr, hpd)
1055 if (hpr-hpd > width || width <-1*(hpr-hpd))
1056
     gau_f(lineshape,quality,hpoint,width,linefunction,laxis,ha
     xis,hpr,hpd)
1057 endif
1058 sim9 += lineshape
1059 lineshape=0
1060 CNT+=1
1061 endfor
1062 endfor
1063 endfor
1064 lineshape=0
1065 I12=0
1066 I5=0
1067 I6=2
1068 H0=(6.626*(10^-34) * freq *
     (10^9))*1000/(g*9.274*10^-24)
1069 for(Iz12=I12;Iz12>=-I12;Iz12-=1)
1070 for(Iz5=I5;Iz5>=-I5;Iz5-=1)
1071 for(Iz6=I6;Iz6>=-I6;Iz6-=1)
1072 hpd =
     getH(hpoint,type,Aciso,dAciso,ani,dani,A5,A6,As,Iz12,I
     z1,Iz2,I5,I6,Iz5,Iz6,Iz56,I12,I1,I2,I56,H0,A1,A2)
1073 hpr =
     getH(hpoint,type,Aciso,dAciso,ani,dani,A5,A6,As,Iz12,I
     z1,Iz2,I5,I6,Iz5,Iz6,Iz56,I12,I1,I2,I56,H0,A1,A2)
1074 makeline(quality,linefunction,hpoint,lineshape, laxis,
     haxis, width, hpr, hpd)
1075 if (hpr-hpd > width || width <-1*(hpr-hpd))
1076
     gau_f(lineshape,quality,hpoint,width,linefunction,laxis,ha
     xis,hpr,hpd)
1077 endif
1078 sim10 += lineshape
1079 lineshape=0
1080 CNT+=1
1081 endfor
1082 endfor
1083 endfor
1084 lineshape=0
1085 I12=0
1086 I5=0
1087 I6=1
1088 H0=(6.626*(10^-34) * freq *
     (10^9))*1000/(g*9.274*10^-24)
1089 for(Iz12=I12;Iz12>=-I12;Iz12-=1)
1090 for(Iz5=I5;Iz5>=-I5;Iz5-=1)
1091 for(Iz6=I6;Iz6>=-I6;Iz6-=1)
```

```
1092 hpd =
     getH(hpoint,type,Aciso,dAciso,ani,dani,A5,A6,As,Iz12,I
     z1,Iz2,I5,I6,Iz5,Iz6,Iz56,I12,I1,I2,I56,H0,A1,A2)
1093 hpr =
     getH(hpoint,type,Aciso,dAciso,ani,dani,A5,A6,As,Iz12,I
     z1,Iz2,I5,I6,Iz5,Iz6,Iz56,I12,I1,I2,I56,H0,A1,A2)
1094 makeline(quality,linefunction,hpoint,lineshape, laxis,
     haxis, width, hpr, hpd)
1095 if (hpr-hpd > width || width <-1*(hpr-hpd))
1096
     gau_f(lineshape,quality,hpoint,width,linefunction,laxis,ha
     xis,hpr,hpd)
1097 endif
1098 sim11 += lineshape
1099 lineshape=0
1100 CNT+=1
1101 endfor
1102 endfor
1103 endfor
1104 lineshape=0
1105 I12=0
1106 I5=0
1107 I6=0
1108 H0=(6.626*(10^-34) * freq *
     (10^9))*1000/(g*9.274*10^-24)
1109 for(Iz12=I12;Iz12>=-I12;Iz12-=1)
1110 for(Iz5=I5;Iz5>=-I5;Iz5-=1)
1111 for(Iz6=I6;Iz6>=-I6;Iz6-=1)
1112 hpd =
     getH(hpoint,type,Aciso,dAciso,ani,dani,A5,A6,As,Iz12,I
     z1,Iz2,I5,I6,Iz5,Iz6,Iz56,I12,I1,I2,I56,H0,A1,A2)
1113 hpr =
     getH(hpoint,type,Aciso,dAciso,ani,dani,A5,A6,As,Iz12,I
     z1,Iz2,I5,I6,Iz5,Iz6,Iz56,I12,I1,I2,I56,H0,A1,A2)
1114 makeline(quality,linefunction,hpoint,lineshape, laxis,
     haxis, width, hpr, hpd)
1115 if (hpr-hpd > width || width <-1*(hpr-hpd))
1116
     gau_f(lineshape,quality,hpoint,width,linefunction,laxis,ha
     xis,hpr,hpd)
1117 endif
1118 sim12 += lineshape
1119 lineshape=0
1120 CNT+=1
1121 endfor
1122 endfor
1123 endfor
1124 lineshape=0
1125
     simallHDH2HD=(sim1+sim2+sim3+sim4+sim5+sim6+si
     m7+sim8+sim9+sim10+sim11+sim12)/CNT
1126 Differentiate simallHDH2HD
1127 end
1128
1129
1130 ////////////////////////////////////////////////////////////////////////////
1131 //
1132 // This is the function to make spectrum of D2H2D2+
1133 //
1134 ////////////////////////////////////////////////////////////////////////////
1135
1136 function D2H2D2()
1137 variable type
1138 variable y
1139 variable laxis, haxis
1140 variable g, freq, width,linefunction,quality,LF
1141 variable hpd,hpr,hpoint
1142 variable Aciso,Acani,dAciso,dAcani,A1,A2,As,A5,A6
1143 variable ani,dani
1144 variable Iz12,Iz1,Iz2,Iz5,Iz6,Iz56
1145 variable I1,I2,I12,I5,I6,I56
1146 variable H0,first,second
1147 type     = 6
1148 laxis    = 300
1149 haxis    = 360
1150 g          = 2.00212
1151 freq     = 9.256
1152 Aciso        = 21.4
1153 A5         = 1.43
1154 A6         = 1.43
1155 width    = 0.13
1156 hpoint = 4096
1157 quality = 100
1158 VARIABLE CNT=0
1159 prompt laxis, "enter start Magnetic Field: "
1160 prompt haxis, "enter end Magnetic Field: "
1161 prompt hpoint, "enter number of points: "
1162 DoPrompt "Enter magnetic field" ,laxis,haxis
1163 if (V_flag)
1164 return -1
1165 endif
1166 prompt g, "enter g-value: "
1167 prompt freq, "enter microwave frequency: "
1168 prompt Aciso, "enter isotropic Actr in mT: "
1169 prompt Acani, "enter anisotropic Actr in mT: "
1170 prompt A5, "enter A5 in mT: "
1171 prompt A6, "enter A6 in mT: "
1172 prompt width, "enter half width at half maximum in mT:
     "
1173 DoPrompt "Enter ESR
     Parameters" ,g,freq,Aciso,A5,A6,width
1174 if (V_flag)
1175 return -1
1176 endif
1177 printf "g = %g¥r",g
1178 printf "freq. = %g¥r",freq
1179 printf "Aciso = %g¥r",Aciso
1180 printf "A5 = %g¥r",A5
1181 printf "A6 = %g¥r",A6
1182 printf "width = %g¥r",width
1183 Make/O/D/N=(hpoint) sim1; SetScale x 0, 2*PI,
     sim1;sim1=0
1184 SetScale/I x laxis,haxis,"mT", sim1
1185 Make/O/D/N=(hpoint) sim2; SetScale x 0, 2*PI,
     sim2;sim2=0
1186 SetScale/I x laxis,haxis,"mT", sim2
1187 Make/O/D/N=(hpoint) sim3; SetScale x 0, 2*PI,
     sim3;sim3=0
1188 SetScale/I x laxis,haxis,"mT", sim3
1189 Make/O/D/N=(hpoint) sim4; SetScale x 0, 2*PI,
     sim4;sim4=0
1190 SetScale/I x laxis,haxis,"mT", sim4
1191 Make/O/D/N=(hpoint) sim5; SetScale x 0, 2*PI,
     sim5;sim5=0
1192 SetScale/I x laxis,haxis,"mT", sim5
1193 Make/O/D/N=(hpoint) sim6; SetScale x 0, 2*PI,
     sim6;sim6=0
1194 SetScale/I x laxis,haxis,"mT", sim6
1195 Make/O/D/N=(hpoint) sim7; SetScale x 0, 2*PI,
     sim7;sim7=0
1196 SetScale/I x laxis,haxis,"mT", sim7
1197 Make/O/D/N=(hpoint) sim8; SetScale x 0, 2*PI,
     sim8;sim8=0
1198 SetScale/I x laxis,haxis,"mT", sim8
1199 Make/O/D/N=(hpoint) sim9; SetScale x 0, 2*PI,
     sim9;sim9=0
1200 SetScale/I x laxis,haxis,"mT", sim9
1201 Make/O/D/N=(hpoint) sim10; SetScale x 0, 2*PI,
     sim10;sim10=0
1202 SetScale/I x laxis,haxis,"mT", sim10
1203 Make/O/D/N=(hpoint) sim11; SetScale x 0, 2*PI,
     sim11;sim11=0
1204 SetScale/I x laxis,haxis,"mT", sim11
1205 Make/O/D/N=(hpoint) sim12; SetScale x 0, 2*PI,
     sim12;sim12=0
1206 SetScale/I x laxis,haxis,"mT", sim12
1207 Make/O/D/N=(hpoint) simani; SetScale x 0, 2*PI,
     simani;simani=0
1208 SetScale/I x laxis,haxis,"mT", simani
1209 Make/O/D/N=(hpoint) simallD2H2D2; SetScale x 0,
     2*PI, simallD2H2D2;simallD2H2D2=0
1210 SetScale/I x laxis,haxis,"mT", simallD2H2D2
1211 Make/O/D/N=(hpoint) lineshape; SetScale x 0, 2*PI,
     lineshape;lineshape=0
1212 SetScale/I x laxis,haxis,"mT", lineshape
1213 I12=1
1214 I5=2
1215 I6=2
1216 H0=(6.626*(10^-34) * freq *
     (10^9))*1000/(g*9.274*10^-24)
1217 for(Iz12=I12;Iz12>=-I12;Iz12-=1)
1218 for(Iz5=I5;Iz5>=-I5;Iz5-=1)
1219 for(Iz6=I6;Iz6>=-I6;Iz6-=1)
```

```
1220 hpd =
     getH(hpoint,type,Aciso,dAciso,ani,dani,A5,A6,As,Iz12,I
     z1,Iz2,I5,I6,Iz5,Iz6,Iz56,I12,I1,I2,I56,H0,A1,A2)
1221 hpr =
     getH(hpoint,type,Aciso,dAciso,ani,dani,A5,A6,As,Iz12,I
     z1,Iz2,I5,I6,Iz5,Iz6,Iz56,I12,I1,I2,I56,H0,A1,A2)
1222 makeline(quality,linefunction,hpoint,lineshape, laxis,
     haxis, width, hpr, hpd)
1223 if (hpr-hpd > width || width <-1*(hpr-hpd))
1224
     gau_f(lineshape,quality,hpoint,width,linefunction,laxis,ha
     xis,hpr,hpd)
1225 endif
1226 sim1 += lineshape
1227 lineshape=0
1228 CNT+=1
1229 endfor
1230 endfor
1231 endfor
1232 lineshape=0
1233 I12=1
1234 I5=2
1235 I6=0
1236 H0=(6.626*(10^-34) * freq *
     (10^9))*1000/(g*9.274*10^-24)
1237 for(Iz12=I12;Iz12>=-I12;Iz12-=1)
1238 for(Iz5=I5;Iz5>=-I5;Iz5-=1)
1239 for(Iz6=I6;Iz6>=-I6;Iz6-=1)
1240 hpd =
     getH(hpoint,type,Aciso,dAciso,ani,dani,A5,A6,As,Iz12,I
     z1,Iz2,I5,I6,Iz5,Iz6,Iz56,I12,I1,I2,I56,H0,A1,A2)
1241 hpr =
     getH(hpoint,type,Aciso,dAciso,ani,dani,A5,A6,As,Iz12,I
     z1,Iz2,I5,I6,Iz5,Iz6,Iz56,I12,I1,I2,I56,H0,A1,A2)
1242 makeline(quality,linefunction,hpoint,lineshape, laxis,
     haxis, width, hpr, hpd)
1243 if (hpr-hpd > width || width <-1*(hpr-hpd))
1244
     gau_f(lineshape,quality,hpoint,width,linefunction,laxis,ha
     xis,hpr,hpd)
1245 endif
1246 sim2 += lineshape
1247 lineshape=0
1248 CNT+=1
1249 endfor
1250 endfor
1251 endfor
1252 lineshape=0
1253 I12=1
1254 I5=0
1255 I6=0
1256 H0=(6.626*(10^-34) * freq *
     (10^9))*1000/(g*9.274*10^-24)
1257 for(Iz12=I12;Iz12>=-I12;Iz12-=1)
1258 for(Iz5=I5;Iz5>=-I5;Iz5-=1)
1259 for(Iz6=I6;Iz6>=-I6;Iz6-=1)
1260 hpd =
     getH(hpoint,type,Aciso,dAciso,ani,dani,A5,A6,As,Iz12,I
     z1,Iz2,I5,I6,Iz5,Iz6,Iz56,I12,I1,I2,I56,H0,A1,A2)
1261 hpr =
     getH(hpoint,type,Aciso,dAciso,ani,dani,A5,A6,As,Iz12,I
     z1,Iz2,I5,I6,Iz5,Iz6,Iz56,I12,I1,I2,I56,H0,A1,A2)
1262 makeline(quality,linefunction,hpoint,lineshape, laxis,
     haxis, width, hpr, hpd)
1263 if (hpr-hpd > width || width <-1*(hpr-hpd))
1264
     gau_f(lineshape,quality,hpoint,width,linefunction,laxis,ha
     xis,hpr,hpd)
1265 endif
1266 sim3 += lineshape
1267 lineshape=0
1268 CNT+=1
1269 endfor
1270 endfor
1271 endfor
1272 lineshape=0
1273 I12=1
1274 I5=0
1275 I6=2
1276 H0=(6.626*(10^-34) * freq *
     (10^9))*1000/(g*9.274*10^-24)
1277 for(Iz12=I12;Iz12>=-I12;Iz12-=1)
1278 for(Iz5=I5;Iz5>=-I5;Iz5-=1)
1279 for(Iz6=I6;Iz6>=-I6;Iz6-=1)
1280 hpd =
     getH(hpoint,type,Aciso,dAciso,ani,dani,A5,A6,As,Iz12,I
     z1,Iz2,I5,I6,Iz5,Iz6,Iz56,I12,I1,I2,I56,H0,A1,A2)
1281 hpr =
     getH(hpoint,type,Aciso,dAciso,ani,dani,A5,A6,As,Iz12,I
     z1,Iz2,I5,I6,Iz5,Iz6,Iz56,I12,I1,I2,I56,H0,A1,A2)
1282 makeline(quality,linefunction,hpoint,lineshape, laxis,
     haxis, width, hpr, hpd)
1283 if (hpr-hpd > width || width <-1*(hpr-hpd))
1284
     gau_f(lineshape,quality,hpoint,width,linefunction,laxis,ha
     xis,hpr,hpd)
1285 endif
1286 sim4 += lineshape
1287 lineshape=0
1288 CNT+=1
1289 endfor
1290 endfor
1291 endfor
1292 lineshape=0
1293 I12=0
1294 I5=2
1295 I6=2
1296 H0=(6.626*(10^-34) * freq *
     (10^9))*1000/(g*9.274*10^-24)
1297 for(Iz12=I12;Iz12>=-I12;Iz12-=1)
1298 for(Iz5=I5;Iz5>=-I5;Iz5-=1)
1299 for(Iz6=I6;Iz6>=-I6;Iz6-=1)
1300 hpd =
     getH(hpoint,type,Aciso,dAciso,ani,dani,A5,A6,As,Iz12,I
     z1,Iz2,I5,I6,Iz5,Iz6,Iz56,I12,I1,I2,I56,H0,A1,A2)
1301 hpr =
     getH(hpoint,type,Aciso,dAciso,ani,dani,A5,A6,As,Iz12,I
     z1,Iz2,I5,I6,Iz5,Iz6,Iz56,I12,I1,I2,I56,H0,A1,A2)
1302 makeline(quality,linefunction,hpoint,lineshape, laxis,
     haxis, width, hpr, hpd)
1303 if (hpr-hpd > width || width <-1*(hpr-hpd))
1304
     gau_f(lineshape,quality,hpoint,width,linefunction,laxis,ha
     xis,hpr,hpd)
1305 endif
1306 sim5 += lineshape
1307 lineshape=0
1308 CNT+=1
1309 endfor
1310 endfor
1311 endfor
1312 lineshape=0
1313 I12=0
1314 I5=2
1315 I6=0
1316 H0=(6.626*(10^-34) * freq *
     (10^9))*1000/(g*9.274*10^-24)
1317 for(Iz12=I12;Iz12>=-I12;Iz12-=1)
1318 for(Iz5=I5;Iz5>=-I5;Iz5-=1)
1319 for(Iz6=I6;Iz6>=-I6;Iz6-=1)
1320 hpd =
     getH(hpoint,type,Aciso,dAciso,ani,dani,A5,A6,As,Iz12,I
     z1,Iz2,I5,I6,Iz5,Iz6,Iz56,I12,I1,I2,I56,H0,A1,A2)
1321 hpr =
     getH(hpoint,type,Aciso,dAciso,ani,dani,A5,A6,As,Iz12,I
     z1,Iz2,I5,I6,Iz5,Iz6,Iz56,I12,I1,I2,I56,H0,A1,A2)
1322 makeline(quality,linefunction,hpoint,lineshape, laxis,
     haxis, width, hpr, hpd)
1323 if (hpr-hpd > width || width <-1*(hpr-hpd))
1324
     gau_f(lineshape,quality,hpoint,width,linefunction,laxis,ha
     xis,hpr,hpd)
1325 endif
1326 sim6 += lineshape
1327 lineshape=0
1328 CNT+=1
1329 endfor
1330 endfor
1331 endfor
1332 lineshape=0
1333 I12=0
1334 I5=0
1335 I6=0
```

```
H0=(6.626*(10^-34) * freq *
    (10^9))*1000/(g*9.274*10^-24)
for(Iz12=I12;Iz12>=-I12;Iz12-=1)
for(Iz5=I5;Iz5>=-I5;Iz5-=1)
for(Iz6=I6;Iz6>=-I6;Iz6-=1)
hpd =
    getH(hpoint,type,Aciso,dAciso,ani,dani,A5,A6,As,Iz12,I
    z1,Iz2,I5,I6,Iz5,Iz6,Iz56,I12,I1,I2,I56,H0,A1,A2)
hpr =
    getH(hpoint,type,Aciso,dAciso,ani,dani,A5,A6,As,Iz12,I
    z1,Iz2,I5,I6,Iz5,Iz6,Iz56,I12,I1,I2,I56,H0,A1,A2)
makeline(quality,linefunction,hpoint,lineshape, laxis,
    haxis, width, hpr, hpd)
if (hpr-hpd > width || width <-1*(hpr-hpd))

    gau_f(lineshape,quality,hpoint,width,linefunction,laxis,ha
    xis,hpr,hpd)
endif
sim7 += lineshape
lineshape=0
CNT+=1
endfor
endfor
endfor
lineshape=0
I12=0
I5=0
I6=2
H0=(6.626*(10^-34) * freq *
    (10^9))*1000/(g*9.274*10^-24)
for(Iz12=I12;Iz12>=-I12;Iz12-=1)
for(Iz5=I5;Iz5>=-I5;Iz5-=1)
for(Iz6=I6;Iz6>=-I6;Iz6-=1)
hpd =
    getH(hpoint,type,Aciso,dAciso,ani,dani,A5,A6,As,Iz12,I
    z1,Iz2,I5,I6,Iz5,Iz6,Iz56,I12,I1,I2,I56,H0,A1,A2)
hpr =
    getH(hpoint,type,Aciso,dAciso,ani,dani,A5,A6,As,Iz12,I
    z1,Iz2,I5,I6,Iz5,Iz6,Iz56,I12,I1,I2,I56,H0,A1,A2)
makeline(quality,linefunction,hpoint,lineshape, laxis,
    haxis, width, hpr, hpd)
if (hpr-hpd > width || width <-1*(hpr-hpd))

    gau_f(lineshape,quality,hpoint,width,linefunction,laxis,ha
    xis,hpr,hpd)
endif
sim8 += lineshape
lineshape=0
CNT+=1
endfor
endfor
endfor
lineshape=0

    simallD2H2D2=(sim1+sim2+sim3+sim4+sim5+sim6+si
    m7+sim8)/CNT
Differentiate simallD2H2D2
end


////////////////////////////////////////////////////////////////////////////
//
// This is the function to make spectrum of H2D2H2+
//
////////////////////////////////////////////////////////////////////////////

function H2D2H2()
variable type
variable y
variable laxis, haxis
variable g, freq, width
variable hpd,hpr,hpoint
variable Aciso,Acani,dAciso,dAcani,A1,A2,As,A5,A6
variable ani,dani
variable Iz12,Iz1,Iz2,Iz5,Iz6,Iz56
variable I1,I2,I12,I5,I6,I56
variable H0,first,second
variable LF, linefunction, quality
type = 7
laxis = 300
haxis = 360
g = 2.00212
freq = 9.256
Aciso = 3.14
Acani = 0
width = 0.07
hpoint = 65536
quality = 100
VARIABLE CNT=0
prompt laxis, "enter start Magnetic Field: "
prompt haxis, "enter end Magnetic Field: "
prompt hpoint, "enter number of points: "
DoPrompt "Enter magnetic field" ,laxis,haxis
if (V_flag)
return -1
endif
prompt LF, "Chose linefunction", popup "laurentian;
    gaussian"
prompt quality, "Enter the value of lineshape quality
    (1-5000)"
DoPrompt "Chose line function" ,LF,quality
if (V_flag)
return -1
endif
if (LF==1)
linefunction=0
endif
if (LF==2)
linefunction=1
endif
prompt g, "enter g-value: "
prompt freq, "enter microwave frequency: "
prompt Aciso, "enter isotropic Actr in mT: "
prompt Acani, "enter anisotropic Actr in mT: "
prompt width, "enter half width at half maximum in mT:
    "
DoPrompt "Enter ESR
    Parameters" ,g,freq,Aciso,Acani,width
if (V_flag)
return -1
endif
printf "g = %g¥r",g
printf "freq. = %g¥r",freq
printf "Aciso = %g¥r",Aciso
printf "Acani = %g¥r",Acani
printf "width = %g¥r",width
Make/O/N=(hpoint) sim1; SetScale x 0, 2*PI,
    sim1;sim1=0
SetScale/I x laxis,haxis,"mT", sim1
Make/O/N=(hpoint) sim2; SetScale x 0, 2*PI,
    sim2;sim2=0
SetScale/I x laxis,haxis,"mT", sim2
Make/O/D/N=(hpoint) sim3; SetScale x 0, 2*PI,
    sim3;sim3=0
SetScale/I x laxis,haxis,"mT", sim3
Make/O/N=(hpoint) simani; SetScale x 0, 2*PI,
    simani;simani=0
SetScale/I x laxis,haxis,"mT", simani
Make/O/N=(hpoint) simallH2D2H2; SetScale x 0, 2*PI,
    simallH2D2H2;simallH2D2H2=0
SetScale/I x laxis,haxis,"mT", simallH2D2H2
Make/O/N=(hpoint) lineshape; SetScale x 0, 2*PI,
    lineshape;lineshape=0
SetScale/I x laxis,haxis,"mT", lineshape
I12 = 2
H0=(6.6260755*(10^-34) * freq *
    (10^9))*1000/(g*9.2740154*10^-24)
for(Iz12=I12;Iz12>=-I12;Iz12-=1)
ani = -Acani
hpd =
    getH(hpoint,type,Aciso,dAciso,ani,dani,A5,A6,As,Iz12,I
    z1,Iz2,I5,I6,Iz5,Iz6,Iz56,I12,I1,I2,I56,H0,A1,A2)//(type,
    Aciso,ani,As,Iz12,I12,H0)//
ani = 2*Acani
hpr =
    getH(hpoint,type,Aciso,dAciso,ani,dani,A5,A6,As,Iz12,I
    z1,Iz2,I5,I6,Iz5,Iz6,Iz56,I12,I1,I2,I56,H0,A1,A2)//(type,
    Aciso,ani,As,Iz12,I12,H0)//
if (hpr < haxis && hpr > laxis)
makeline(quality,linefunction,hpoint,lineshape, laxis,
    haxis, width, hpr, hpd)
if (hpr-hpd > width || width <-1*(hpr-hpd))
```

```
1462
      gau_f(lineshape,quality,hpoint,width,linefunction,laxis,ha
      xis,hpr,hpd)
1463 endif
1464 sim1 += lineshape
1465 lineshape=0
1466 else
1467 sim1=sim1
1468 endif
1469 CNT+=1
1470 endfor
1471 I12 = 1
1472 H0=(6.6260755*(10^-34) * freq *
      (10^9))*1000/(g*9.2740154*10^-24)
1473 for(Iz12=I12;Iz12>=-I12;Iz12-=1)
1474 ani = -Acani
1475 hpd =
      getH(hpoint,type,Aciso,dAciso,ani,dani,A5,A6,As,Iz12,I
      z1,Iz2,I5,I6,Iz5,Iz6,Iz56,I12,I1,I2,I56,H0,A1,A2)//(type,
      Aciso,ani,As,Iz12,I12,H0)//
1476 ani = 2*Acani
1477 hpr =
      getH(hpoint,type,Aciso,dAciso,ani,dani,A5,A6,As,Iz12,I
      z1,Iz2,I5,I6,Iz5,Iz6,Iz56,I12,I1,I2,I56,H0,A1,A2)//(type,
      Aciso,ani,As,Iz12,I12,H0)//
1478 if (hpr < haxis && hpr > laxis)
1479 makeline(quality,linefunction,hpoint,lineshape, laxis,
      haxis, width, hpr, hpd)
1480 if (hpr-hpd > width || width <-1*(hpr-hpd))
1481
      gau_f(lineshape,quality,hpoint,width,linefunction,laxis,ha
      xis,hpr,hpd)
1482 endif
1483 sim2 += lineshape
1484 lineshape=0
1485 else
1486 sim2=sim2
1487 endif
1488 CNT+=1
1489 endfor
1490 I12 = 0
1491 Iz12 = 0
1492 ani = -Acani
1493 hpd =
      getH(hpoint,type,Aciso,dAciso,ani,dani,A5,A6,As,Iz12,I
      z1,Iz2,I5,I6,Iz5,Iz6,Iz56,I12,I1,I2,I56,H0,A1,A2)//(type,
      Aciso,ani,As,Iz12,I12,H0)//
1494 ani = 2*Acani
1495 hpr =
      getH(hpoint,type,Aciso,dAciso,ani,dani,A5,A6,As,Iz12,I
      z1,Iz2,I5,I6,Iz5,Iz6,Iz56,I12,I1,I2,I56,H0,A1,A2)//(type,
      Aciso,ani,As,Iz12,I12,H0)//
1496 if (hpr < haxis && hpr > laxis)
1497 makeline(quality,linefunction,hpoint,lineshape, laxis,
      haxis, width, hpr, hpd)
1498 if (hpr-hpd > width || width <-1*(hpr-hpd))
1499
      gau_f(lineshape,quality,hpoint,width,linefunction,laxis,ha
      xis,hpr,hpd)
1500 endif
1501 sim3 += lineshape
1502 lineshape=0
1503 else
1504 sim3=sim3
1505 endif
1506 CNT+=1
1507 simallH2D2H2=(sim1+sim2+sim3)/CNT
1508 Differentiate simallH2D2H2
1509 end
1510
1511
1512 ////////////////////////////////////////////////////////////////////////////
1513 //
1514 // This is the function to make spectra of H2D2D2+
1515 //
1516 ////////////////////////////////////////////////////////////////////////////
1517
1518 function H2D2D2()
1519 variable type
1520 variable y
1521 variable laxis, haxis
1522 variable g, freq, width,linefunction,quality,LF
1523 variable hpd,hpr,hpoint
1524 variable Aciso,Acani,dAciso,dAcani,A1,A2,As,A5,A6
1525 variable ani,dani
1526 variable Iz12,Iz1,Iz2,Iz5,Iz6,Iz56
1527 variable I1,I2,I12,I5,I6,I56
1528 variable H0,first,second
1529 type      = 1
1530 laxis    = 300
1531 haxis    = 360
1532 g          = 2.00212
1533 freq      = 9.256
1534 Aciso    = 3.17
1535 Acani    = 0
1536 dAciso = 0.18
1537 dAcani = 0
1538 As         = 1.44
1539 width    = 0.16
1540 hpoint=4096
1541 quality = 100
1542 VARIABLE CNT=0
1543 prompt laxis, "enter start Magnetic Field: "
1544 prompt haxis, "enter end Magnetic Field: "
1545 prompt hpoint, "enter number of points: "
1546 DoPrompt "Enter magnetic field" ,laxis,haxis
1547 if (V_flag)
1548 return -1
1549 endif
1550 prompt LF, "Chose linefunction", popup "laurentian;
      gaussian; mix0.5"
1551 prompt quality, "Enter the value of lineshape quality
      (1-5000)"
1552 DoPrompt "Chose line function" ,LF,quality
1553 if (V_flag)
1554 return -1
1555 endif
1556 if (LF==1)
1557 linefunction=0
1558 endif
1559 if (LF==2)
1560 linefunction=1
1561 endif
1562 if (LF==3)
1563 linefunction=2
1564 endif
1565 prompt g, "enter g-value: "
1566 prompt freq, "enter microwave frequency: "
1567 prompt Aciso, "enter isotropic Actr in mT: "
1568 prompt Acani, "enter anisotropic Actr in mT: "
1569 prompt dAciso, "enter (A1iso-A2iso)/2 in mT: "
1570 prompt dAcani, "enter (A1ani-A2ani)/2 in mT: "
1571 prompt As, "enter Asid in mT: "
1572 prompt width, "enter half width at half maximum in mT:
      "
1573 DoPrompt "Enter ESR
      Parameters" ,g,freq,Aciso,Acani,dAciso,dAcani,As,width
1574 if (V_flag)
1575 return -1
1576 endif
1577 printf "g = %g¥r",g
1578 printf "freq. = %g¥r",freq
1579 printf "Aciso = %g¥r",Aciso
1580 printf "Acani = %g¥r",Acani
1581 printf "dAciso = %g¥r",dAciso
1582 printf "dAcani = %g¥r",dAcani
1583 printf "As = %g¥r",As
1584 printf "width = %g¥r",width
1585 Make/O/D/N=(hpoint) sim1; SetScale x 0, 2*PI,
      sim1;sim1=0
1586 SetScale/I x laxis,haxis,"mT", sim1
1587 Make/O/D/N=(hpoint) sim2; SetScale x 0, 2*PI,
      sim2;sim2=0
1588 SetScale/I x laxis,haxis,"mT", sim2
1589 Make/O/D/N=(hpoint) simani; SetScale x 0, 2*PI,
      simani;simani=0
1590 SetScale/I x laxis,haxis,"mT", simani
1591 Make/O/D/N=(hpoint) simallH2D2D2; SetScale x 0,
      2*PI, simallH2D2D2;simallH2D2D2=0
1592 SetScale/I x laxis,haxis,"mT", simallH2D2D2
1593 Make/O/D/N=(hpoint) lineshape; SetScale x 0, 2*PI,
      lineshape;lineshape=0
1594 SetScale/I x laxis,haxis,"mT", lineshape
1595 I1=1
```

```
1596 I2=1
1597 I56=2
1598 H0=(6.626*(10^-34) * freq *
     (10^9))*1000/(g*9.274*10^-24)
1599 for(Iz1=I1;Iz1>=-I1;Iz1-=1)
1600 for(Iz2=I2;Iz2>=-I2;Iz2-=1)
1601 for(Iz56=I56;Iz56>=-I56;Iz56-=1)
1602 ani = -Acani
1603 dani = -dAcani
1604 hpd =
     getH(hpoint,type,Aciso,dAciso,ani,dani,A5,A6,As,Iz12,I
     z1,Iz2,I5,I6,Iz5,Iz6,Iz56,I12,I1,I2,I56,H0,A1,A2)
1605 ani = 2*Acani
1606 dani = 2*dAcani
1607 hpr =
     getH(hpoint,type,Aciso,dAciso,ani,dani,A5,A6,As,Iz12,I
     z1,Iz2,I5,I6,Iz5,Iz6,Iz56,I12,I1,I2,I56,H0,A1,A2)
1608 if (hpr < haxis && hpr > laxis)
1609 makeline(quality,linefunction,hpoint,lineshape, laxis,
     haxis, width, hpr, hpd)
1610 if (hpr-hpd > width || width <-1*(hpr-hpd))
1611
     gau_f(lineshape,quality,hpoint,width,linefunction,laxis,ha
     xis,hpr,hpd)
1612 endif
1613 sim1 += lineshape
1614 lineshape=0
1615 else
1616 sim1=sim1
1617 endif
1618 CNT+=1
1619 endfor
1620 endfor
1621 endfor
1622 lineshape=0
1623 for(Iz1=I1;Iz1>=-I1;Iz1-=1)
1624 for(Iz2=I2;Iz2>=-I2;Iz2-=1)
1625 Iz56=0
1626 I56=0
1627 ani = -Acani
1628 dani = -dAcani
1629 hpd =
     getH(hpoint,type,Aciso,dAciso,ani,dani,A5,A6,As,Iz12,I
     z1,Iz2,I5,I6,Iz5,Iz6,Iz56,I12,I1,I2,I56,H0,A1,A2)
1630 ani = 2*Acani
1631 dani = 2*dAcani
1632 hpr =
     getH(hpoint,type,Aciso,dAciso,ani,dani,A5,A6,As,Iz12,I
     z1,Iz2,I5,I6,Iz5,Iz6,Iz56,I12,I1,I2,I56,H0,A1,A2)
1633 if (hpr < haxis && hpr > laxis)
1634 makeline(quality,linefunction,hpoint,lineshape, laxis,
     haxis, width, hpr, hpd)
1635 if (hpr-hpd > width || width <-1*(hpr-hpd))
1636
     gau_f(lineshape,quality,hpoint,width,linefunction,laxis,ha
     xis,hpr,hpd)
1637 endif
1638 sim2 += lineshape
1639 lineshape=0
1640 else
1641 sim2=sim2
1642 endif
1643 CNT+=1
1644 endfor
1645 endfor
1646 lineshape=0
1647 simallH2D2D2=(sim1+sim2)/CNT
1648 Differentiate simallH2D2D2
1649 end
1650
1651
1652 ////////////////////////////////////////////////////////////////////////////
1653 //
1654 // This is the function to make spectra of D6+
1655 //
1656 ////////////////////////////////////////////////////////////////////////////
1657
1658 function D2D2D2()
1659 variable type
1660 variable y
1661 variable laxis, haxis
1662 variable g, freq, width,linefunction,quality,LF
1663 variable hpd,hpr,hpoint
1664 variable Aciso,Acani,dAciso,dAcani,A1,A2,As,A5,A6
1665 variable ani,dani
1666 variable Iz12,Iz1,Iz2,Iz5,Iz6,Iz56
1667 variable I1,I2,I12,I5,I6,I56
1668 variable H0,first,second
1669 type      = 5
1670 laxis    = 300
1671 haxis    = 360
1672 g          = 2.00212
1673 freq      = 9.256
1674 Aciso        = 3.285
1675 A5         = 1.43
1676 A6         = 1.43
1677 width    = 0.13
1678 hpoint = 4096
1679 quality = 100
1680 VARIABLE CNT=0
1681 prompt laxis, "enter start Magnetic Field: "
1682 prompt haxis, "enter end Magnetic Field: "
1683 prompt hpoint, "enter number of points: "
1684 DoPrompt "Enter magnetic field" ,laxis,haxis
1685 if (V_flag)
1686 return -1
1687 endif
1688 prompt g, "enter g-value: "
1689 prompt freq, "enter microwave frequency: "
1690 prompt Aciso, "enter isotropic Actr in mT: "
1691 prompt Acani, "enter anisotropic Actr in mT: "
1692 prompt A5, "enter A5 in mT: "
1693 prompt A6, "enter A6 in mT: "
1694 prompt width, "enter half width at half maximum in mT:
     "
1695 DoPrompt "Enter ESR
     Parameters" ,g,freq,Aciso,A5,A6,width
1696 if (V_flag)
1697 return -1
1698 endif
1699 printf "g = %g¥r",g
1700 printf "freq. = %g¥r",freq
1701 printf "Aciso = %g¥r",Aciso
1702 printf "A5 = %g¥r",A5
1703 printf "A6 = %g¥r",A6
1704 printf "width = %g¥r",width
1705 Make/O/D/N=(hpoint) sim1; SetScale x 0, 2*PI,
     sim1;sim1=0
1706 SetScale/I x laxis,haxis,"mT", sim1
1707 Make/O/D/N=(hpoint) sim2; SetScale x 0, 2*PI,
     sim2;sim2=0
1708 SetScale/I x laxis,haxis,"mT", sim2
1709 Make/O/D/N=(hpoint) sim3; SetScale x 0, 2*PI,
     sim3;sim3=0
1710 SetScale/I x laxis,haxis,"mT", sim3
1711 Make/O/D/N=(hpoint) sim4; SetScale x 0, 2*PI,
     sim4;sim4=0
1712 SetScale/I x laxis,haxis,"mT", sim4
1713 Make/O/D/N=(hpoint) sim5; SetScale x 0, 2*PI,
     sim5;sim5=0
1714 SetScale/I x laxis,haxis,"mT", sim5
1715 Make/O/D/N=(hpoint) sim6; SetScale x 0, 2*PI,
     sim6;sim6=0
1716 SetScale/I x laxis,haxis,"mT", sim6
1717 Make/O/D/N=(hpoint) sim7; SetScale x 0, 2*PI,
     sim7;sim7=0
1718 SetScale/I x laxis,haxis,"mT", sim7
1719 Make/O/D/N=(hpoint) sim8; SetScale x 0, 2*PI,
     sim8;sim8=0
1720 SetScale/I x laxis,haxis,"mT", sim8
1721 Make/O/D/N=(hpoint) sim9; SetScale x 0, 2*PI,
     sim9;sim9=0
1722 SetScale/I x laxis,haxis,"mT", sim9
1723 Make/O/D/N=(hpoint) sim10; SetScale x 0, 2*PI,
     sim10;sim10=0
1724 SetScale/I x laxis,haxis,"mT", sim10
1725 Make/O/D/N=(hpoint) sim11; SetScale x 0, 2*PI,
     sim11;sim11=0
1726 SetScale/I x laxis,haxis,"mT", sim11
1727 Make/O/D/N=(hpoint) sim12; SetScale x 0, 2*PI,
     sim12;sim12=0
1728 SetScale/I x laxis,haxis,"mT", sim12
1729 Make/O/D/N=(hpoint) simani; SetScale x 0, 2*PI,
     simani;simani=0
```

```
1730 SetScale/I x laxis,haxis,"mT", simani
1731 Make/O/D/N=(hpoint) simallD2D2D2; SetScale x 0,
     2*PI, simallD2D2D2;simallD2D2D2=0
1732 SetScale/I x laxis,haxis,"mT", simallD2D2D2
1733 Make/O/D/N=(hpoint) lineshape; SetScale x 0, 2*PI,
     lineshape;lineshape=0
1734 SetScale/I x laxis,haxis,"mT", lineshape
1735 I12=0
1736 I5=2
1737 I6=2
1738 H0=(6.626*(10^-34) * freq *
     (10^9))*1000/(g*9.274*10^-24)
1739 for(Iz12=I12;Iz12>=-I12;Iz12-=1)
1740 for(Iz5=I5;Iz5>=-I5;Iz5-=1)
1741 for(Iz6=I6;Iz6>=-I6;Iz6-=1)
1742 hpd =
     getH(hpoint,type,Aciso,dAciso,ani,dani,A5,A6,As,Iz12,I
     z1,Iz2,I5,I6,Iz5,Iz6,Iz56,I12,I1,I2,I56,H0,A1,A2)
1743 hpr =
     getH(hpoint,type,Aciso,dAciso,ani,dani,A5,A6,As,Iz12,I
     z1,Iz2,I5,I6,Iz5,Iz6,Iz56,I12,I1,I2,I56,H0,A1,A2)
1744 makeline(quality,linefunction,hpoint,lineshape, laxis,
     haxis, width, hpr, hpd)
1745 if (hpr-hpd > width || width <-1*(hpr-hpd))
1746
     gau_f(lineshape,quality,hpoint,width,linefunction,laxis,ha
     xis,hpr,hpd)
1747 endif
1748 sim1 += lineshape
1749 lineshape=0
1750 CNT+=1
1751 endfor
1752 endfor
1753 endfor
1754 lineshape=0
1755 I12=0
1756 I5=2
1757 I6=0
1758 H0=(6.626*(10^-34) * freq *
     (10^9))*1000/(g*9.274*10^-24)
1759 for(Iz12=I12;Iz12>=-I12;Iz12-=1)
1760 for(Iz5=I5;Iz5>=-I5;Iz5-=1)
1761 for(Iz6=I6;Iz6>=-I6;Iz6-=1)
1762 hpd =
     getH(hpoint,type,Aciso,dAciso,ani,dani,A5,A6,As,Iz12,I
     z1,Iz2,I5,I6,Iz5,Iz6,Iz56,I12,I1,I2,I56,H0,A1,A2)
1763 hpr =
     getH(hpoint,type,Aciso,dAciso,ani,dani,A5,A6,As,Iz12,I
     z1,Iz2,I5,I6,Iz5,Iz6,Iz56,I12,I1,I2,I56,H0,A1,A2)
1764 makeline(quality,linefunction,hpoint,lineshape, laxis,
     haxis, width, hpr, hpd)
1765 if (hpr-hpd > width || width <-1*(hpr-hpd))
1766
     gau_f(lineshape,quality,hpoint,width,linefunction,laxis,ha
     xis,hpr,hpd)
1767 endif
1768 sim2 += lineshape
1769 lineshape=0
1770 CNT+=1
1771 endfor
1772 endfor
1773 endfor
1774 lineshape=0
1775 I12=0
1776 I5=0
1777 I6=0
1778 H0=(6.626*(10^-34) * freq *
     (10^9))*1000/(g*9.274*10^-24)
1779 for(Iz12=I12;Iz12>=-I12;Iz12-=1)
1780 for(Iz5=I5;Iz5>=-I5;Iz5-=1)
1781 for(Iz6=I6;Iz6>=-I6;Iz6-=1)
1782 hpd =
     getH(hpoint,type,Aciso,dAciso,ani,dani,A5,A6,As,Iz12,I
     z1,Iz2,I5,I6,Iz5,Iz6,Iz56,I12,I1,I2,I56,H0,A1,A2)
1783 hpr =
     getH(hpoint,type,Aciso,dAciso,ani,dani,A5,A6,As,Iz12,I
     z1,Iz2,I5,I6,Iz5,Iz6,Iz56,I12,I1,I2,I56,H0,A1,A2)
1784 makeline(quality,linefunction,hpoint,lineshape, laxis,
     haxis, width, hpr, hpd)
1785 if (hpr-hpd > width || width <-1*(hpr-hpd))
1786
     gau_f(lineshape,quality,hpoint,width,linefunction,laxis,ha
     xis,hpr,hpd)
1787 endif
1788 sim3 += lineshape
1789 lineshape=0
1790 CNT+=1
1791 endfor
1792 endfor
1793 endfor
1794 lineshape=0
1795 I12=0
1796 I5=0
1797 I6=2
1798 H0=(6.626*(10^-34) * freq *
     (10^9))*1000/(g*9.274*10^-24)
1799 for(Iz12=I12;Iz12>=-I12;Iz12-=1)
1800 for(Iz5=I5;Iz5>=-I5;Iz5-=1)
1801 for(Iz6=I6;Iz6>=-I6;Iz6-=1)
1802 hpd =
     getH(hpoint,type,Aciso,dAciso,ani,dani,A5,A6,As,Iz12,I
     z1,Iz2,I5,I6,Iz5,Iz6,Iz56,I12,I1,I2,I56,H0,A1,A2)
1803 hpr =
     getH(hpoint,type,Aciso,dAciso,ani,dani,A5,A6,As,Iz12,I
     z1,Iz2,I5,I6,Iz5,Iz6,Iz56,I12,I1,I2,I56,H0,A1,A2)
1804 makeline(quality,linefunction,hpoint,lineshape, laxis,
     haxis, width, hpr, hpd)
1805 if (hpr-hpd > width || width <-1*(hpr-hpd))
1806
     gau_f(lineshape,quality,hpoint,width,linefunction,laxis,ha
     xis,hpr,hpd)
1807 endif
1808 sim4 += lineshape
1809 lineshape=0
1810 CNT+=1
1811 endfor
1812 endfor
1813 endfor
1814 lineshape=0
1815 I12=2
1816 I5=2
1817 I6=2
1818 H0=(6.626*(10^-34) * freq *
     (10^9))*1000/(g*9.274*10^-24)
1819 for(Iz12=I12;Iz12>=-I12;Iz12-=1)
1820 for(Iz5=I5;Iz5>=-I5;Iz5-=1)
1821 for(Iz6=I6;Iz6>=-I6;Iz6-=1)
1822 hpd =
     getH(hpoint,type,Aciso,dAciso,ani,dani,A5,A6,As,Iz12,I
     z1,Iz2,I5,I6,Iz5,Iz6,Iz56,I12,I1,I2,I56,H0,A1,A2)
1823 hpr =
     getH(hpoint,type,Aciso,dAciso,ani,dani,A5,A6,As,Iz12,I
     z1,Iz2,I5,I6,Iz5,Iz6,Iz56,I12,I1,I2,I56,H0,A1,A2)
1824 makeline(quality,linefunction,hpoint,lineshape, laxis,
     haxis, width, hpr, hpd)
1825 if (hpr-hpd > width || width <-1*(hpr-hpd))
1826
     gau_f(lineshape,quality,hpoint,width,linefunction,laxis,ha
     xis,hpr,hpd)
1827 endif
1828 sim5 += lineshape
1829 lineshape=0
1830 CNT+=1
1831 endfor
1832 endfor
1833 endfor
1834 lineshape=0
1835 I12=2
1836 I5=2
1837 I6=0
1838 H0=(6.626*(10^-34) * freq *
     (10^9))*1000/(g*9.274*10^-24)
1839 for(Iz12=I12;Iz12>=-I12;Iz12-=1)
1840 for(Iz5=I5;Iz5>=-I5;Iz5-=1)
1841 for(Iz6=I6;Iz6>=-I6;Iz6-=1)
1842 hpd =
     getH(hpoint,type,Aciso,dAciso,ani,dani,A5,A6,As,Iz12,I
     z1,Iz2,I5,I6,Iz5,Iz6,Iz56,I12,I1,I2,I56,H0,A1,A2)
1843 hpr =
     getH(hpoint,type,Aciso,dAciso,ani,dani,A5,A6,As,Iz12,I
     z1,Iz2,I5,I6,Iz5,Iz6,Iz56,I12,I1,I2,I56,H0,A1,A2)
```

```
1844 makeline(quality,linefunction,hpoint,lineshape, laxis,
     haxis, width, hpr, hpd)
1845 if (hpr-hpd > width || width <-1*(hpr-hpd))
1846
     gau_f(lineshape,quality,hpoint,width,linefunction,laxis,ha
     xis,hpr,hpd)
1847 endif
1848 sim6 += lineshape
1849 lineshape=0
1850 CNT+=1
1851 endfor
1852 endfor
1853 endfor
1854 lineshape=0
1855 I12=2
1856 I5=0
1857 I6=0
1858 H0=(6.626*(10^-34) * freq *
     (10^9))*1000/(g*9.274*10^-24)
1859 for(Iz12=I12;Iz12>=-I12;Iz12-=1)
1860 for(Iz5=I5;Iz5>=-I5;Iz5-=1)
1861 for(Iz6=I6;Iz6>=-I6;Iz6-=1)
1862 hpd =
     getH(hpoint,type,Aciso,dAciso,ani,dani,A5,A6,As,Iz12,I
     z1,Iz2,I5,I6,Iz5,Iz6,Iz56,I12,I1,I2,I56,H0,A1,A2)
1863 hpr =
     getH(hpoint,type,Aciso,dAciso,ani,dani,A5,A6,As,Iz12,I
     z1,Iz2,I5,I6,Iz5,Iz6,Iz56,I12,I1,I2,I56,H0,A1,A2)
1864 makeline(quality,linefunction,hpoint,lineshape, laxis,
     haxis, width, hpr, hpd)
1865 if (hpr-hpd > width || width <-1*(hpr-hpd))
1866
     gau_f(lineshape,quality,hpoint,width,linefunction,laxis,ha
     xis,hpr,hpd)
1867 endif
1868 sim7 += lineshape
1869 lineshape=0
1870 CNT+=1
1871 endfor
1872 endfor
1873 endfor
1874 lineshape=0
1875 I12=2
1876 I5=0
1877 I6=2
1878 H0=(6.626*(10^-34) * freq *
     (10^9))*1000/(g*9.274*10^-24)
1879 for(Iz12=I12;Iz12>=-I12;Iz12-=1)
1880 for(Iz5=I5;Iz5>=-I5;Iz5-=1)
1881 for(Iz6=I6;Iz6>=-I6;Iz6-=1)
1882 hpd =
     getH(hpoint,type,Aciso,dAciso,ani,dani,A5,A6,As,Iz12,I
     z1,Iz2,I5,I6,Iz5,Iz6,Iz56,I12,I1,I2,I56,H0,A1,A2)
1883 hpr =
     getH(hpoint,type,Aciso,dAciso,ani,dani,A5,A6,As,Iz12,I
     z1,Iz2,I5,I6,Iz5,Iz6,Iz56,I12,I1,I2,I56,H0,A1,A2)
1884 makeline(quality,linefunction,hpoint,lineshape, laxis,
     haxis, width, hpr, hpd)
1885 if (hpr-hpd > width || width <-1*(hpr-hpd))
1886
     gau_f(lineshape,quality,hpoint,width,linefunction,laxis,ha
     xis,hpr,hpd)
1887 endif
1888 sim8 += lineshape
1889 lineshape=0
1890 CNT+=1
1891 endfor
1892 endfor
1893 endfor
1894 lineshape=0
1895
     simallD2D2D2=(sim1+sim2+sim3+sim4+sim5+sim6+si
     m7+sim8)/CNT
1896 Differentiate simallD2D2D2
1897 end
```

# Publication lists

1. J. Kumagai, H. Inagaki, S. Kariya, T. Ushida, Y. Shimizu, and T. Kumada, Electron spin resonance study on $H_6^+$, $H_5D^+$, $H_4D_2^+$, and $H_2D_4^+$ in solid parahydrogen, J. Chem. Phys **127** 024505 (2007).

2. 熊田高之、牛田考洋、清水裕太、熊谷　純、固体パラ水素中に生成した $H_6^+$の ESR 分光研究、電子スピンサイエンス, **5** 134 (2007)

3. Y. Shimizu, T. Kumada, and J. Kumagai, Electron spin resonance spectroscopy of molecules in large precessional motion: A case of $H_6^+$ and $H_4D_2^+$ in solid parahydrogen, J. Magn. Reson. **194** 76 (2008).

4. T. Kumada, Y. Shimizu, T. Ushida, and J. Kumagai, H atom, $e^-$, and $H_6^+$ ions produced in irradiated solid hydrogens: An electron spin resonance study Rad. Phys. Chem. **77** 1318 (2008).

5. Y. Kurosaki, Y. Shimizu, and J. Kumagai, Isotope effects on the spin-density distribution in the $H_6^+$ clusters: Direct ab initio molecular dynamics study, Chem. Phys. Lett. **455** 59 (2008).

6. 清水裕太, 熊谷　純, 固体パラ水素中の $H_6^+$同位体イオンと捕捉電子の放射線化学、放射線化学 **87** 23 (2009).

7. Y. Shimizu, M. Inagaki, T. Kumada, and J. Kumagai, Negative and positive ion trapping by isotopic molecules in cryocrystals in case of solid parahydrogen containing electrons and $H_6^+$ radical cations, J. Chem. Phys. **132** 244503 (2010).

# International conferences

1. Y. Shimizu, T. Kumada, J. Kumagai, Deffusion of $H_6^+$ ion in γ-ray irradiated solid parahydrogen studied by isotope condensation, 2nd Asia-Pacific Symposium on Radiation Chemistry (APSRC-2008), **2P-18** 162 (Aug. 2008, Tokyo, Japan).

2. Y. Shimizu, T. Kumada, J. Kumagai, $H_6^+$ ions and electrons diffusing irradiated solid parahydrogen are trapped by isotopic hydrogen molecules, The 1st G-COE International Symposium on Elucidation and Design of Materials and Molecular Functions, **P67** 101 (2009)

3. Y. Shimizu, T. Kumada, J. Kumagai, Negative and positive ions produced by radiolysis of solid parahydrogen are trapped by deuterium molecules, Horiba-ISSP International Symposium (ISSP-11) "Hydrogen and water in condensed matter physics", **P48** 192 (Oct. 2009, Chiba, Japan).

# Awards

1. NatureCOE 若手研究奨励賞, 名古屋大学 21 世紀 COE, 2006 年 1 月

2. 名古屋大学学術奨励賞, 名古屋大学, 2008 年 7 月

3. 優秀発表賞, 第 47 回電子スピンサイエンス学会年会 (SEST2008), 2008 年 10 月, 福岡

4. 若手研究奨励賞, 材料バックキャストテクノロジー研究センター, 2009 年 3 月

5. 学生講演賞, 日本化学会第 90 春季年会, 2010 年 3 月, 大阪

6. 若手優秀講演賞, 第 53 回放射線化学討論会, 2010 年 9 月, 名古屋

7. 若手研究奨励賞, 材料バックキャストテクノロジー研究センター, 2010 年 12 月

# Acknowledgement

The present investigation has been carried out from 2006 to 2011 in the Physical Chemistry laboratory, Graduate School of Engineering, Nagoya University as a doctoral course student.

The author wishes to profound gratitude to Associate Professor KUMAGAI Jun of Nagoya University, Professor OKAZAKI Susumu of Nagoya University, and Dr. KUMADA Takayuki of Japan Atomic Energy Research Institute for their variable advice and continuous encouragement through the work. The author wishes to his appreciation to Dr. KITANO Toshiaki, who advised me to take a doctoral course.

The author would like to thank for Mr. IMAI Shigefumi of $^{60}$Co γ-ray irradiation facility at Nagoya University for his helpful collaborations for γ-ray irradiations. Hearty thanks are made to all members in Radiation Chemistry group led by Associate Professor KUMAGAI Jun, especially Mr. USHIDA Takahiro, Mr. KOBAYASHI Hiroharu, Mr. SATO Fumiaki, Mr. INAGAKI Makoto, and Mr. HARA Hidetoshi for their collaborations.

The author gratefully acknowledge to Dr. KUROSAKI Yuzuru of Japan Atomic Energy Research Institute and Assistant Professor KOMAGUCHI Kenji of Hiroshima University, Professor FUKUTANI Katsuyuki of the University of Tokyo, and Mr. SUGIMOTO Toshiki of the University of Tokyo for helpful discussions. The author also thanks a lot for Mr. ISHIGAKI Tatsuya for kindly advice about computer programming.

This work was partly supported by the Global-COE program in Chemistry at Nagoya University and Iue Memorial Foundation.

Last but far from least, appreciation must be expressed to the author's family and relatives for their continual encouragement without which the present study could not have been done.

March 2011

SHIMIZU Yuta